CHAPTER TWO

Advances in Catalysis for Methanol-to-Olefins Conversion

Shutao Xu[*,1], Yuchun Zhi[*,1], Jingfeng Han[*], Wenna Zhang[*,†], Xinqiang Wu[*,†], Tantan Sun[*,†], Yingxu Wei[*,2], Zhongmin Liu[*,‡,2]

[*]National Engineering Laboratory for Methanol to Olefins, Dalian National Laboratory for Clean Energy, iChEM (Collaborative Innovation Center of Chemistry for Energy Materials), Dalian Institute of Chemical Physics, Chinese Academy of Sciences, Dalian, PR China
[†]University of Chinese Academy of Sciences, Beijing, PR China
[‡]State Key Laboratory of Catalysis, Dalian Institute of Chemical Physics, Chinese Academy of Sciences, Dalian, PR China
[2]Corresponding authors: e-mail address: weiyx@dicp.ac.cn; liuzm@dicp.ac.cn

Contents

[1] Shutao Xu and Yuchun Zhi contributed equally.

Advances in Catalysis, Volume 61
ISSN 0360-0564
https://doi.org/10.1016/bs.acat.2017.10.002

Abstract

Methanol-to-olefins (MTO) conversion is one of the most important reactions in C1 chemistry, which provides a path for producing basic petrochemicals from non-petroleum resources such as coal and natural gas. Since the 1970s, the processes of methanol conversion to olefins have been developed, and with the great research efforts in the past 30 years, commercialization of MTO process has been achieved in 2010. Many institutions and companies have made great effort in the research on MTO reaction, and significant progresses have been made with respect to the fundamental principle, catalyst synthesis, and process research and development. The application of shape-selective catalysts, such as ZSM-5 and SAPO-34, realizes the efficient conversion of methanol with high selectivity to light olefins, ethene and propene. This review first gives a brief overview of the MTO catalysts and MTO technology development, including fixed-bed and fluidized-bed technologies. The advances in catalysis for MTO conversion have been summarized, and the proposals of the direct reaction mechanism and the indirect reaction mechanism, the strategy for the control of product selectivity, the complicated reaction network of methanol conversion over zeolite and zeotype catalysts, and deactivation of MTO reaction have been discussed in detail. The reaction mechanism for initial carbon–carbon bond formation in the early stage of MTO reaction, and some new insights into initial methanol conversion are discussed by reviewing the latest literature in this field.

ABBREVIATIONS

BAS	Brønsted acid sites
CHA	structure code for chabazite framework
DFT	density functional theory
DICP	Dalian Institute of Chemical Physics
DME	dimethyl ether
DMTO	methanol-to-olefin technology developed by DICP
FCC	fluid catalytic cracking
FMTP	fluidized methanol-to-propene technology developed by Tsinghua University
H-mordenite	proton form MOR zeolite
H-SAPO-5	proton form SAPO-5 zeolite
H-SSZ-13	proton form SSZ-13 zeolite
H-SSZ-24	proton form SSZ-24 zeolite
H-Y	proton form Y-zeolite
IM-5	an aluminosilicate zeolite of the IMF framework
LAS	Lewis acid sites
MAS NMR	magic angle spinning nuclear magnetic resonance
MeAPSO-34	metal heteroatoms modified SAPO-34 molecular sieve through isomorphous substitution (MeAPSO-34)
Me/SAPO-34	metal heteroatoms modified SAPO-34 molecular sieve through ion exchange or impregnation
MFI	structure code for ZSM-5 framework
MTG	methanol to gasolines

MTH	methanol to hydrocarbons
MTO	methanol to olefins
NMR	nuclear magnetic resonance
R&D	research and development
SAPO	silicoaluminophosphate molecular sieve
SAPO-34	a silicoaluminophosphate molecular sieve with the chabazite framework
SAPO-5	a silicoaluminophosphate molecular sieve with the AFI framework
SMS	surface methoxy species
SMTO	methanol-to-olefin technology developed by Sinopec Group
SSZ-13	an aluminosilicate zeolite of the chabazite framework
SSZ-24	an aluminosilicate zeolite of the AFI framework
TNU-9	an aluminosilicate zeolite of the TUN framework
UCC	Union Carbide Corporation
UV/Vis	ultraviolet–visible spectroscopy
Y-zeolite	an aluminosilicate zeolite of the faujasite framework (Si/Al > 1.5)
ZSM-5	an aluminosilicate zeolite of the MFI framework
ZSM-22	an aluminosilicate zeolite of the TON framework
ZSM-35	an aluminosilicate zeolite of the FER framework.

1. INTRODUCTION

The process development of methanol conversion to hydrocarbons (MTH) began with two seminal discoveries by Mobil central research group in the 1970s *(1)*. During the study of methanol conversion to other oxygen-containing compounds and of methanol and isobutane alkylation over ZSM-5 catalysts, unexpected hydrocarbons in gasoline fraction were discovered, which initiated methanol to gasoline (MTG) process *(2,3)*. Thereafter, MTO conversion process over molecular sieve catalyst was reported by Mobile Company *(4)*. These two processes could produce petrochemical products using methanol as raw material instead of petroleum *(5,6)*.

It is believed that MTO process includes the conversion of methanol to dimethyl ether (DME) and methanol and DME to olefins over solid acid catalysts (Fig. 1). Amorphous solid acids like Al_2O_3 and Al_2O_3–SiO_2

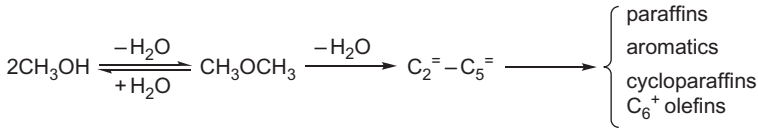

Fig. 1 The reaction path of methanol to hydrocarbons *(1)*.

could convert methanol to DME; however, the selectivity for light olefins is low. Light olefin selectivity could be significantly improved by employing appropriate molecular sieve catalysts *(1,5,7,8)*. Secondary reaction of olefin products would generate paraffins, aromatics, and higher hydrocarbons.

MTO process using ZSM-5 zeolite with the MFI structure was first disclosed by Chang et al. from Mobil Company in the 1970s *(1,4)*. Focusing on the production of propene, Lurgi Company employed ZSM-5 for methanol catalytic conversion and developed methanol-to-propene (MTP) process *(9)*. In 1984, the Union Carbide Corporation (UCC) developed a new series of silicoaluminophosphate (SAPO) molecular sieves *(10)*. SAPO molecular sieves have the pore structure with 6- to 12-ring windows ranging from 0.3 to 0.8 nm in diameter and moderate acidity. Through the application of SAPO-34 molecular sieve with chabazite (CHA) topology, the selectivity for light olefins is highly enhanced in MTO process. The selectivity for ethene and propene over SAPO-34 catalyst reached up to 90%, and the formation of butene and higher olefins was largely suppressed *(7,8)*. Thus, after the R&D on MTO reaction for more than 40 years, based on the small pore SAPO-34 catalyst, Dalian Institute of Chemical Physics (DICP) developed methanol-to-olefin (DMTO) technology and realized the world's first commercialization of MTO reaction *(11)*. At present, ZSM-5 and SAPO-34 have become the most important catalysts for MTO process. Besides the development of new processes and catalysts for methanol conversion, research efforts have also been devoted to the mechanistic study of methanol reaction, which is desirable to optimize the reaction process and guide the development of new catalysts.

2. MTO CATALYST DEVELOPMENT

As a central component of MTO technology, the catalyst development has always been attracting substantial interests from both academic and industrial community. A better understanding of distinct catalytic performance and the structure–activity relationship for a specific catalyst enables us to gain insights into the underlying catalytic MTO chemistry, eventually to establish selectivity control principle for effectively manipulating product distribution. Being two utmost important commercial catalysts, ZSM-5 and SAPO-34 have been drawing sustained attention for decades, always being at the core of catalyst research.

2.1 ZSM-5 Catalyst

ZSM-5 zeolite was synthesized by Argauer and Landolt in 1972 *(12)*. Chang et al. first found that ZSM-5 is capable of converting methanol to gasoline in 1975 *(2,3,13)*, and immediately after this, Mobil Company developed the MTO process on ZSM-5 in 1977 *(1)*. ZSM-5 had played a critical role in the early stage of development of MTG and MTO processes. Even now, as to the MTG process, no other zeolites outweigh ZSM-5 in catalytic activity, and meanwhile, almost all the practical MTO processes based on the fixed-bed reactor adopt ZSM-5 as a catalyst. The feature of ZSM-5 is embodied by the distinctive MFI structure consisting of a straight 10-membered ring channel with dimensions of 5.1×5.5 Å intersected by a sinusoidal 10-membered ring channel of 5.3×5.6 Å, forming the large space with a diameter of around 8.9 Å at channel intersection *(14,15)* as shown in Fig. 2.

The stronger acidity of ZSM-5 endows it with high activity to convert methanol. The spacious channel size cannot constrain the generation of long-chain hydrocarbons and aromatics to a rather low extent, especially over ZSM-5 with higher Brønsted acid sites (BAS) density, and yet this feature is beneficial for MTG process. Rather, ZSM-5 with high Si/Al ratio corresponding to a lower BAS density can effectively circumvent the secondary reaction of the produced olefins, yielding more propene *(16)*. Nanosized and micropore/mesopore composited ZSM-5, advantageous for the diffusion of reactants and products, is considered as potential candidates to enhance the propene selectivity and prolong the catalyst lifetime as well *(16)*. Besides multiple modification strategies, e.g., high-temperature

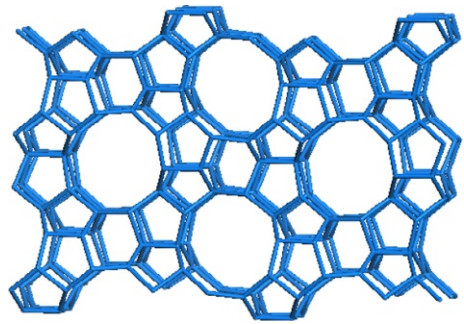

Fig. 2 Illustration of MFI structure viewed along [010] (the framework image was redrawn according to the database of the International Zeolite Association).

steaming treatment, P and metal (such as Ma, Ca, Ce, and Ni) modification have also been applied to adjust the acidity and decelerate the catalytic activity loss *(17)*. Although the approximate consensus could be reached in some aspects, e.g., elements modification can irreversibly reduce the BAS content by dealumination or by covering the strong BAS, and accordingly improve the light olefins selectivity and prolong the catalyst lifetime. However, given the complexity of the interplay of inherent acid sites and the introduced steam, P, and metal additives, there is no definitive conclusion regarding the nature and catalytic origin of the adventitious element itself and its interaction with the local zeolitic structure.

Even though a higher propene to ethene ratio can be achieved on the basis of the unique MFI structure and especially with posttreatment of ZSM-5 catalyst, the yield of propene in one single-path operation is usually no more than 50%. Hence, developing effective catalyst with high single-path propene selectivity remains challenging for exploring the new generation of MTO technology.

Except for ZSM-5, researchers also attempt to apply other silicoaluminate zeolites for MTO reaction. The H-Y and H-mordenite zeolites possessing a larger pore size are inclined to form aromatics deactivating the catalyst fast, resulting in inferior olefins selectivity *(18,19)*. Concerning the small pore zeolites, such as ZK-5, ZSM-34, and ZSM-35, prominent amounts of lower olefins can be obtained by the product shape selectivity conferred by the small pore opening. Nevertheless, the intrinsically lower Si/Al ratio associated with the poor diffusivity makes these zeolites subject to liable accumulation of deposits, accompanied by considerable undesired alkanes *(20–22)*.

2.2 SAPO-34 Catalyst

Ever since the invention of series of SAPO molecular sieves *(23)*, SAPO-34 typical for CHA framework topology with cage dimensions of $10 \times 6.7 \times 6.7$ Å connected by eight-membered ring opening of 3.8×3.8 Å (Fig. 3), has drawn much research concern owing to its medium acidity strength, high hydrothermal stability, and exceptional light olefins selectivity *(24,25)*. DICP in Chinese Academy of Sciences reported the MTO catalytic activity on SAPO-34 for the first time in 1990 *(7)*. In this foundation work, almost 100% methanol conversion was achieved and the selectivity of C_2–C_4 olefins amounted to around 90% with less C_{5+} products *(7)*. This unprecedented finding has been unequivocally viewed as an essential step

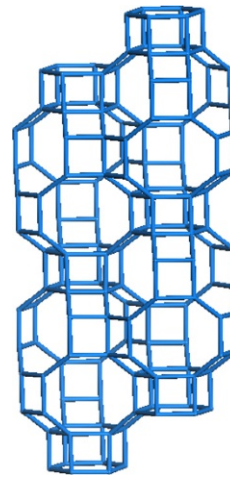

Fig. 3 Illustration of CHA structure viewed along [001] (the framework image was redrawn according to the database of the International Zeolite Association).

forward in developing MTO technology and in turn highly encourages the researchers to devote more effects to optimize the synthesis protocol of SAPO-34 and to unveil the MTO mechanism over this exceptional catalyst. Liu and coworkers from DICP systemically studied the synthesis of SAPO-34 and proposed the SAPO-34 crystallization and the Si incorporation mechanism *(26,27)*. They found that SAPO-34 with single Si(4Al) coordination state favors selective production of light olefins. For this, crystallization conditions and starting materials should be carefully controlled to achieve a successful synthesis *(26,28)*.

Metal heteroatom modification, through isomorphous substitution (MeAPSO-34) or ion exchange and impregnation (Me/SAPO-34), has been extensively investigated to tune the acidity and local structure of SAPO-34 cavity in order to lower the undesired side products, improve the product distribution, and enhance the catalyst lifetime *(29–31)*. An important work demonstrated by Inui and Kang *(29)* showed the surprising ethene selectivity up to 88% in NiAPSO-34 with Si/Ni of 40. Subsequently, van Niekerk made efforts trying to synthesize SAPO-34 containing Ni and Co metal elements, but, no evidence can be given to support the incorporation of the metal into the framework of SAPO-34 and, in contrast, the addition of Ni and Co cannot improve the ethene selectivity apparently *(30)*, whereas CoAPSO-34, ZnAPSO-34, and MgAPSO-34 have been successfully synthesized by Liu and coworkers which exhibited enhanced

C_2–C_3 olefins selectivity above 90%, especially for CoAPSO-34 with C_2–C_3 olefins selectivity up to 93% and 60% ethene *(31)*.

Intriguingly, a ship-in-a-bottle scenario was proposed by Song and Haw *(32)* to modify the acidity of SAPO-34, in such a way that the reaction of the introduced PH_3 and methanol inside the cavity of SAPO-34 in situ generated the large-sized $P(CH_3)_3$ and $P(CH_3)_4^+$ species followed by high-temperature calcination to partly consume BAS and concurrently shrink the cage volume. This peculiar treatment increased ethene selectivity from 37% to 46% compared with the parent SAPO-34, albeit somewhat of decline of methanol conversion *(32)*. In addition, silanization modification of SAPO-34 by leading SiH_4 and Si_2H_6 to the cavity engendered irreversible transformation of part of BAS to LAS, along with the diminution of effective cavity space *(33)*. Turning to MTO reaction, parallel to the degree of silanization, ethene to ethane ratio steadily increased, and concomitantly coke deposition apparently decreased. However, silanization treatment is such as to lower down the selectivity of the total light olefins *(33)*.

Light olefins, especially ethene and propene, which can be produced from MTO reaction on SAPO-34, are highly desirable for commercially applicable MTO process. With the aid of process and technology, optimization, recycling, and cracking the low-valued butene and other by-products could generate more light olefins. However, such an added procedure would incur heavier recycling load and stress the apparatus burden. So, more efforts still need to be devoted to develop more effective catalysts to enhance sing-path light olefins selectivity. Moreover, even under the industrial operation, it is observed that propene selectivity is almost invariable and, however, the ethene selectivity, quite lower at the initial period, ascends with reaction going on, resulting in a rather narrow "operation window" for optimum light olefins production *(6)*. How to significantly promote the ethene selectivity at the early stage of MTO process, being a profit-related crucial issue in view of industrial application, remains to be explored.

3. MTO TECHNOLOGY DEVELOPMENT

Research and development of coal or natural gas to olefin technology was inspired by the serious impact of the first and second oil crises on the world economy in 1973 and 1978. Many countries have put their research effort on the technology development of producing light olefins from nonoil resources. Up to date, methanol-to-light olefin technology has become the bridge linking coal or natural gas chemical industry with petrochemical

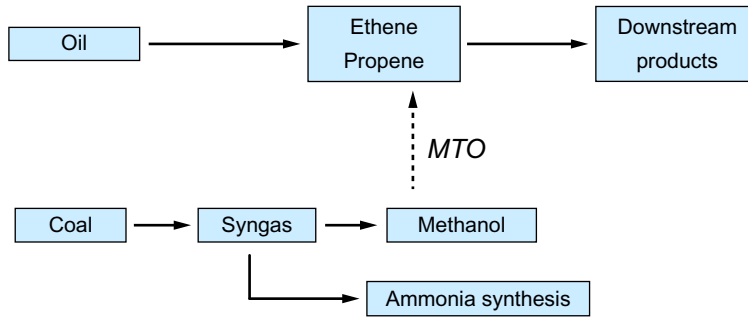

Fig. 4 MTO process linking petrochemical industry and coal chemical industry.

industry. The nonoil route light olefins production from coal or natural gas contains several steps (Fig. 4), including syngas preparation, manufacture of methanol, methanol to olefins, and olefin polymerization. Except the MTO process, the other processes have already been commercialized, so MTO process development attracts more and more attention from academy and industry fields. Following summarizes the MTO process development in the past 40 years, including fixed-bed and fluidized-bed MTO technologies with the application of ZSM-5 and SAPO-34 as the catalysts.

3.1 MTO Technology of Mobil Company and ExxonMobil Company

The MTO process was first reported in the early 1970s by Chang and Silvestri of Mobil Company *(1,34,35)*. In these initiative work, the researchers were trying to produce high-octane gasoline by passing mixture of methanol and isobutene through H-ZSM-5. What they produced from these experiments were indeed high-octane rating products mainly consisting of aromatics, along with gaseous products of light olefins and alkanes. However, careful control experiments suggested that similar product distributions were formed without co-feeding isobutene, and mass balance analysis indicated that isobutene was not consumed when being co-fed with methanol. What they observed is actually a new route to produce hydrocarbon directly from methanol, known as MTG process. After this discovery, MTG and MTO processes were fast developed in the 1970s. Subsequently, Mobil Company developed fixed-bed and fluidized-bed MTO processes. After the development of MTG process for converting methanol to high-octane rating gasoline from nonpetroleum sources, a commercial plant was established in New Zealand in 1982 *(36–38)*. This plant converts natural

gas from the Maui and Kapuni fields into methanol and then into ca. 570,000 tons per year of gasoline via Mobil's fixed-bed MTG process *(36–38)*.

In the 1980s, the fluidized-bed MTO process has been developed and realized successfully in the plant in Wesseling (Germany) shown in Fig. 5 *(36)*. The fluidized-bed process has the following advantages compared to the fixed-bed process: excellent heat transfer properties, continuous regeneration of the catalyst (constant catalyst activity), uniform bed temperature, uniform and stable transient temperature profiles during heat-up and cool-down, the higher specific throughput, lower cost, and so on *(36)*.

In 1999, Exxon Company merged with Mobil Company to build up the largest international oil and gas company. Then, ExxonMobil established the unit for demonstration test of MTO technology, including the product separation and polymerization system. This operation unit was also equipped with MOGD system (Mobil olefins to gasoline/distillate), which could realize the olefin transformation to gasoline and distillate *(39,40)*. In this process, gasoline and distillates selectivity is greater than 95% and gasoline/distillate product ratios range from 0.2 to 100. In order to obtain gasoline with high-octane number, the local acid environment of catalyst was delicately tuned based on the shape-selectivity control theory for preferable production of methyl-branched iso-olefins (C_5–C_{20}). A large-scale MOGD test run was executed in a Mobil refinery in 1981.

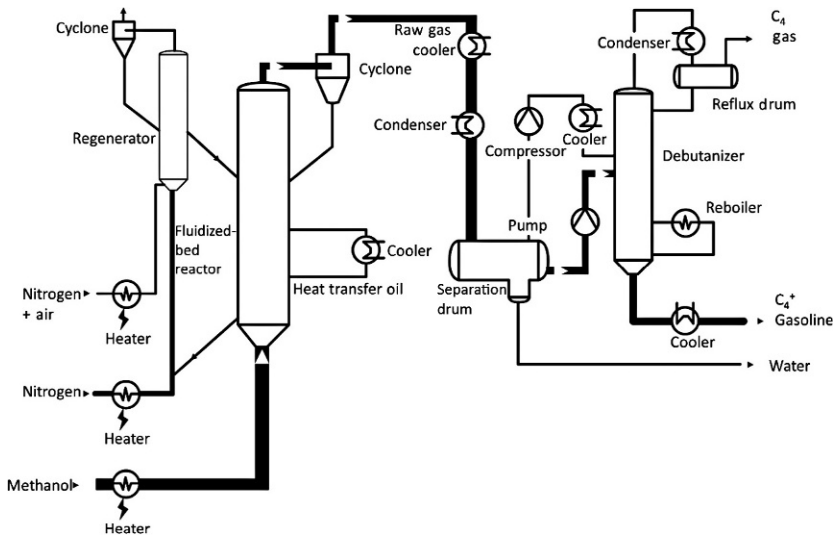

Fig. 5 Fluidized-bed MTG and MTO demonstration plant of Mobil Company *(36)*.

3.2 MTP Technology of Lurgi

Stimulated by the high propene demand worldwide, Lurgi Company developed MTP process with high propene selectivity utilizing ZSM-5 produced by Süd-Chemie as the catalyst *(9,41,42)*. MTP process is a fixed-bed technology based on the combination of a suitable reactor system and a selective zeolite-based catalyst. Methanol is introduced to a prereactor loaded with acidic catalysts, where methanol is converted into an equilibrium mixture including methanol, DME, and water vapor and then the mixture is converted into olefins (mainly propene) in fixed-bed reactors installed in series at reaction temperature of 450–500°C. Finally, the propene is separated and the other products are recycled to reactors to further enhance propene yield. Methanol and DME are converted by more than 90% with propene as the predominant product. Based on the microscale tests in the laboratory, the Demo Unit of MTP process was built by Lurgi in Statoil methanol plant at Tjeldbergodden, Norway in 2001 *(9,41,42)*. The demonstration unit completed the scheduled 8000 tests and met the commercial target with regeneration period of 500–600 h. Propene selectivity was higher than 60% and propene purity attained the polymerization grade. The product yield on large-scale MTP units was announced by Lurgi as follows: for MTP unit with the processing capacity of 5000 tons methanol per day (1.67 million tons annually), approximately 474,000 tons propylene annually, 185,000 tons gasoline annually, 41,000 tons LPG annually, small amount of fuel gas, and 935,000 tons water annually could be produced *(9)*. The recommended MTP process flow diagram is shown in Fig. 6 *(9)*. Since 2010, commercialized MTP plants of Lurgi Company have been built in China.

3.3 MTO Technology of UOP/Hydro and Combined MTO and Olefin Cracking Technology

In the 1980s, UCC Company discovered SAPO molecular sieves, which presents high selectivity to light olefins in MTO reaction. Based on the SAPO-34 molecular sieve, UOP (Des Plaines, Illinois) and Norsk Hydro (Oslo, Norway) developed the gas-to-olefins process and the MTO process. The MTO process employs a fluidized-bed continuous reaction-regeneration technology and the simplified flow sheet is presented in Fig. 7 *(36)*. The catalyst is transferred continuously to the regenerator to remove the coke to keep the high activity of the catalyst. MTO reaction conducted by the fluidized-bed reactor, dealing with 0.75 tons/day methanol, had been successfully verified at Porsgrunn in

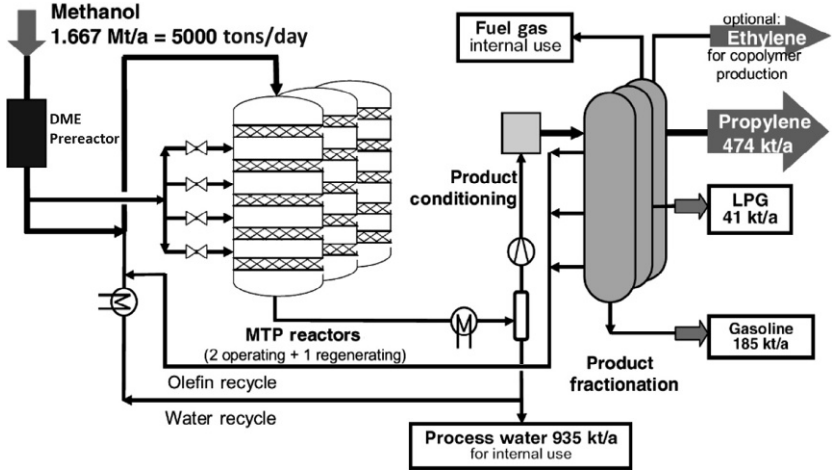

Fig. 6 Lurgi MTP-simplified process flow diagram *(9)*.

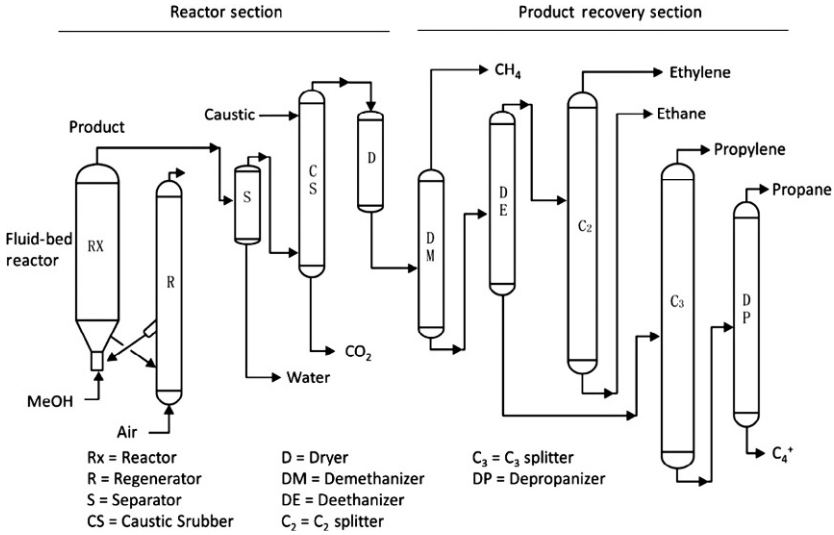

Fig. 7 UOP/Hydro MTO process flow sheet *(36)*.

Norway. In 1995, pilot test results were published and it was claimed that MTO industrial setup could be designed for producing 0.3–0.5 million tons light olefins every year, and that the catalyst showed higher attrition resistance performance and good stability. During the 90-day continuous test, methanol conversion was kept close to 100%, and total selectivity of ethene and

propene (based on carbon number) was about 75%–80% *(43)*. The ratio of ethene to propene could be varied from 0.75 to 1.25 by controlling the reaction conditions, and the total selectivity of ethene and propene reached its maximum when the selectivity of ethene was close to that of propene *(36,43,44)*.

For improving the selectivity of ethene and propene, olefin-cracking process (OCP) was suggested by UOP Company for converting higher olefins to smaller ones, ethene and propene. OCP process was substantiated in 1988 and further developed and demonstrated by Total Petrochemicals. It was reported that the MTO process combined with the OCP process could further improve the selectivity of light olefins to about 85%–90%, and the ratio of propene to ethene could be tuned to 2.1. The integration of MTO and OCP techniques recycles and cracks the C_{4+} products of MTO process for more ethene and propene production. Catalytic cracking is usually in favor of producing propene, which in turn enhances the propene to ethene ratios. In the OCP process, fixed-bed reactors and zeolite catalyst were adopted for the cracking of C_4–C_7 mixtures to produce light olefins, under the reaction conditions of high space velocity, low pressure (0.1–0.3 MPa), and high reaction temperature (500–600°C) *(44)*.

3.4 MTO Technology of DICP

In China, DICP started to develop methanol-to-olefins process from the early 1980s. DMTO technology (DME/methanol to olefin, DMTO) developed by DICP has been successfully applied in the world's first commercialized MTO process in 2010 *(6)*.

3.4.1 Fixed-Bed MTO Technology of DICP

The MTO research in DICP started since 1982 as a project supported by Chinese government and Chinese Academy of Sciences due to the concerns for the shortage of oil supply originated from the oil crisis in the 1970s *(6)*. DICP developed the modified ZSM-5 as a catalyst for fixed-bed MTO reaction with ethene selectivity of around 30% or higher and propene selectivity of 50%–60%. The pilot test of fixed-bed MTO reaction was carried out with 300 tons methanol feed annually. The catalyst stability test for 1000 h was successfully achieved with seven regeneration cycles. To avoid the overheating of catalyst bed and remove the reaction heat quickly, the diluted methanol (30 wt%) was used as the feedstock and two reactor systems were applied. Methanol was partly dehydrated in the first reactor loaded with the Al_2O_3 catalyst to get the mixture of methanol, DME, and water, and then in the second reactor, the mixture was transformed to hydrocarbon

products. In this way, severe reaction heat release could be avoided. Furthermore, the catalyst was loaded segmentedly in the second reactor to achieve an appropriate bed temperature distribution.

3.4.2 Fluidized-Bed MTO Technology of DICP

3.4.2.1 Technology Development

The fixed-bed MTO technology was based on the modified ZSM-5 catalyst; although proven to be successful, the selectivity of ethene and the overall selectivity of ethene and propene were not high enough. In the meantime, the researchers in DICP reported the application of SAPO-34 in the MTO reaction *(7)*; the selectivity of C_2–C_4 alkenes could reach 89% with ethene selectivity of 57%–59% at methanol conversion of 100%.

The MTO reaction is highly exothermal and the released heat must be effectively removed from the reaction bed to keep the catalyst bed temperature constant. Besides, the MTO reaction over SAPO-34 catalyst usually encounters rapid catalyst deactivation due to the coke deposition. Therefore, the fluidized-bed reactor with excellent heat transfer effect was considered *(6)*. With the successful scale-up of the catalyst and the reactor, DMTO reaction (DME to olefins) performed on the fluidized-bed reactor presented excellent performance with DME conversion of 100%, $C_2^=$–$C_4^=$ selectivity of 90% and $C_2^=$ selectivity of ~60% at 550°C and DME WHSV of 6 h^{-1}, confirming the scale-up method for SAPO-34 synthesis and catalyst preparation *(45)*.

Different types of fluidized-bed reactors were adopted and tested for DMTO process as well, which includes two downer reactors and a dense-phase fluidized-bed reactor. Benefiting from the experiences from FCC practice and the in-depth understanding of the fluidization mode, dense-phase fluidized-bed reactor system was eventually adopted for DMTO process under the consideration of the unique characteristics of MTO reaction *(6)*. Dense-phase fluidized-bed reactor tests optimize the reaction conditions and lay the foundation for further scale-up of DMTO process.

3.4.2.2 Industrial Test of DMTO Technology

In order to verify and optimize the DMTO process and provide basic data for designing and constructing large-scale industrial plant, the industrial testing plant of DMTO technology with 10,000 tons methanol feeding per year (50–75 tons/day) started to be built from August 2004 jointly by DICP and engineering corporations in China. The plant includes

reaction–regeneration part, heat removal unit, quenching-stripping part, air compressors, and power station. The flow diagram of the industrial testing unit is shown in Fig. 8 *(6)*. The industrial test was completed in June 2006 after running for nearly 1200 h. The basic data for designing large-scale industrial plant were obtained and the feasibility of catalysts and technologies were verified *(11)*. The industrial testing results under typical operation conditions are shown in Fig. 9 *(6)*. The total methanol conversion was realized

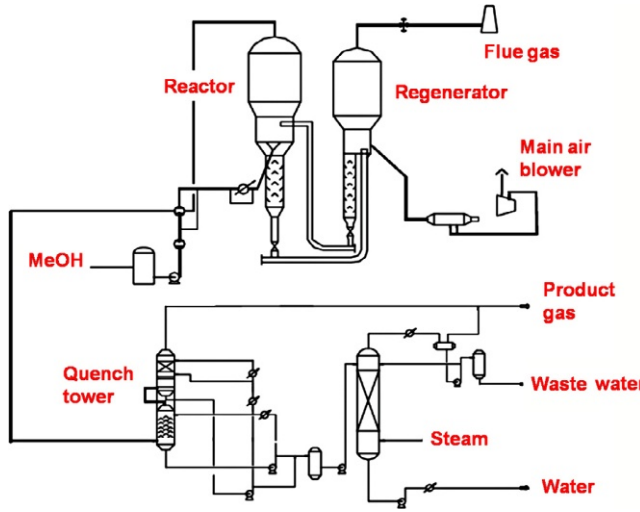

Fig. 8 Flow diagram of DMTO industrial test unit *(6)*.

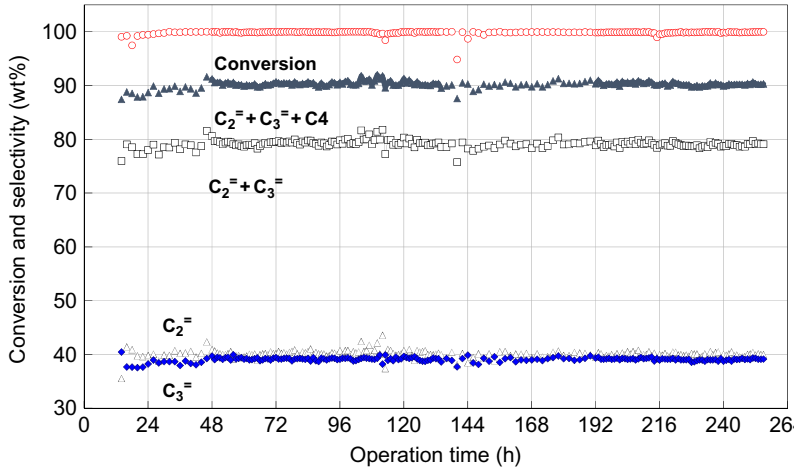

Fig. 9 Typical results obtained from DMTO industrial test plant *(6)*.

with both ethene and propene selectivity of 80% and the total selectivity of ethene, propene, and C_4 amounting to 90% under the continuous and stable operation of more than 150 h.

3.4.2.3 DMTO Technology Commercialization

In May 2010, the world's first DMTO commercial unit was constructed in Baotou, China, by Shenhua group. The capacity of the unit is to produce 0.6 million tons polyethene and polypropene per year. The employed reactor is based on a shallow turbulent fluidized bed with a diameter of 11 m and a bed height of 3 m. In August 2010, this unit was successfully started up with the methanol conversion of 100% and the ethene and propene selectivity higher than 80%. The light olefins selectivity is superior to the results obtained in small-scale unit, due to the good fluidization effect in the commercial DMTO reactor. In March 2011, a 72-h performance test was carried out on this DMTO unit. Analysis of the obtained data showed that the methanol consumption is 2.96 tons for production of 1 ton ethene and propene.

After the success of industrial practice, DICP developed the second generation of DMTO process (DMTO-II), in which the by-products of C_{4+} are separated from the products stream and further converted to ethene and propene in the fluidized-bed cracking reactor. From 2009 to 2010, the DMTO-II process has been substantiated. The results obtained from the demonstration unit showed that the selectivity of both ethene and propene increased from 79.21% in DMTO process to 85.68% in DMTO-II process with 60 wt% of C_{4+} recycling, and the methanol consumption for producing 1 ton ethene and propene reduced from 2.96 to 2.67 tons. In December 2014, the first commercial DMTO-II unit was successfully started up in Pucheng Clean Energy Chemical Co. Ltd. in China.

Since 2006, DICP started to license DMTO technology worldwide. Up to July 2017, 23 licenses have been approved with a total capacity of 11 million tons/a ethene and propene production. More than 10 commercial DMTO units and 1 commercial DMTO-II unit have been commercialized with olefins production capacity exceeding 5.6 million tons/a.

In China, besides DMTO technology developed by DICP, Tsinghua University also developed fluidized methanol-to-propene process (FMTP) based on a small pore SAPO molecular sieve and a fluidized-bed technique and also accomplished the industrial test with 100 tons methanol feed per day in recent years. China Petrochemical Corporation (Sinopec Group) also

developed methanol-to-olefin (SMTO) process and completed industrial test. It has been reported that the SMTO technology has been applied for ethene plant expansion and reconstruction in Zhongyuan Oil field in China *(46)*.

4. REACTION MECHANISM OF METHANOL TO OLEFINS CONVERSION

4.1 Direct Mechanism of Methanol Conversion

MTO conversion is a reaction converting C1 raw material, methanol, or DME, to the new compounds with the successive construction of C—C bond. The C—C bond generation mechanism is one of the most important scientific issues in the mechanistic study on MTO *(5,15,47)*. The main mechanisms proposed by early researchers were focused on direct conversion mechanisms, in which olefin products are considered to be produced through the direct coupling reaction of C1 reactants *(5,15)*. In order to explain the first C—C bond generation from methanol, researchers have proposed more than 20 direct mechanisms *(5)* as identified by the involved reaction intermediates, such as oxonium ylide *(48–50)*, carbocation *(51,52)*, carbine *(1,34,53)*, and radical species *(54,55)*. But in these mechanisms, a direct coupling of C1 entities has to overcome high reaction energy barrier *(47,56)*. These direct mechanisms have suffered from the lack of experimental evidences and could not explain some of the experimental phenomena successfully.

In recent years, several research groups reported new progresses in revealing the reaction pathway of initial C—C bond formation in methanol conversion. The following summarizes these studies based on the direct capture of reactive intermediates and confirmation of different reaction routes from both experimental and theoretical aspects.

Fan et al. *(57)* compared the reaction behavior of methanol and DME on a fully calcined SAPO-34 (FC-SAPO-34) catalyst using a pulse reactor, showing that in the initial reaction stage, DME was more reactive than methanol. By in situ IR spectroscopy (Fig. 10) *(57)*, when appropriate amount of DME was introduced into SAPO-34 catalyst with pregenerated surface methoxy species (SMS), an increase in the temperature from 30°C to 180°C led to the appearance of a new band at 2960 cm^{-1}, which is attributed to the asymmetric C—H stretching vibration of the CH_2 group in CH_3OCH_2OZ (Z = zeolite). Based on this observation, methoxymethyl carbocation ($CH_3OCH_2^+$), formed by the interaction of SMS and DME,

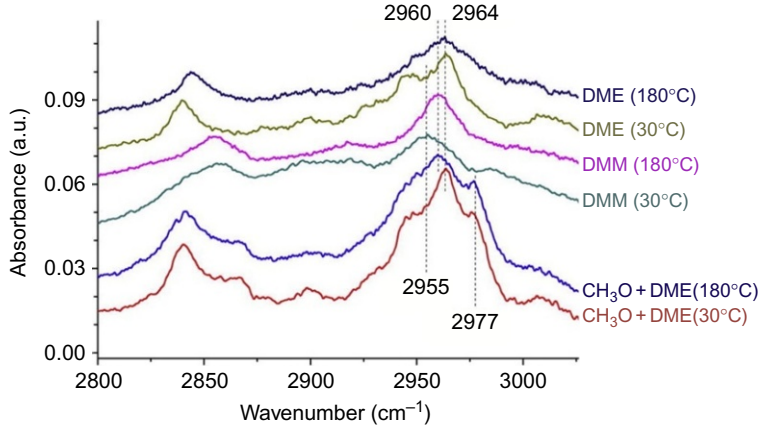

Fig. 10 IR spectra for the formation of $CH_3OCH_2^+$ by the reaction of methoxy groups and DME *(57)*.

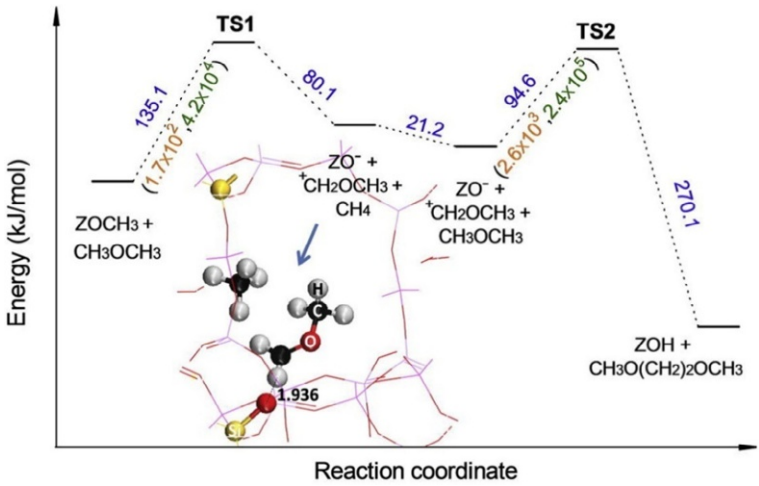

Fig. 11 Route for the formation of the first C—C bond *(57)*.

is proposed as a crucial intermediate. The $CH_3OCH_2^+$ species further couples with another DME or methanol molecule to give 1,2-dimethoxy ethane or 2-methoxyethanol, forming the first C—C bond. Theoretically, it was predicted that the energy barriers of the first and second steps are 135 and 95 kJ mol^{-1}, and the corresponding rate constants at 400°C are 4.2×10^4 and 2.4×10^5 s^{-1}, respectively (Fig. 11) *(57)*. Ethene and propene were also calculated as initial alkene products through the formation of a series of

oxonium cations via methylation, deprotonation, dealkylation, H-transfer, and olefin elimination steps. It should be noted that the direct formation of 1,2-dimethoxy ethane or 2-methoxyethanol from methoxymethyl cations and DME or methanol is still lack of sufficient experimental evidences. Additionally, in the theoretical calculation work of Hu et al. *(58)*, the formation of methoxymethyl carbocation was predicted more energetically favorable via the interaction of SMS and formaldehyde.

Tajima et al. *(59)* proposed the methane–formaldehyde mechanism using theoretical calculations based on the small cluster zeolite model. Methane and formaldehyde were predicted to be formed by the interaction of SMS (H acceptor) and methanol (H donor), and followingly, the interaction of these two surface-formed species would give rise to a surface-adsorbed ethanol and further dehydration to form framework-bound ethoxy species. Although ethene could be quite rapidly formed by ethoxy decomposition, the rate constant for ethanol formation step was theoretically predicted in a range of 1.2×10^{-7}–$7.4 \times 10^{-1}\,s^{-1}$, which indicates the difficulty in converting formaldehyde and methane to C_2 species *(57,60,61)*. In addition, in 2015, Sautet et al. *(62)* showed that the Lewis acidic Al sites on the 110 facet of γ-Al_2O_3 can readily activate DME to yield CH_4, alkenes, and surface formate species according to spectroscopic studies combined with the computational approach. A transient oxonium ion intermediate, generated by the hydrogen transfer between SMS and coordinated methanol on adjacent Al sites, can further react with methane yielding the first carbon–carbon bond or react with one additional DME to form a surface formate species (Fig. 12) *(62)*. This research implied that extra framework Al centers in acidic zeolites might play a key role in the formation of the first carbon–carbon bond during the initial stage of MTH process *(62)*.

Lercher and coworkers *(63)* showed that the decomposition of methanol to form HCHO and CO took place easily even over inert surfaces, such as silicate, Na-ZSM-5, or γ-Al_2O_3. The C atom in MeOH, DME, and HCHO is electrophilic, while the carbon atom in CO is nucleophilic. They postulated that the formation of the first C—C bond was originated from the carbonylation of DME or methanol to form acetic acid and methyl acetates (Fig. 13) *(63)*. Feeding methylal onto H-ZSM-5 zeolite at 400°C led to the detection of trace amount of methyl acetate and acetic acid as primary products, while olefins appeared as secondary products. Furthermore, the olefin formation would be promoted when methanol and CO were co-fed on H-ZSM-5 at increased temperatures (Fig. 14) *(63)*. Thus, either methyl acetate or acetic acid generated from the CO carbonylation reaction was

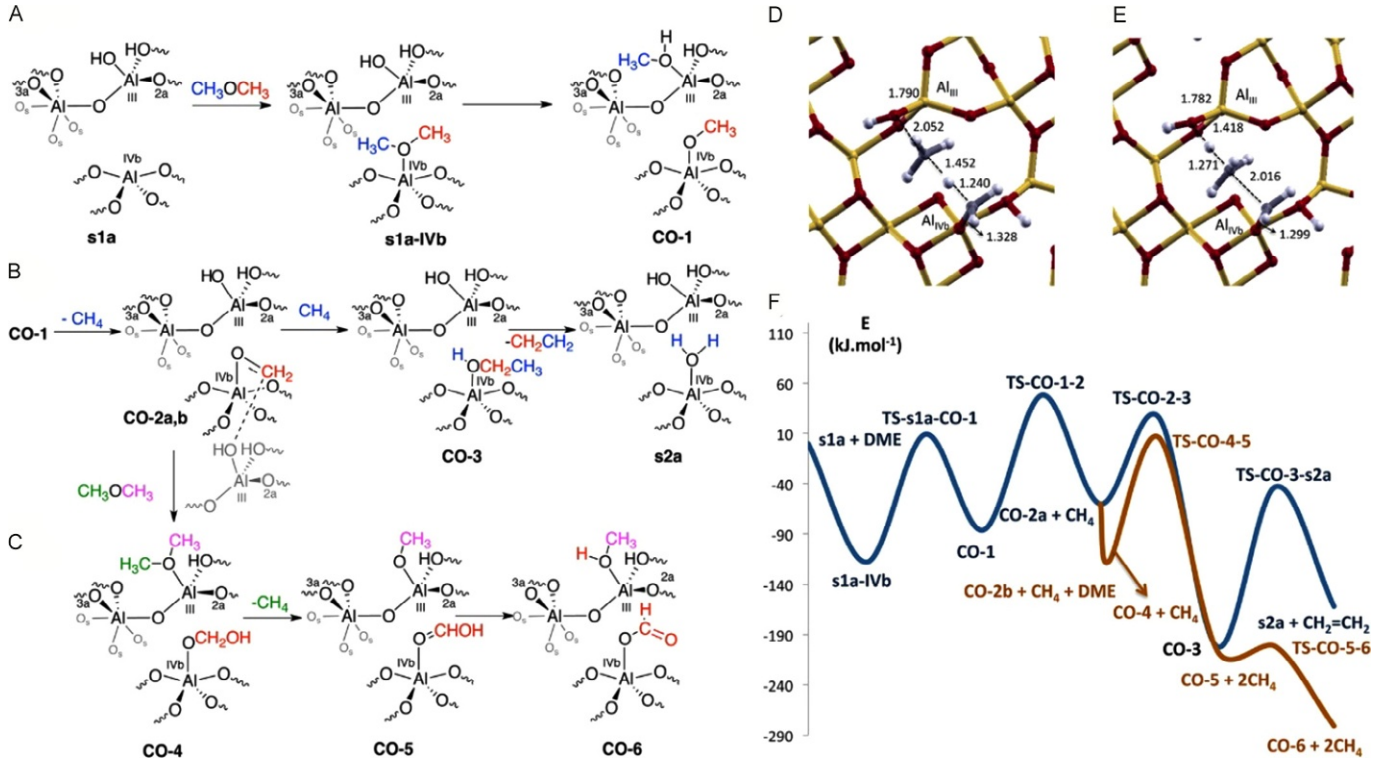

Fig. 12 (A) C–OCH_3 activation process assisted by an OH group of the CH_3OCH_3 molecule on γ-Al_2O_3. (B) Formation of methane and oxonium, carbon–carbon bond formation step (from CO-1 to CO-3) and subsequent ethylene formation along with s2a surface. (C) Formate route from the CO-2 species. (D) Transition state structures corresponding to the formation of methane and oxonium (TS-CO-1-2) and (E) carbon–carbon bond formation steps (TS-CO-2-3). (F) Electronic energy profiles (in kJ mol^{-1}) for the ethylene and formate formation. The energies refer to two CH_3OCH_3 and the γ-Al_2O_3 surface. For the ethylene route (*dark blue*), the second DME molecule is not depicted since it does not participate in the reaction. The formate route is depicted in *brown (62)*.

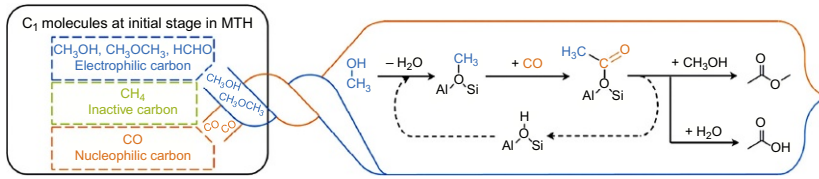

Fig. 13 First C—C bond formation in MTH through coupling between nucleophilic and electrophilic carbon atoms *(63)*.

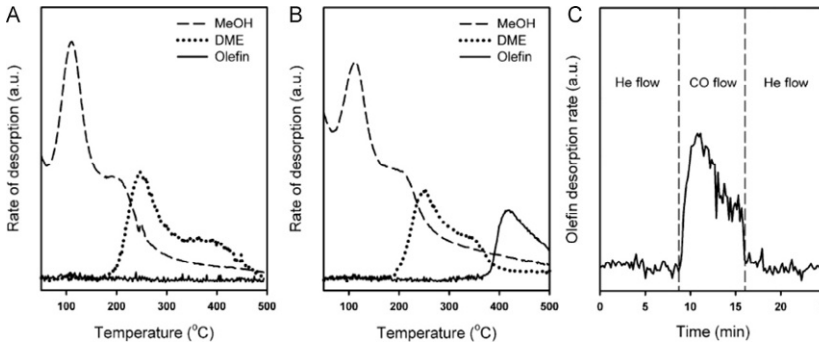

Fig. 14 (A) Temperature-programmed surface reaction of MeOH on H-ZSM-5 under (A) He flow and (B) CO flow. (C) Olefin desorption rate in the surface reaction of MeOH on H-ZSM-5 under alternate He and CO flow at 400°C (conditions: He or CO 25 mL min^{-1}, 25 mg H-ZSM-5, temperature ramping rate 10°C min^{-1}) *(63)*.

thought to be the initially formed important surface intermediates, and a series of acid-catalyzed reactions including acetylation, decarboxylation, aldol condensation, and cracking would occur in sequence and convert these surface species into the initial hydrocarbon pool species as well as the first olefin. This carbonylation-based mechanism has an energy barrier of 80 kJ mol^{-1} for the formation of the first C—C bond, which was significantly lower than the barriers of the earlier proposed mechanisms *(63)*.

The direct mechanism of C—C bond generation by the oxonium ion–ylide pathway was first suggested by Olah and coworkers *(50,64)* in the 1980s, but the significance of trimethyloxonium ions (TMO) was not acknowledged by Haw et al. *(65)*. The direct deprotonation of TMO to form dimethyl oxonium methylide (DOMY) and subsequent methylation to generate an ethyl dimethyl oxonium ion (EDMO), which could further give ethene and DME by way of β-hydride elimination, were theoretically predicted to be too difficult to be realized *(60,61)*. Nevertheless, methylation of DME to form TMO caused a large decrease in the CO stretching

force constant (from 5.22 to 4.05 mdyn $Å^{-1}$) and this also made TMO a potential methylation agent just as SMS *(66)*. Lately, Weckhuysen et al. *(67)* provided ssNMR spectroscopic evidence for the formation of surface acetate and methyl acetate, which gives a good support to the above mentioned carbonylation-based mechanism. Moreover, by the aid of 2D $^{13}C—^{13}C$ ssNMR, the close proximity of surface-adsorbed methanol (52.3 ppm) and SMS (57.7 ppm) was directly observed (Fig. 15) *(67)* and thus the carbene/ylide intermediate was speculated to be formed through the polarization of the C—H bond of SMS by a neighboring oxygen. Surface-ethanolic species could be easily formed by the typical insertion reaction of carbene/ylide from SMS into the sp^3 C—H bond of methanol/DME and undergoes dehydration to form ethylene and regenerates the acid site. Therefore, they proposed the surface species-assisted "direct mechanism" for the formation of the first C—C bond *(67)*.

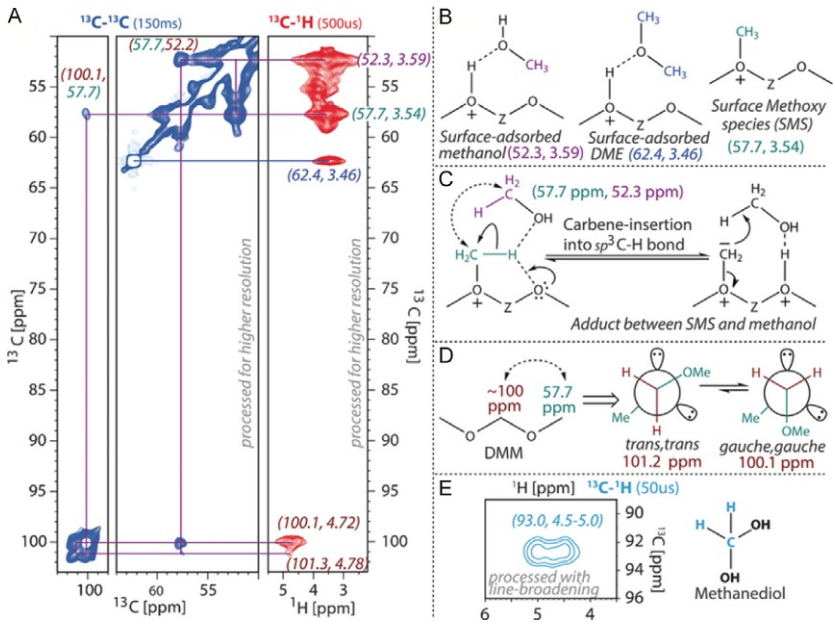

Fig. 15 ssNMR spectra of methanol, methoxy, and acetyl species in H-SAPO-34 after MTO reaction for 30 min at 673 K *(67)*. (A) Zooms from 2D $^{13}C–^{13}C$ (blue) and $^{13}C–^{1}H$ ssNMR spectra with long mixing (150 ms) or CP contact time (500 ms), respectively. (B) NMR assignment of surface species. (C) Identification of a surface adduct between SMS and methanol (normal arrows: electron flows, dotted arrows: $^{13}C–^{13}C$ NMR correlation). (D) Chemical exchange of anomeric conformations of DMM observed in $^{13}C–^{13}C$ spectra. (E) Identification of methanediol in $^{13}C–^{1}H$ spectrum (light blue) with short CP contact time (50 μs).

In an early density functional theory (DFT) calculation study of the first C—C bond in the MTG process, when water was introduced to assist the reaction, SMS-mediated methanol or DME transformation to form adsorbed ethanol and methyl ethyl ether, respectively, was predicted with corresponding activation barriers of 251 and 211 kJ mol^{-1}, indicating the feasibility of the direct pathway for C—C bond formation in terms of the energy *(68)*. In a very recent work by Liu and coauthors *(69)*, accompanied with the detection of the initial formation of ethene product in the effluents, SMS, TMO, and DME/methanol were captured on the catalyst surface by ex situ ssNMR spectroscopy (Fig. 16). More importantly, a new signal at about 70 ppm was directly observed when methanol conversion was detected by in situ ssNMR spectroscopy (Fig. 17) *(69)*. Due to the absence of the signal of the methyl carbon moiety, the possibility of its originating from framework-bound ethoxy was ruled out.

Compared with the result from ex situ ssNMR, it was attributed to methyleneoxy-analogue species originated from activated DME and was also recognized to be the most crucial intermediate for the formation of the first C—C bond. The GIPAW periodic method was employed for the prediction of the ^{13}C chemical shift in the ssNMR spectroscopy. Interestingly, the chemical shift of the carbon atom from DME is theoretically predicted to appear between $\delta = 59.5$ and 71.9 ppm when stretching the bond distance of one of the C—H bonds of DME from 1.108 to 1.309 Å. Based on the experimental evidence and the theoretical calculations, new insights into the formation of the first C—C bond are provided, thus suggesting SMS/TMO-mediated DME/methanol activation over an acid zeolite catalyst and a direct mechanism for C—C bond formation from surface C1 species during the initial stage of the MTH reaction *(69)*. Herein, we summarize the critical steps of the first C—C bond formation in methanol reaction over zeolites proposed in recent years demonstrated in Fig. 18.

Methanol conversion rate is very low in the initial stage, but it rises to 100% abruptly after reacting for a period of time *(70–72)*. This initial stage called "dynamic induction period" is difficult to be explained by any direct mechanism *(73)*. Actually, the direct mechanism of methanol or DME to hydrocarbons operates only at the very initial stage of MTH reaction. Once olefin products are initially formed, methanol conversion will propagate via efficient indirect pathways with the regeneration of olefins or active cyclic organic compounds *(74)*. Therefore, indirect mechanism, with organic species retained inside the catalyst as cocatalysts, was proposed *(75–77)*. At

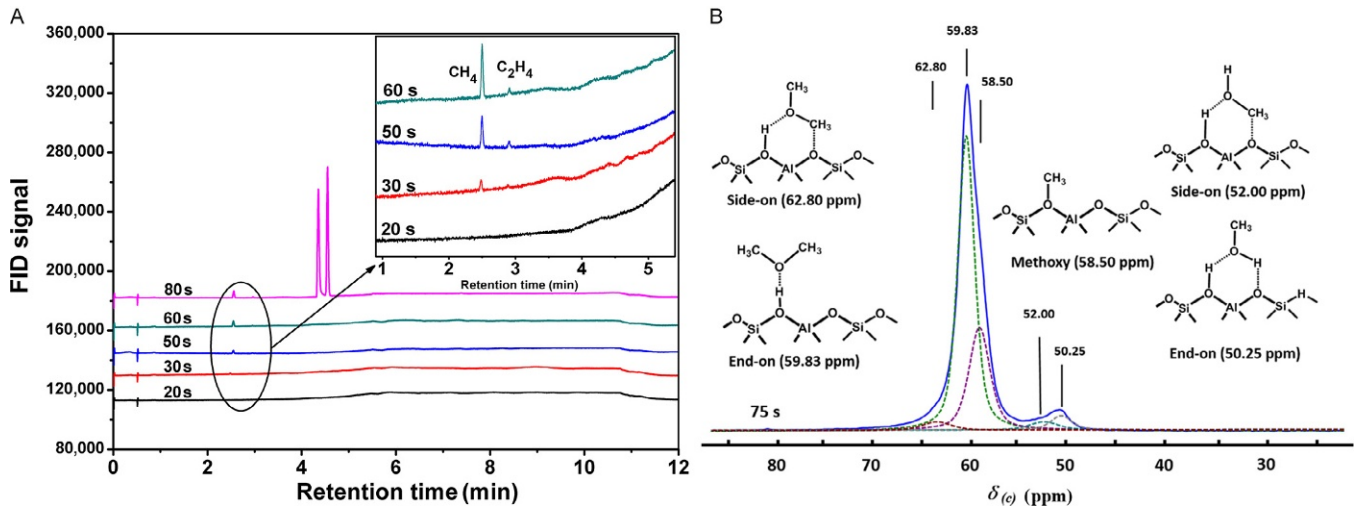

Fig. 16 (A) GC–MS chromatograms of effluent products from the MTH reaction run over the H-ZSM-5 catalyst at 300°C with a methanol weight hourly space velocity (WHSV) of 2.0 h^{-1}. Details within the *circle* are enlarged in the inserted picture. (B) ^{13}C CP/MAS NMR spectrum of reacted H-ZSM-5 after ^{13}C-methanol conversion at 300°C for 75 s *(69)*.

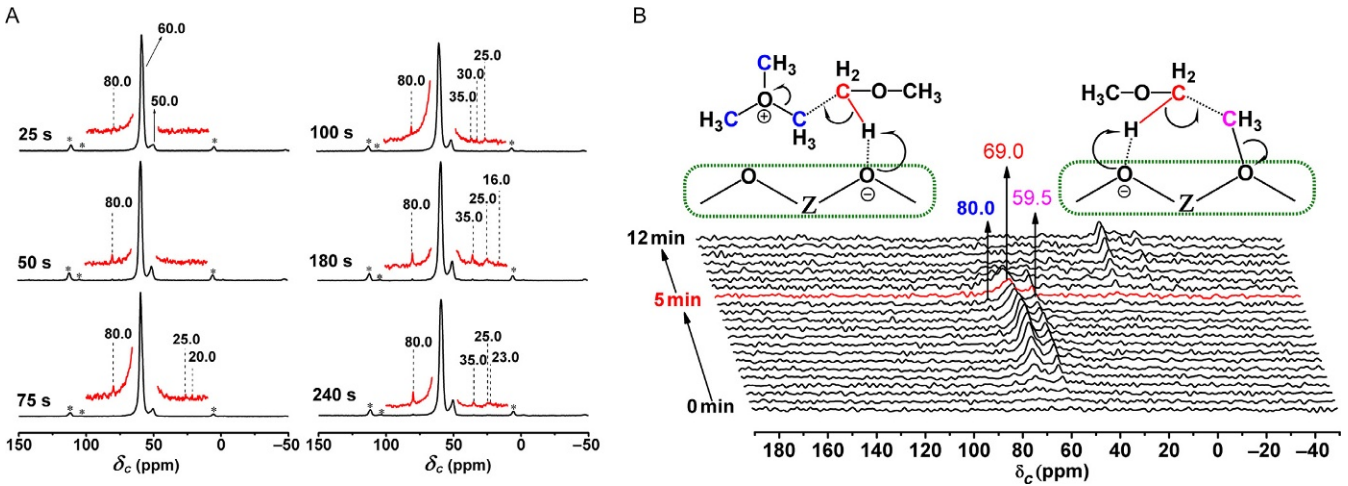

Fig. 17 (A) Ex situ ^{13}C CP/MAS NMR spectra of the H-ZSM-5 catalyst after ^{13}C-methanol conversion at 300°C for 25–240 s. *The spinning band. (B) In situ solid-state ^{13}C MAS NMR spectra recorded during ^{13}C-methanol conversion over H-ZSM-5 at 300°C. The spectra were recorded every 20 s from 0 to 5 min and then every 60 s from 5 to 12 min *(69)*.

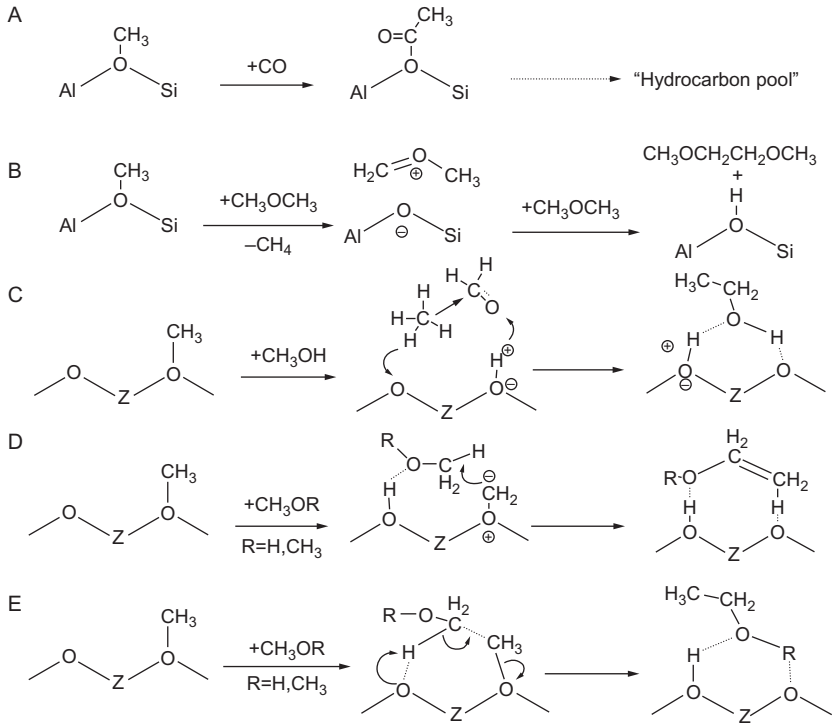

Fig. 18 Direct mechanisms for the conversion of methanol/dimethyl ether to olefins: (A) carbonylation-based mechanism *(63)*; (B) methoxymethyl cation mechanism *(57)*; (C) methane-formaldehyde mechanism *(59)*; (D) carbene insertion mechanism *(67)*; (E) methoxy-mediated DME/methanol activation mechanism *(69)*.

present, it is widely believed that MTO reaction follows an indirect mechanism and some formed hydrocarbon species play an active role during the methanol conversion process *(15,47,75–77)*. These species as active reaction center could be aromatic species *(15,73,78–83)*, olefin species *(84,85)*, or both of them *(86–88)*.

4.2 Autocatalysis Character of Methanol Conversion

In the early 1970s and 1980s, autocatalytic phenomenon in methanol reaction was revealed gradually. By reprocessing the data published by Chang in 1977, Chen and Reagan *(89)* found the S-curve feature of methanol or DME conversion as a function of reaction time. The conversion rate of methanol or DME is very slow at short residence times. However, the

conversion rate rises rapidly as the residence time increases. When processing the methanol conversion reaction over H-ZSM-5 at 643 K, the earlier observation was confirmed. These results indicated that the initial olefin products slowly generate from methanol and the methanol conversion is further accelerated with the increase of hydrocarbon products. Ono and Mori *(52)* studied the methanol conversion reaction over H-ZSM-5 using a closed system at 492 K with a methanol partial pressure of 7.71 kPa. As shown in Fig. 19 *(52)*, during the first 8 h, the main products are DME with trace amount of hydrocarbon compounds; with further prolonging reaction time, the hydrocarbon products exhibit an exponential increment feature, which is the character of autocatalytic reaction. The autocatalysis phenomenon was also observed with the increase of temperature. At 512 K, the reaction products show the similar increasing tendency, but even more rapid increase of hydrocarbon formation occurring at initial 4–5 h. At 531 K, the abrupt change in the olefin yield was observed after 1.5–2.5 h feeding *(52)*. These results indicate that the reaction rate of autocatalytic process is much higher than that of initial olefin production. Therefore, the methanol conversion reaction can be divided into the following two steps:

$$CH_3OH \rightarrow \text{olefins (the first step)}$$

$$\text{Olefins} + CH_3OH \rightarrow \text{olefins (+ paraffins) (the second step, autocatalytic process)}$$

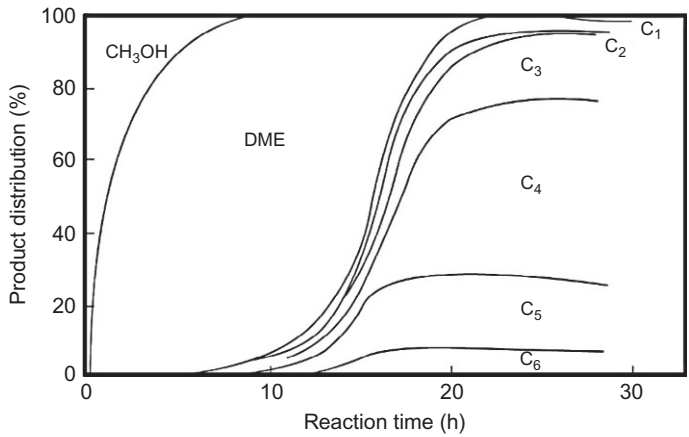

Fig. 19 Product distribution in methanol conversion over H-ZSM-5 at 492 K *(52)*. Methanol initial pressure: 7.71 kPa.

Based on these considerations, Ono et al. *(52)* studied reaction kinetics of autocatalytic reaction. A stands for raw material (i.e., methanol or DME) and B stands for olefin products, the reaction formulas can be simplified as follows:

$$A + A \xrightarrow{k_1} B \tag{1}$$

$$A + B \xrightarrow{k_2} B \tag{2}$$

Supposing that reaction (1) is of second order and reaction (2) is of first order to A and B, if putting x for the conversion of A, the concentration of A, $[A] = A_0(1-x)$, and the concentration of B, $[B] = [B]_0 + [A]_0 x$, where k_1 and k_2 are the rate constants of (1) and (2), respectively, setting $k_1/k_2 = \alpha$ and $[B]_0/[\mathrm{A}]_0 = \beta$, W for the weight of the catalyst, Eq. (3) is obtained

$$\frac{\mathrm{d}x}{\mathrm{d}t} = k_2 W[A]_0(1-x)[(\alpha+\beta) + (1-\alpha)x] \tag{3}$$

Integration of Eq. (3) yields Eq. (4)

$$\ln\frac{\alpha+\beta+(1-\alpha)x}{(\alpha+\beta)(1-x)} = k_2 W[A]_0(1+\beta)t \tag{4}$$

At $t = 0$, initial concentration of olefin B_0 is 0, thus $\beta = 0$ and α is much smaller than 1, and Eq. (4) is reduced to

$$\ln\frac{\alpha+x}{\alpha(1-x)} = k_2 \mathrm{W}[A]_0 t \tag{5}$$

Supposing that reaction (1) is of first order and that initial concentration of olefin B_0 is 0 and $k_1 \ll k_2$, the S-curve of conversion rate vs reaction time can be obtained from Eq. (4).

In early studies, researchers used the reaction of methyl carbenium ion and surface methoxy group to explain initial olefin generation in reaction (1), and regarded reaction (2) as the chain growth reaction of methyl carbenium ion and olefin *(52)*. Since then, the development of the methanol conversion mechanism, especially the proposed indirect mechanism, provided more reasonable and detailed explanation for the autocatalytic process of methanol conversion.

Liu and coworkers *(90)* studied the reaction behaviors during induction period of methanol reaction using kinetic method. Methanol conversion over H-ZSM-5 zeolite has been investigated in a fixed-bed reactor. A prolonged induction period at low reaction temperature favors the

detailed study of the initial period of MTH reaction. The methanol conversion and product distribution at 245°C plotted in Fig. 20 *(90)* as a function of time on stream present for the first time, three different reaction stages, i.e., the initial C—C bond formation stage, the hydrocarbon pool (HCP) species formation stage, and the autocatalysis reaction stage.

Liu's work *(90)* found that in the very beginning of the reaction, only ethene is generated as the effluent product containing a C—C bond, and propene is not detected. It is supposed that some other species containing

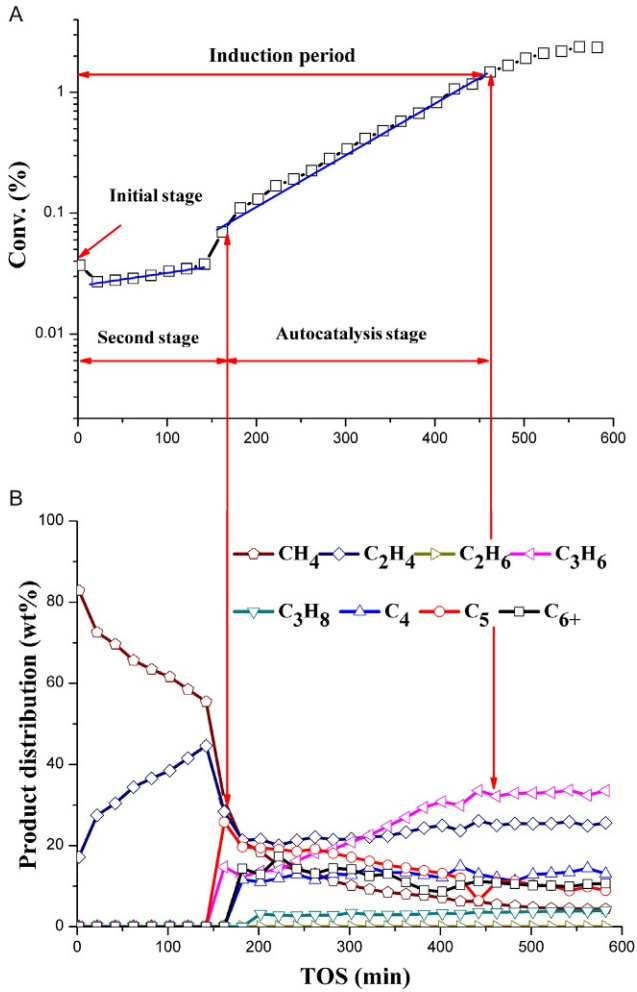

Fig. 20 Conversion of methanol (A) and product distribution (B) as a function of time on zeolite H-ZSM-5 at 245°C *(90)*.

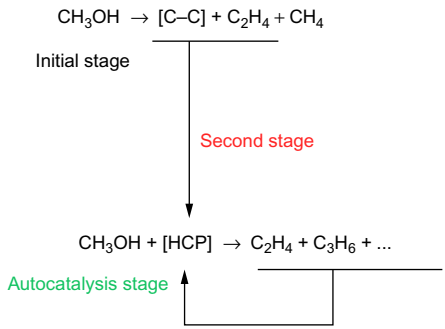

Scheme 1 Three-stage MTH induction reaction mechanism *(90)*.

C—C bond are also generated and adsorbed on the surface of the catalyst, which cannot be detected by GC analysis. As a result, in the second stage, the formation of initial HCP species should be very complicated given the multisteps including ethene methylation, ethene dimerization, ethene reaction with surface organic species, or a combination of these reactions. When the HCP species accumulate to a critical amount, the HCP mechanism will start to work. This leads to an efficient olefin production, in turn speeds up the formation of HCP species, and further accelerates methanol conversion in an autocatalysis way. After the formation of HCP species, the methanol conversion is further enhanced by the aromatics-based and olefins-based indirect pathways. The proposed MTH induction reaction as a kinetic process is shown in Scheme 1 *(90)*.

After the confirmation of the three reaction stages *(90)*, the kinetic parameters as well as the apparent activation energies were also evaluated. Among the three reaction stages, the HCP species formation stage is the rate-controlling step due to the highest energy barrier. A critical value of the concentration of HCP species is proposed to explain the occurrence of the autocatalysis reaction during the third stage. It is suggested that this critical value can be reached via the formation with methanol reaction or co-feeding of HCP species on the catalyst. The kinetic study showed that the co-feeding of ppm amount of benzene, toluene, or *p*-xylene can lower down the activation energies for the second and third stages and in turn shortens the induction period *(90)*.

4.3 Indirect Mechanism of Methanol Conversion

4.3.1 The Proposal of Indirect Mechanism of MTO Reaction

In 1982, for the first time, Dessau et al. *(84,85)* from Mobil Company used ^{13}C-methanol and ^{12}C-olefins or ^{12}C-aromatics co-feeding on H-ZSM-5

to investigate the MTO reaction mechanism. The results of the co-feeding reaction on the H-ZSM-5 catalyst showed that MTO reaction follows an indirect reaction mechanism including the continuous methylation reaction and the cracking reaction (Fig. 21) *(84)*. They thought that once the methanol conversion reaches a stable state, ethene and higher olefins are mainly produced by repeated methylation reactions, oligomerization, and cracking reactions. They proposed an autocatalytic reaction mechanism of methanol conversion which is also suggested by Chen et al. *(89)*, putting forward that the first olefin molecule may be derived from the C—C bond-forming reactions, or come from the impurities of molecular sieve catalyst used in the reaction, feedstock of methanol, or carrier gas. The initial olefin products play an important role in the initiation of the reaction. The actual product forming process begins with the formation of a certain amount of olefins in the reaction induction period, and a single olefin molecule is considered to be sufficient to trigger the MTH reaction. According to the MTH reaction mechanism proposed by Dessau et al. *(84,85)*, ethene is not the initially observed olefin produced from methanol, but is formed by secondary reequilibration of the primary olefin products, propene and butene. At the same time, the aromatic species generated in the MTH reaction, as the secondary products and coke precursors from hydrogen transfer reaction, have no contribution to the formation of olefins, which are mainly produced with olefin methylation–cracking mechanism (Fig. 21) *(84)*.

During this period, Langner *(91)* studied the effect of the co-feeding of high carbon alcohol in the MTO reaction induction period and obtained the evidence of the indirect mechanism of methanol conversion. When a trace of higher alcohols (such as 3.6×10^{-3} mol% cyclohexanol) was added to the

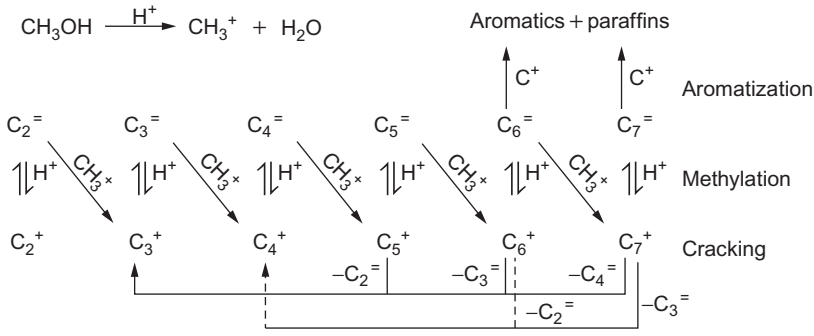

Fig. 21 Olefin methylation–cracking mechanism proposed by Dessau *(84)*.

methanol feed, it was found that the duration of induction period is reduced by 18 times, which is consistent with the mechanism proposed by Dessau *(84)*. Langner *(91)* speculated that cyclic reaction intermediates in the reaction play an important role. He proposed the reaction mechanism with the involvement of multiple methyl-substituted cyclic reaction intermediates and considered that the light olefins formation follows the paring reaction route, involving ring-contraction and ring-expansion reactions of the reaction intermediates, which is first proposed by Sullivan in 1961 *(92)* for explanation of the reaction mechanism of hexamethylbenzene to olefins (especially for the isobutene).

Mole et al. *(93,94)* proposed an indirect reaction mechanism of aromatics-cycle route based on the co-feeding experimental study. They found the cocatalyst function of methylbenzenes in the reaction of co-fed toluene and methanol on H-ZSM-5 catalyst and observed the enhancement of methanol conversion if 1 wt% toluene or xylene was added to methanol feed. In order to explain the cocatalytic effect of toluene observed in the experiment, they proposed the side-chain alkylation mechanism. This proposal is very similar to the hydrocarbon pool mechanism, which is widely accepted at present. The mechanism proposed by Mole et al. *(93,94)* involves an alkyl side-chain formation from the reaction of polymethylbenzenes and methanol and the release of a water molecule. The ethene formation occurs from the alkyl side-chain elimination, generating a methylbenzene molecule with less methyl substitution groups than the initial methylbenzene species at the same time.

4.3.2 Hydrocarbon Pool Mechanism

At the beginning of the 1990s, inspired by the early reaction mechanism of MTO, Dahl and Kolboe *(75–77)* proposed the hydrocarbon pool mechanism of methanol conversion. They carried out the co-feeding reaction of ^{13}C-methanol and ^{12}C-ethene or -propene on SAPO-34 and found that almost all the hydrocarbon products contain ^{13}C atoms and only a small amount of reaction products contains ^{12}C atoms. This means that only a small amount of reaction products comes from ^{12}C-ethene or propene, and most of the reaction products are derived from the active organic species formed methanol itself. The co-feeding of ethene or propene almost has no influence on the conversion of methanol, implying that these olefinic molecules are not reactive. The low olefins reactivity on SAPO-34 prompted Dahl and Kolboe *(75–77)* to propose a hydrocarbon pool mechanism presented in Fig. 22 *(77)*, in which $(CH_2)_n$ represent the hydrocarbon pool

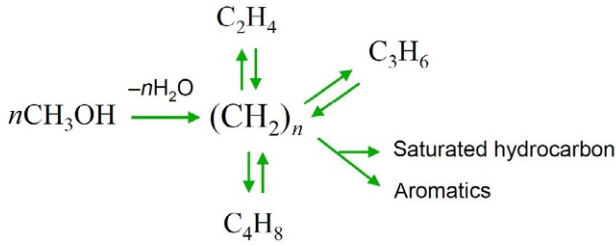

Fig. 22 The hydrocarbon pool mechanism proposed by Dahl and Kolboe *(77)*.

species adsorbed in the molecular sieve catalyst and are active intermediates for olefin formation. The presence of these hydrocarbon pool species in the catalyst plays the role as a cocatalyst in the process of methanol conversion to olefins. These hydrocarbon species go through successive methylation reactions and subsequent elimination of side chain to produce light olefins, which enables the hydrocarbon pool species to be regenerated for the completion of the catalytic cycle *(77)*.

At the initial stage of the reaction, methanol reaction first forms active hydrocarbon pool species in molecular sieve catalyst, and then the methanol conversion increases gradually and the reaction goes into the steady-state stage. Methanol reacts with the active hydrocarbon pool species to produce light olefins, such as ethene, propene, and butene, and then these olefins are further transformed by condensation, alkylation, cyclization, and hydrogen transfer reactions to produce higher olefins, alkanes, and aromatic hydrocarbons. These reactions are generally referred to as the secondary reactions. The two core questions of hydrocarbon pool mechanism are "what are hydrocarbon pool species composed of?" and "how do methanol react with hydrocarbon pool species to produce light olefins?" Many research work have been made on the catalysts with different topological structures to attempt to answer these two questions after the hydrocarbon pool mechanism was put forward.

4.3.2.1 Identification of Hydrocarbon Pool Species

The hydrocarbon pool species are important active organic intermediates in the MTO reaction. It is important to study the nature and the function of hydrocarbon pool species in the production of the olefin products for the deep understanding of the MTO reaction mechanism. The experiment results reported by Dahl and Kolboe *(75–77)* indicated the nonactivity feature of ethene and propene on H-SAPO-34 catalysts and suggested the participation of aromatic compounds in the reaction of methanol.

Moreover, in the 1980s, Mole *(93,94)* reported that methanol conversion had been greatly improved for the MTO reaction with adding a small amount of aromatic hydrocarbons, such as toluene and xylene. These results prompted many research groups to confirm the hypothesis that aromatic compounds are the main components of hydrocarbon pool species and resultantly a series of progresses have been obtained.

Mikkelsen et al. *(80)* performed the co-feeding reaction of ^{13}C-methanol and ^{12}C-benzene or toluene on H-ZSM-5, H-mordenite, and H-beta zeolite catalysts. The results showed that the products of ethene and propene contain 50%–75% ^{13}C atoms, while the ^{13}C isotopic distribution of the polymethylbenzenes is in disorder. This demonstrates that polymethylbenzenes do participate in the reaction of olefin formation and that the active species in H-beta is mainly hexamethylbenzene (HMB), while for H-ZSM-5 and H-mordenite zeolites tri/tetramethylbenzenes and pentamethylbenzene function as active HCP species. The work by Song et al. *(82)* using solid nuclear magnetic resonance spectroscopy confirmed that methylbenzenes are the reactive center of MTO reaction in SAPO-34, and revealed the relationship between the presence of methylbenzenes in SAPO-34 cage and the formation of olefins. Besides, Arstad and Kolboe *(79)* analyzed the reaction activity of the organic species after the short time reaction in the SAPO-34, and further confirmed that the main components of the reaction active center of SAPO-34 are methylbenzenes. Sassi et al. *(95)* performed the reaction of polymethylbenzenes on H-beta zeolite with the 12-membered ring channel, and the results showed a high activity for the production of olefins. The yield of olefins and selectivity of propylene were improved with the increase of the numbers of methyl-substituted groups on the benzene ring, even if feeding hexamethylbenzene alone can produce light olefins.

From 1998, by the aid of pulse-quench reaction technique and solid-state NMR spectroscopy (ssNMR), Haw and coworkers *(83,96–99)* have studied the mechanism of hydrocarbon pool and made some important progresses. They confirmed that 1,3-dimethylcyclopentenyl (diMCP$^+$) is formed in the H-ZSM-5 zeolite catalyst *(97)*. Further work on SAPO-34 molecular sieve and H-beta zeolite catalysts demonstrated the existence of other cyclic carbenium ions, such as pentamethylcyclopentenyl (pentaMCP$^+$) and heptamethylbenzenium (heptaMB$^+$) *(83,98)*, and these cyclic carbenium ions and methylbenzenes play an important role in the hydrocarbon pool mechanism as the important intermediates *(73,95,97,100)*.

The interaction between the hydrocarbon pool species and the molecular sieve catalyst is of great importance in the MTO reaction.

Haw et al. *(73,81)* proposed the concept of supramolecular catalyst in the MTO reaction. They considered that the properties of molecular sieve (composition, framework structure, and acid strength) and the specific properties of hydrocarbon pool species located in the molecular sieve catalyst determine the unique activity of the supramolecular catalyst. The concept of supramolecular is shown in Fig. 23 *(73)*. The organic methylbenzene molecules and the occupied inorganic SAPO-34 nanocage are regarded as a supramolecular system. Haw and Marcus *(73)* found that the ethene and propene selectivity are related to the number of methyl groups (Me_{ave}) on benzene rings of methylbenzenes trapped in the nanocages of H-SAPO-34. By correlating the Me_{ave} and the volatile product distribution, they found that propene formation is favored by the intermediate of methylbenzenes with four to six methyl groups, but ethene is predominantly formed over the catalyst with methylbenzenes with two or three methyl groups. And they also found that the increase of Me_{ave} will improve the reaction activity. For example, hexamethylbenzene, which is conducive to the formation of propene, is more active than trimethylbenzene, which is beneficial to the formation of ethene. Song et al. *(101)* pointed out that in addition to the methylbenzenes, methylnaphthalene is also active hydrocarbon pool species, and high ethene selectivity is attained when methylnaphthalene is present as the confined organic species.

Based on the experimental studies, researchers confirmed that methylbenzene, methylcyclopentadiene, and their corresponding carbenium ions are the active hydrocarbon pool species *(78,82,102)*. By the aid of ssNMR, some carbenium ions have been identified as intermediates confined within zeolite or SAPO catalysts, such as the cations 1,3-dimethylcyclopentadienyl, indanyl, and 1,1,2,4,6-pentamethylbenzenium within H-ZSM-5; $heptaMB^+$

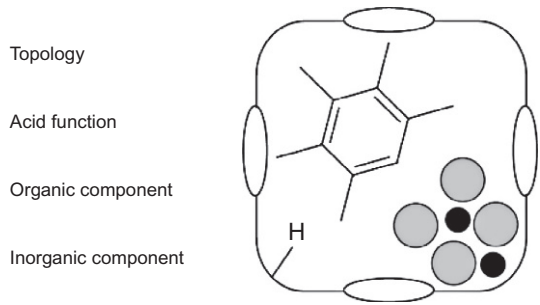

Fig. 23 Schematic of a single cage in a zeolite supramolecule catalyst for MTO conversion *(73)*.

within H-beta and heptamethylcyclopentenyl (heptaCP$^+$) within SAPO-34 *(83,97–99,103)*. Wang et al. also observed several larger alkyl-substituted cyclopentenyl cations in the MTH reaction on ZSM-5 *(104–107)*.

However, the formation of most of these carbenium ions during methanol conversion was proved via an indirect way. Up to present, it has been found that the carbenium ions of the hydrocarbon pool species include two categories, i.e., methylcyclopentenyl cations and methylbenzenium cations (Table 1). The structure of these carbenium ions is closely related to the structure of molecular sieve catalysts. The confinement effect of the chemical environment of catalyst on the size or structure of the active intermediates is an important characteristic of zeolite-catalyzed MTO reaction *(108–115)*. Moreover, the direct observation of such HCP species and their roles in methanol conversion over zeolites or SAPO catalysts under real working conditions is still a huge challenge.

HeptaMB$^+$ cation is of particular importance as a reaction intermediate in MTO reaction *(15,116)* and its direct capture and identification has been made by the co-reaction of benzene and methanol over H-beta, H-MCM-22, and H-mordenite *(81,117,118)*. However, over the molecular sieve catalysts with narrow eight-membered ring pore opening, such as SAPO-34, the co-reaction of benzene and methanol is unfeasible because of the diffusion limitations. In order to fully understand the catalytic process of MTO and to reveal the energetically feasible mechanism of hydrocarbon pool reaction route, it is very important to realize the direct observation of the carbenium ions under the real MTO reaction condition. Difficulties in the direct observation of heptaMB$^+$ formed in the nanocage of SAPO-34 seem to be related to the very high reactivity of heptaMB$^+$ and the relatively weak acidity of SAPO catalysts compared to liquid acids or zeolites. A catalyst with a particular structure and/or a strong acidic environment might be required to accommodate and stabilize this bulky carbenium cation. A breakthrough of heptaMB$^+$ observation was made in 2012 by Liu and coworkers using a newly synthesized catalyst DNL-6 *(108,119)*, an eight-membered ring SAPO molecular sieve with the RHO structure possessing large α cavity, and relatively high acid concentration and strength, which can accommodate and stabilize the bulky carbenium cations. For the first time, heptaMB$^+$ was directly captured over DNL-6 by ssNMR during methanol conversion under real working conditions (Fig. 24) *(74)*, and this observation was consolidated by the capture of its deprotonated form of 1,2,3,3,4,5-hexamethyl-6-methylene-1,4-cyclohexadiene (HMMC) in the catalyst with GC–MS measurement *(108)*. This is the first time for the direct

Table 1 The Series of Carbenium Ions Observed in Zeolites With Solid-State NMR Spectroscopy During Methanol Conversion Reaction

Carbenium Ions	Reaction and Catalyst
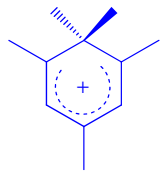 1,1,2,4,6-Pentamethylbenzenium cation	Methanol + benzene, H-ZSM-5 *(99)* Methanol, H-ZSM-5 *(104)*
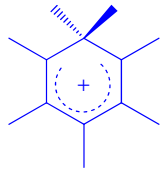 Heptamethylbenzenium cation	Methanol + benzene, H-Beta *(83)* Methanol, DNL-6 *(108)* or H-SSZ-13 *(74)*
 1,3-Dimethylcyclopentenyl cation	Methanol, H-ZSM-5 *(97)*
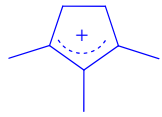 1,2,3-Trimethylcyclopentenyl cation	Methanol, H-ZSM-5 *(104)*
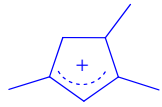 1,3,4-Trimethylcyclopentenyl cation	Methanol, H-ZSM-5 *(104)*
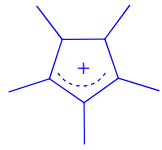 1,2,3,4,5-Pentamethylcyclopentenyl cation	Methanol, H-SSZ-13 *(74)* or SAPO-34 *(109)*

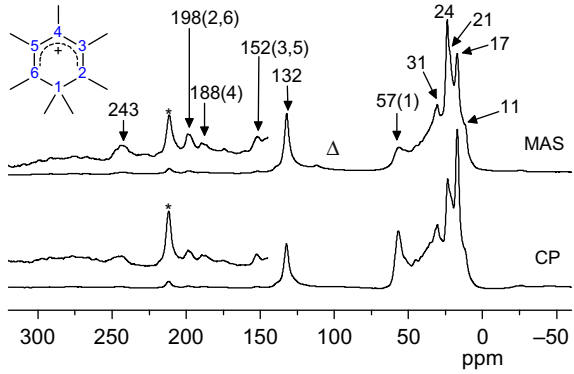

Fig. 24 ^{13}C MAS and CP/MAS NMR spectra of the DNL-6 catalyst after ^{13}C-methanol conversion at 275°C for ~50 min *(74)*. *The spinning sideband and Δ the background.

observation and confirmation of the very important carbenium ions in an eight-membered ring small pore molecular sieve during methanol conversion under real reaction condition.

In a more detailed work, the ^{12}C/^{13}C-methanol switch experiments confirmed the higher reactivity of polymethylbenzenes than that of methylbenzenes with less methyl group substitutions, implying the important role of these intermediates in the olefin formation *(108,120)*. Liu's group succeeded in observing the simultaneous formation of heptaMB$^+$ cation and pentaMCP$^+$ cation under the real working conditions of methanol conversion over the catalyst with CHA topology *(74)*, which makes it possible to elucidate the reaction mechanism over the industrial DMTO catalyst. The results of experimental study and theoretical calculation showed that the detection of the carbenium ions depends on the acid-catalytic environment and the reactivity of these ions during the catalytic transformation. PentaMCP$^+$ is more facile to be observed than heptaMB$^+$ in the CHA nanocage owing to the higher activation energy required for its further transformation. ^{13}C MAS NMR measurements and isotopic switch experiment provided substantial proofs that both pentaMCP$^+$ and heptaMB$^+$ are important intermediates for the MTO reaction *(74)*. Recently, Liu's group systemically investigated batch-like and continuous-flow methanol conversions over H-beta zeolites with ^{13}C MAS NMR spectroscopy *(121)*. The important reaction intermediates, heptaMB$^+$ and methylcyclopentenyl (MCP$^+$) cations, have been directly observed during methanol conversion by the aid of ssNMR technique. Brönsted acid sites of H-beta zeolite

catalysts play an important role in carbenium ion formation and observation. It was found that the competitive adsorption of reactants and products on the catalyst surface may cause the deprotonation of the carbenium ions. In the continuous-flow reactions, both the heptaMB$^+$ and MCP$^+$ cations are formed and more easily observed compared with batch-like reactions due to the improved methanol conversion and the reduced competitive adsorption on the Brönsted acid sites.

4.3.2.2 Origin of Hydrocarbon Pool Species

How the hydrocarbon pool species are generated has been a puzzle for researchers. With the application of a stopped-flow protocol, pure surface methoxy groups [SiO(CH_3)Al] were prepared by Wang et al. *(72)* on various acidic zeolite catalysts (H-Y, H-ZSM-5, H-SAPO-34) at temperatures lower than 473 K, and the further co-reactions of these SMS with toluene and cyclohexane molecules showed the high reactivity of SMS by in situ ^{13}C MAS NMR spectroscopy. The conversion of pure methoxy groups alone to aliphatics and aromatics was observed at temperatures of $\geq$523 K. These findings indicate that SMSs are important for the initial C—C bond formation in the kinetic induction period of MTO process. However, Haw et al. *(122)* performed a very careful experimental using highly purified reagents, carrier gas, and catalysts, which shows that methanol/DME is not reactive on either of the two most important catalysts of H-ZSM-5 and H-SAPO-34 in the absence of the primordial hydrocarbon pool species. They believed that the rate of the direct C—C coupling reaction is so slow as to be eclipsed by even trace impurities in the methanol feed, the catalyst, or the carrier gas. Therefore, the direct C—C bond coupling reaction may never happen, and hydrocarbon pool species are derived from the reaction of carbon impurities from ordinary methanol and/or catalyst. These results are in contradiction with the experimental results of Jiang et al. *(123)*; they believed that the trace organic impurities in methanol do not affect the formation of the initial hydrocarbon species by SMS. Vandichel et al. *(124)* proposed a theoretically feasible reaction path to explain the formation of cyclic hydrocarbon pool species in the H-ZSM-5 channel starting from light olefins. In recent years, several work report the progress on the study of initial olefin generation of methanol conversion over SAPO or zeolite catalysts. Experimental and theoretical studies confirm the feasibility of the reaction mode of initial C—C bond generation. Starting from the initially generated olefin hydrocarbon, important cyclic organic species, including the important five-membered

ring and six-membered ring carbenium ion, can be formed and work as the hydrocarbon pool species for the assembly of the C—C bond in the following reaction period with a more efficient indirect pathway.

4.3.2.3 Reaction Pathway of Olefins Formation Following Hydrocarbon Pool Mechanism

At present, one of the widely recognized hydrocarbon pool reaction mechanisms for MTO reaction is an aromatics-based cycle, including methylation reaction of methylbenzene and subsequent elimination reaction to produce olefins, but the detailed step for the production of olefins has been the focus of debate. In order to explain the methanol reaction to olefins through the aromatics-based cycle, the researchers proposed two kinds of olefin formation pathways including paring mechanism and side-chain methylation mechanism. The schematic diagram of two reaction paths is shown in Fig. 25 *(125)*. Both catalytic cycles include the formation of heptaMB$^+$ by methylation of HMB as the initial step. The paring mechanism was first proposed by Sullivan et al. *(92)*, and it can be considered as a reaction route with repeated ring contraction and expansion. Specifically, the paring route involves the rearrangement reaction of hexa- or heptamethylbenzenium cations to produce an alkyl-substituted five-membered ring species; then the five-membered ring species directly undergo an elimination reaction

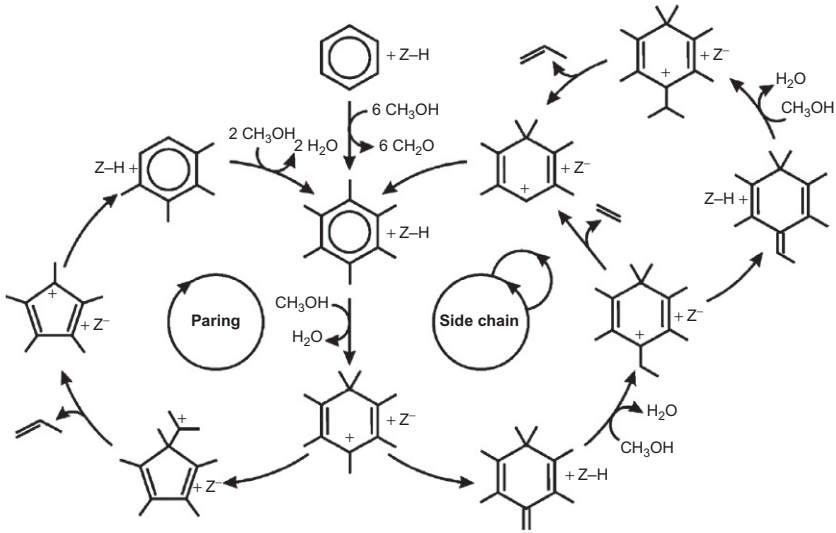

Fig. 25 The paring and side-chain reaction concepts in MTO catalysis *(125)*.

to produce propene or undergo a further rearrangement reaction following an elimination step for the production of isobutene. After this contraction step, the five-membered ring intermediate is expanded back to the original six-membered ring intermediate (left side of Fig. 25) *(125)*. Mole et al. *(93,94)* proposed the side-chain alkylation mechanism in the study of the role of aromatic species on ZSM-5 zeolite-catalyzed methanol reaction, and then Haw et al. *(95,126)* carried out a more detailed study. This reaction cycle goes through the steps of carbenium ion deprotonation to form an exocyclic double bond and successive side-chain methylation to form olefin products. In the side-chain mechanism, the polymethylbenzenes first successively undergo a *gem*-methylation (just as in the paring mechanism) to form a methylbenzenium ion, followed by a deprotonation step to form an intermediate with exocyclic double bond, which can work as the starting material for side-chain methylation rather than ring methylation, after elimination of ethene and propene, the original hydrocarbon pool species can be regenerated. More specifically, the deprotonation of heptaMB$^+$ yields the neutral species HMMC. In the next step of methylation of HMMC, one or two methanol molecules attack the exocyclic double bond of HMMC to form a side ethyl group or an isopropyl group, respectively. Then the side-chain groups will be eliminated to produce ethene or propene (right side of Fig. 25) *(125)*. Both mechanisms go through repeated methylation until the formation of ethyl-, propyl-, or isobutyl-substituted cyclic organic species.

The remarkable difference between the paring and the side-chain alkylation mechanism is that with regard to the paring mechanism the ring carbon atoms participate to form alkyl side chains, while the side-chain alkylation mechanism keeps the structure of the aromatic ring. Bjørgen et al. *(118)* and Sassi et al. *(95)* thoroughly investigated the differences of these two mechanisms. They perform a lot of isotope labeling and co-feeding reactions to reveal the dealkylation reaction mechanism on H-beta zeolite. Bjørgen et al. *(118)* found that if the reaction temperature is lower than 300°C, a lot of propene and isobutane molecules are generated (isobutane is considered from hydrogen transfer reaction of isobutene) containing carbon atoms of benzene ring from the paring reaction pathway, while Sassi et al. *(95)* found that under the high-temperature (350–450°C) reaction conditions, the side-chain alkylation mechanism is the main reaction pathway to produce olefins.

The key intermediate in the side-chain alkylation mechanism distinguished from the paring mechanism is the simultaneous formation of

polymethylbenzene containing with the ethyl, propyl, or other alkyl groups. Haw et al. *(95)* studied co-reaction of ^{13}C-methanol and ^{12}C-ethylbenzene and ^{12}C-cumene on H-beta zeolite at 350°C, and the reaction results showed that the reaction of these species can generate large amounts of ethene and propene. Ethylbenzene (alone) was almost unreactive on H-beta at 350°C, when the reaction of cumene on H-beta can generate propene. And in the presence of methanol, the activity of elimination to generate olefins from ethylbenzene and cumene was enhanced largely *(95)*. The reactions of butylbenzene isomers on H-beta at 350°C without methanol participation were also performed, and the results showed that the reaction activity of these molecules eliminating to form butenes is related to the structure of the alkyl chain; *tert*-butylbenzene is the most reactive with 96% conversion, *sec*-butylbenzene was slightly less reactive with 87% conversion, and isobutylbenzene and *n*-butylbenzene were much less active, with conversions of 13% and 11%, respectively *(126)*. The above results indicate that the side-chain alkylation mechanism is a feasible pathway to produce olefins.

In the work of Liu and coworkers, the reaction mechanism of methanol conversion over eight-membered ring and cage structure catalysts was studied using a newly synthesized SAPO catalyst, DNL-6, and the differences between side-chain methylation route and paring route were recognized based on the observation of the intermediates of aromatic carbenium ions and the ^{12}C/^{13}C-methanol switch experiments *(108)*. The very important intermediate of heptaMB$^+$ was observed and the analysis of the mass spectra of HMB and HMMC (the deprotonated form of heptaMB$^+$) after isotope switch experiments was used to determine the specific reaction pathway of hydrocarbon pool mechanism for the formation of olefins.

In the mass spectra of HMB and HMMC after isotope switch experiments (Fig. 26) *(108)*, one notable observation is that the number of ^{13}C atoms incorporated into HMB or HMMC is less than that of the substituted methyl groups (6 or 7). The most incorporated ^{13}C atoms are exactly the total count of methyl groups in the molecules. The other notable observation is that the M/Z gap between molecular ions of HMB (or HMMC) and the molecular ions with one methyl group lost is 16, indicating the location of all six ^{13}C atoms of hexamethylbenzene (or seven ^{13}C atoms of HMMC) in the methyl groups rather than in the benzene ring. These two observations prove the feasibility of methanol conversion via side-chain methylation mechanism, which involves a key step of methylation of hexaMB to form heptaMB$^+$ for further methylation and elimination to generate olefin products (Fig. 27) *(120)*.

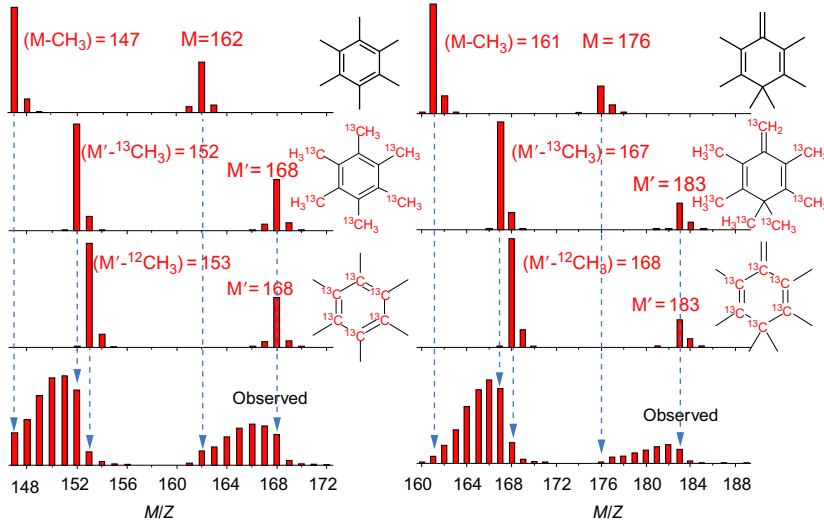

Fig. 26 Comparison of mass spectra of HMB (*left*) and HMMC (*right*) obtained in the isotopic switch experiments over DNL-6 (9 μL of ^{13}C-methanol injection after continuous-flow ^{12}C-methanol conversion for 60 min at 275°C, WHSV of MeOH = 2.0 h^{-1}, He/MeOH (in mol) = 3) with the mass spectra of ^{12}C-HMB and HMMC (M) and simulated mass spectra of ^{13}C-labeled HMB and HMMC (M′) *(108)*.

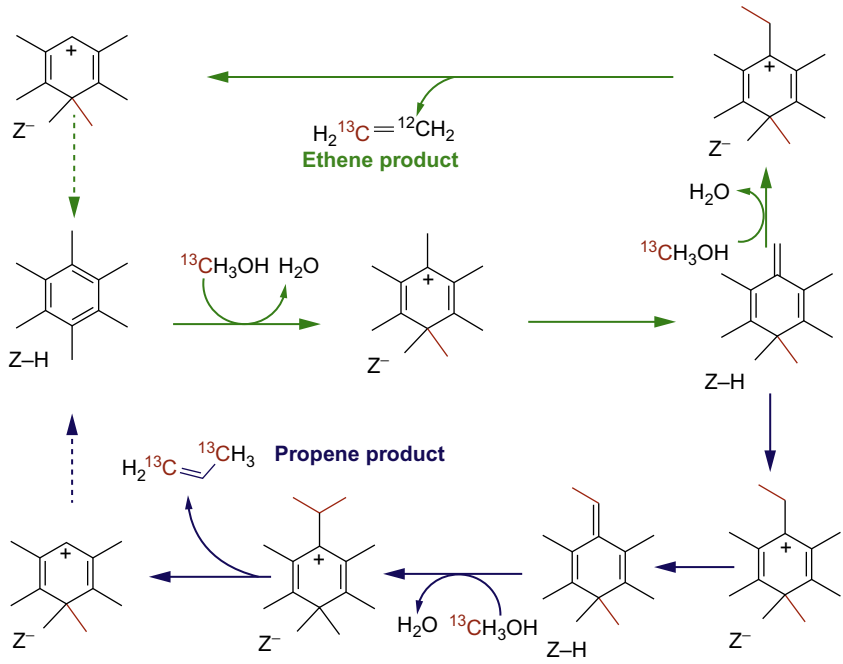

Fig. 27 Side-chain methylation mechanism for olefin generation over DNL-6 *(120)*.

Kolboe and coworkers *(118,127)* conducted the co-reaction of benzene and ^{13}C-methanol over H-beta at a relatively low reaction temperature and concluded that the paring reaction mechanism is the major reaction route for olefin formation. Then, the extended studies of the reaction over H-MCM-22 and H-mordenite drew similar conclusions *(117)*. Erichsen et al. *(162,163)* performed the isotope labeling experiments on H-SSZ-24 (AFI) zeolite and SAPO-5 (AFI) with the same topological structure at low temperature. They also gave the similar conclusion that the formation of olefins with aromatic species as the reaction intermediates over the two catalysts mainly follows the paring mechanism. It was also observed that a carbon atom from a benzene ring enters into the olefin product on both of the catalysts, indicating that the dealkylation reaction of methylbenzene in the catalytic cycle contains a ring-expansion or a ring-contraction reaction step. But whether side-chain alkylation mechanism becomes more and more important at higher temperature is still a problem yet to be studied. Some exchange of carbon atoms still exists even no occurrence of dealkylation reaction, which leads to the scrambling of the carbon atoms between benzene ring and exocyclic methyl groups *(95,118)*. Moreover, the olefins may be produced from the alkene cycle parallel to the aromatic cycle, and therefore, it is sometimes very difficult to analyze the data of isotope labeling experiment under a typical MTO reaction conditions.

4.3.2.4 Theoretical Studies of the Paring and Side-Chain Alkylation Mechanisms

Great efforts have been devoted to the studies of paring and side-chain alkylation mechanisms by theoretical calculation; however, the comparative study of two reaction mechanisms over the same catalyst has been less provided. McCann et al. *(128)* and Lesthaeghe et al. *(125)* theoretically studied the paring and side-chain route over H-ZSM-5 for the formations of different products (isobutene and ethene). The work of McCann et al. *(128)* demonstrated the rationality of the formation of isobutene through paring mechanism on H-ZSM-5, which does not contain the bottleneck step. Lesthaeghe et al. *(125)* proposed that *ortho*-xylene can convert to the ethyl side chain by methylation and finally the ethene elimination needs to overcome a high energy barrier of 200 kJ mol^{-1}. Subsequently, Kolboe et al. *(129–131)* found that the existence of a stable π-electron complex between an alkyl side chain and a benzene ring can greatly decrease the energy barriers of splitting off the alkyl groups. Based on this stable structure, Wispelaere

et al. *(132)* proposed a low-barrier catalytic cycle for ethene and propene formation, and the energy barriers of all the reaction steps are lower than 100 kJ mol^{-1}.

McCann et al. *(128)* first established a complete catalytic cycle (Fig. 28) for MTO conversion over H-ZSM-5 in combination of theoretical and experimental studies. Starting from toluene, 1,1,2,4,6-pentamethylbenzenium and 1,3-dimethylcyclopentadienyl observed previously were considered as reactive intermediates, and the complete catalytic cycle of paring route was established to rationalize the formation of isobutene on H-ZSM-5. Toluene methylation is the rate-determining step in the paring cycle. It is noteworthy that the paring route is started from the methylbenzene with less methyl groups, which is consistent with the result that the methylbenzenes with less methyl groups have higher reactivity for MTO conversion over H-ZSM-5 *(88,133–135)*. Furthermore, the theoretical calculation demonstrated the importance of transition-state shape selectivity for the conversion of methanol to light olefins, and the space of the intersecting channel in H-ZSM-5 limits the formation of the transition-state species for methylation of durene *(136)*. As so far, theoretical calculations are still lack of precise simulation for zeolite framework, and aromatic-based reaction cycle for hydrocarbon pool mechanism could not fully explain the product distribution observed on H-ZSM-5. Therefore, it is necessary to study the reaction mechanisms of product generation on H-ZSM-5 at large.

It is essential to understand the formation mechanisms of light olefins for regulating the selectivity of ethene and propene. In order to confirm the main reaction route of methanol to olefins, Liu and colleagues explored the MTO reaction on H-SSZ-13 under the real working conditions of methanol conversion *(74)*. Based on the direct observation of five-membered ring cation (pentaMCP$^+$) and six-membered cation (heptaMB$^+$), the main reaction routes were theoretically predicted according to the two cyclic carbenium ions considered as the important intermediates in the MTO reaction. Fig. 29 provides the catalytic cycles and activation energies of the paring and side-chain reaction mechanisms for the MTO conversion on H-SSZ-13 zeolite with the involvement of pentaMCP$^+$ and heptaMB$^+$ *(74)*. For the two catalytic cycles, the elimination of propene, with activation energies of 36.66 and 26.65 kcal mol^{-1}, is the rate-determining step for the paring and the side-chain methylation mechanisms. In the reaction systems with competitive reaction routes, the reaction usually follows the pathway with low activation energy, so the side-chain methylation mechanism may be more dominant in the MTO reaction over H-SSZ-13 zeolite. But noticeably,

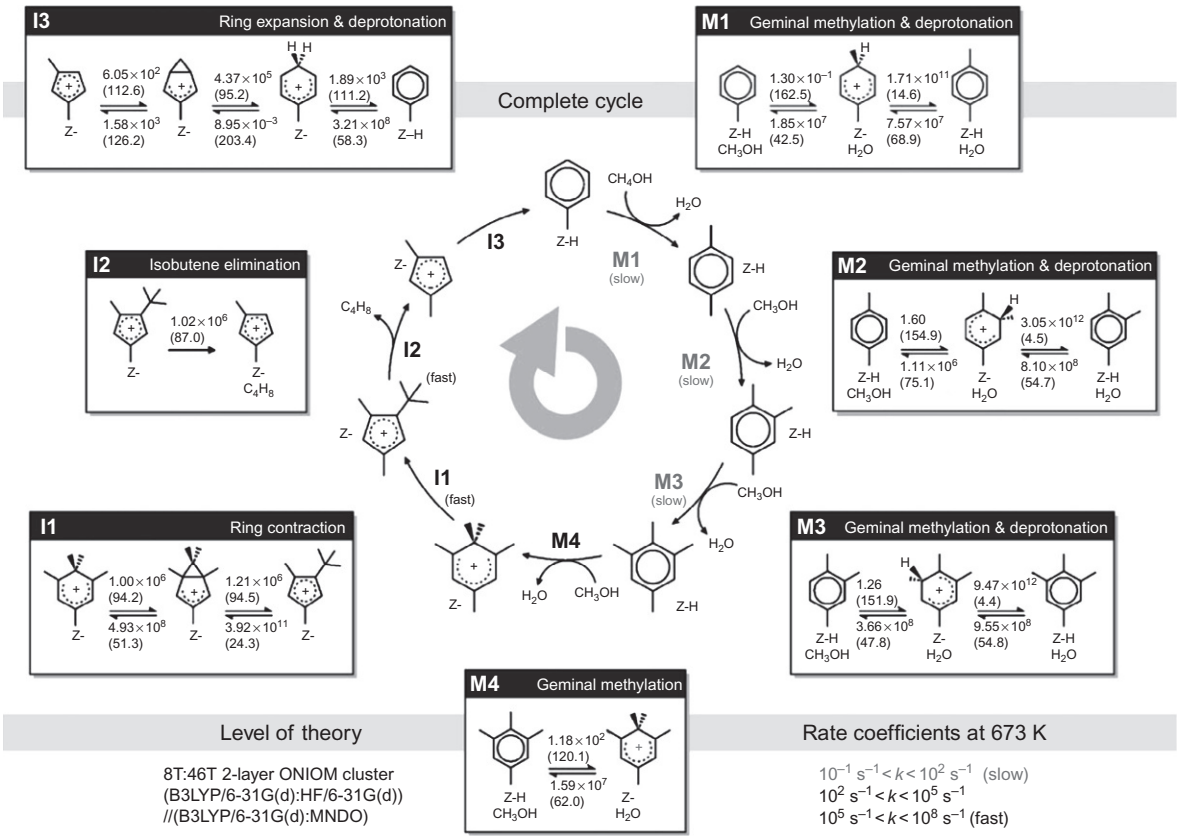

Fig. 28 Full catalytic cycle for isobutene formation from methanol through a combined methylbenzene/cyclopentenyl cation pool in H-ZSM-5 *(128)*. Calculated rate constants at 673 K are given in s^{-1} and reaction barriers at 0 K (in brackets) are given in kJ mol^{-1}.

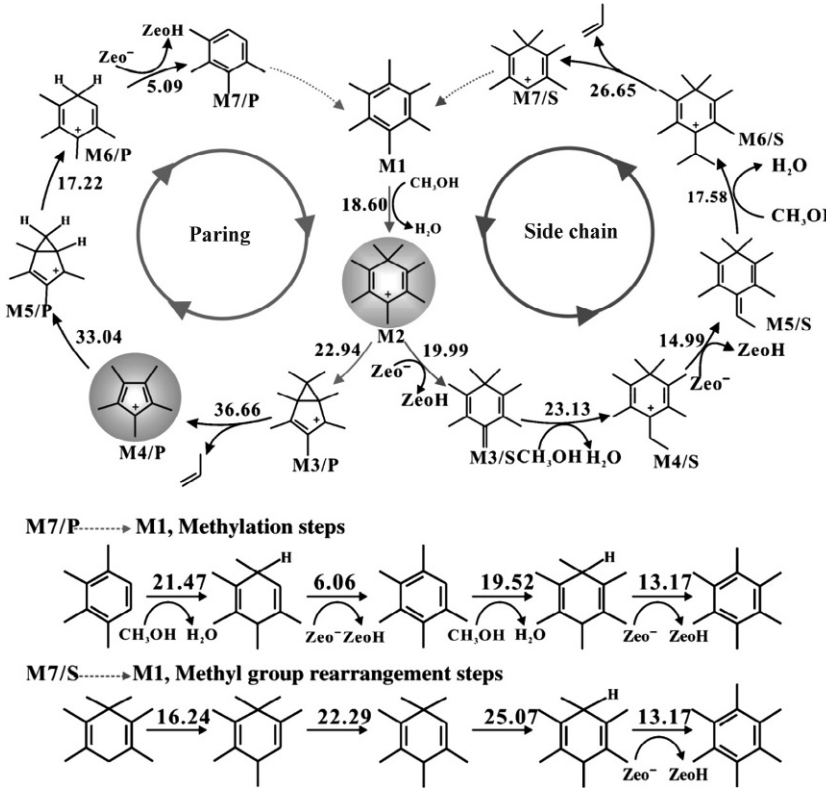

Fig. 29 Catalytic cycles of the paring and side-chain reaction mechanisms for the MTO conversion with the involvement of pentaMCP$^+$ and heptaMB$^+$ in H-SSZ-13 zeolite *(74)*. The calculated energy barriers are given in kcal mol^{-1}.

the difference in activation energy between the two mechanisms is not very large (ca. 10 kcal mol^{-1}), and thus parallel occurrence of the two reaction cycles is also very possible in the MTO reaction *(74)*. This result is also supported by the detailed isotopic distribution analysis of the main olefin products in ^{13}C-labeled methanol reaction. PentaMCP$^+$ formation and its accommodation in the CHA cage of zeolite or SAPO catalysts (H-SAPO-34 and H-SSZ-13), and their participation in methanol conversion is the direct evidence of paring mechanism with the five-membered-ring carbenium ions involvement. However, considering the activation barriers, the contribution of paring mechanism for olefin generation is not of significance, and the side-chain methylation mechanism is more important route for MTO reaction over the catalyst with CHA topology. Based on the proposed reaction cycles with carbenium ions as the important intermediates, the

capture of the heptaMB$^+$ and pentaMCP$^+$ deserves to be discussed in detail. As their generation is energetically favorable, the capture of them is determined by their stability, which are closely related to their further transformation to other intermediates. According to the catalytic cycle presented in Fig. 29 *(74)*, the transformation of pentaMCP$^+$ ions needs to overcome relative higher energy barriers (32.45 and 33.04 kcal mol^{-1}) than the heptaMB$^+$ ions (17–23 kcal mol^{-1}). Therefore, the generated pentaMCP$^+$ ion is more stable than the heptaMB$^+$ ion in H-SSZ-13, which makes it more readily observed by solid-state NMR spectroscopy. This trend is also in good agreement with our experimental results that heptaMB$^+$ ions only can be captured at low reaction temperature.

Wang et al. *(116)* utilized periodic DFT calculations to verify the side-chain alkylation mechanism of the MTO reaction via hexamethylbenzene intermediate over H-SAPO-34 zeolite. It is concluded that the propene formation follows the side-chain alkylation mechanism with lower activation energy and that the ethene splitting from the ethyl side chain needs to overcome higher energy barrier. For the paring route, the bottleneck step of the reaction corresponds to the ring expansion of five-membered ring cation to methylbenzene species. The overall reaction barriers in the paring route of hydrocarbon pool mechanism are much higher than those in the side-chain mechanism. Therefore, they concluded that the paring hydrocarbon pool mechanism *(137)* has a minor role on forming light olefins in the MTO reaction over H-SAPO-34.

4.3.3 Dual-Cycle Reaction Mechanism

The hydrocarbon pool mechanism with the involvement of cyclic organic intermediates has been considered as the indirect reaction mechanism of methanol conversion, which provides a reasonable explanation for the reaction pathway on the zeolite or the SAPO catalyst with a cavity structure, e.g., H-SAPO-34, and with a broad channel structure, e.g., H-beta. The bulky methylbenzenes and their corresponding protonated species formed in the supercage and 12-membered ring channel act as the main reactive intermediates *(81,82,95,126,138)* on the two catalysts. HeptaMB$^+$ shows higher reactivity over H-beta catalyst, but on H-SAPO-34, the hexamethylbenzene is a very important intermediate during the MTO reaction, which illustrates that the reaction intermediates are different with the change of crystal structure. Olsbye et al. *(86–88)* studied the reaction mechanisms of methanol-to-hydrocarbons reaction over H-ZSM-5 zeolite in 2006. The reactivity of the organics confined in the zeolite voids during the reaction was assessed

by transient $^{12}C/^{13}C$-methanol switch experiments, and the species with higher reactivity present more ^{13}C atoms incorporation. Fig. 30 displayed the tendency of ^{13}C content variation in the effluent compounds and the organic species confined in zeolite with different switch time *(87)*. It is demonstrated that the content of the incorporated ^{13}C atoms in methylbenzenes decreased with the increase of the number of methyl groups; that is, the higher methylbenzenes have lower reactivity, which is not consistent with the results on H-SAPO-34 *(73,78,79,81,82,101,138)* and H-beta *(15,95,97,100,102,118,126,134,139,140)*. As to ^{13}C distribution in gas products, ethene displays the same ^{13}C content as *p/m*-xylene and triMBs after switch experiments. This implies that the main formation route of ethene is related to the hydrocarbon pool mechanism on H-ZSM-5. In contrast to ethene and the most active methylbenzenes, the higher ^{13}C content of propene and higher alkenes illustrated that propene and higher alkenes are formed to a considerable extent from the reaction of alkenes, such as the reaction of alkene methylation and cracking *(86–88)*. The difference of this proposed route of alkene methylation and cracking, compared to the previous mechanism proposed by Dessau *(84,85)*, is that ethene is not generated from the cracking reaction of higher olefins *(141)*. Therefore, as shown in Fig. 31, Olsbye et al. *(86–88)* established

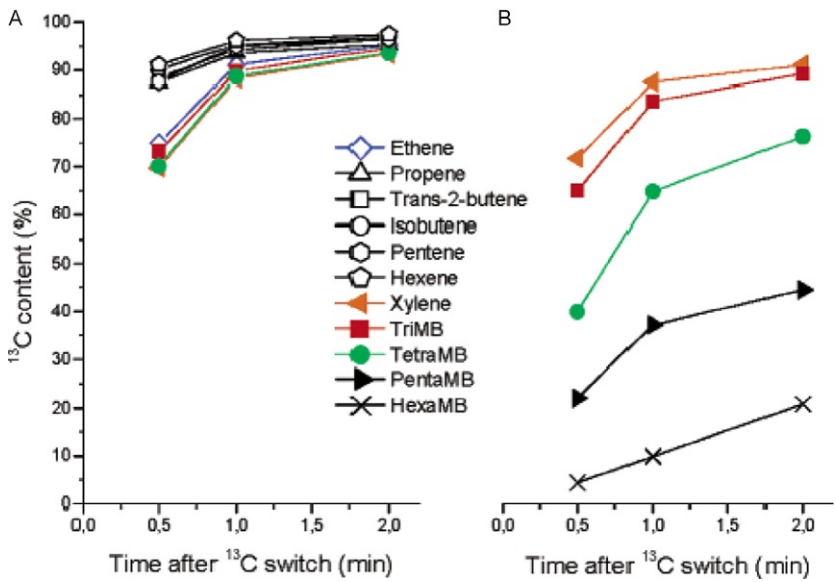

Fig. 30 Time evolution of ^{13}C content in effluent (A) and retained material (B) after $^{12}C/^{13}C$-methanol feed switch *(87)*.

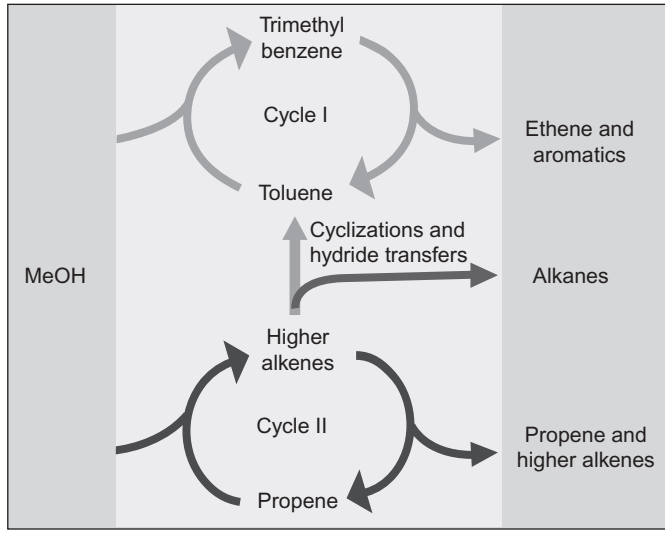

Fig. 31 Suggested dual-cycle concept for the conversion of methanol over H-ZSM-5 *(86)*.

the dual-cycle mechanism that two cycles run simultaneously during the MTH reaction over H-ZSM-5; ethene and propene are formed from the lower methylbenzenes' methylation and side-chain elimination, while propene and higher alkenes are from alkene methylation and cracking cycle. The relationship of aromatics-based and alkenes-based cycles was also described as follows: propene can be formed by the aromatics-based cycle, which plays the cocatalytic role in the alkenes-based cycle, and simultaneously, alkenes can convert to methylbenzenes by the oligomerization and cyclization reactions. The different formation route of ethene and propene implies a possible strategy for selectivity control by varying the reaction route. The dual-cycle mechanism is a development of hydrocarbon pool mechanism proposed by Dahl and Kolboe *(75–77)*.

In recent years, many studies about the hydrocarbon pool mechanism for MTO conversion identified alkene species as the intermediates for light olefins formation over H-SAPO-41 *(142,143)*, H-SAPO-34 *(144–147)*, H-SAPO-18 *(148)*, and H-MCM-22 *(149)*. Dai et al. *(144)* observed three-membered ring compounds, trimethylcyclopropane and dienes confined in H-SAPO-34 via UV/Vis and ^{1}H and ^{13}C MAS NMR spectroscopy and proposed that the olefin-based catalytic cycle is the primary reaction pathway during the early stage of the MTO reaction based on these olefins-like active species. And then, Bhan *(146)* illustrated the role of olefins methylation and cracking reaction via the isotopic tracer studies, which

expands the dual-cycle mechanism for methanol conversion over solid acidic zeotype catalysts to H-SAPO-34 catalyst. In addition, Wang et al. *(145,147)* demonstrated the energy feasibility of olefins-based routes for ethene and propene formation during methanol conversion over H-SAPO-34 by comparing computed overall reaction barriers of aromatics-based side-chain dealkylation and olefins-based β-scission process via density functional theoretical calculation. For the dual-cycle mechanism, many researchers found that the pore structure, the acidity, and the temperature will influence the predominance of the catalytic cycle. For example, the theoretical study was conducted to elucidate MTO reaction route in different pore environments of H-MCM-22 with three types of pore structure. It is predicted that propene can be produced through both alkenes-based cycle and aromatics-based cycle, while the contribution in the sinusoidal channels is minor *(149)*. Wang et al. *(150)* studied the two cycle routes of MTO reaction over H-ZSM-5 and found that catalytic reactivity of H-ZSM-5 zeolite is directly related to its acid strength, and weaker acid sites depress the aromatics-based catalytic cycle and then enhance the contribution of the alkenes-based cycle to form light olefins.

4.3.4 Alkenes Methylation Reaction With Methanol

The MTO reaction over zeolite catalysts is a complicated reaction system which involves many competitive reaction routes, such as methanol itself reaction, alkenes themselves reaction, and interconversion of methanol and alkenes. After establishment of the dual-cycle mechanism, more attentions are paid to the control of the reaction routes and product selectivity on the basis of the in-depth interpretation of the reaction mechanism. Concerning the association of dual-cycle mechanism, one argument is that the single cycle could not be completely independent, rather in such a way that the aromatic species should be formed through the aromatization reaction of higher alkenes derived from the alkenes-based cycle via the alkenes methylation and cracking reactions. Researchers have devoted efforts to attempt to circumvent one of the cycles on a specific catalyst. Initially, it has been believed that H-ZSM-22 with one-dimensional 10-membered ring channels, without the enough space of the intersecting channel, may limit the reaction via the aromatics-based cycle during MTO reaction *(151,152)*. However, the obvious conversion of methanol and a relatively long catalyst life were observed *(113,153–156)*, and a wide range of product distributions were present, including larger C_{5+} alkenes and aromatic compounds.

Co-reaction of ethene and methanol was carried out over H-ZSM-5 and H-ZSM-22 and the reactions, such as methanol reaction, ethene reaction, and methylation of methanol and ethene, occur at the same time. Different reactions when co-feeding ethene and methanol on the catalyst could be controlled by modifying the acidity of the catalysts. The sole methanol conversion can be limited *(156–158)*, and consequently the co-reaction of methanol and ethene became predominant. Complete suppression of conversion of methanol only or ethene could only be achieved over precoked H-ZSM-22, enabling the methylation of ethene dominantly taking place with propene selectivity higher than 80% when reaction time was extended (Table 2) *(156)*. After hydrothermal treatment of P—La-modified H-ZSM-5, the obtained catalyst with a small amount of weak acid sites was used in the co-reaction of ^{12}C-ethene and ^{13}C-methanol. The results illustrated that the

Table 2 Reaction Results of Methanol, Ethene, and Co-feed of Them Over H-ZSM-22 *(156)*

Run No.	**1**			**2**		**3**		
Feed/mL/min								
CH_3OH	20			0		20		
C_2H_4	0			40		40		
He	40			20		0		
TOS/min	6	60	87	6	25	6	33	60
Outlet/C mol%								
C_2H_4	12.3	0.23	0.22	98.7	98.8	61.8	73.8	77.5
C_3H_6	29.0	0.10	0.06	0.11	0.09	14.1	5.62	2.35
C_{4+}	51.1	0.37	0.13	1.18	1.08	17.6	3.94	0.37
CH_3OH/CH_3OCH_3	3.47	98.5	99.2			6.11	16.5	19.7
C_1^o–C_3^o	4.13	0.8	0.42	0.04	0.03	0.31	0.16	0.11
CH_3OH conv. %[a]	96.5	1.51	0.83	—	—	71.0	21.7	6.60
C_2H_4 conv. %	—	—	—	1.33	1.21	21.6	6.51	1.78
C_3H_6 sel. C mol%	30.0	6.80	6.64	8.15	7.47	44.0	57.8	83.0

[a]Conversion was calculated with CH_3OCH_3 included.
T = 773 K, ethene WHSV = 18 h^{-1}, methanol WHSV = 10 h^{-1}.

main product is propene and 89% propene molecules possess one ^{13}C atom from $^{13}CH_3OH$, confirming that the alkene methylation reaction is operative over the almost nonacidic catalyst *(157)*. Thus, lowering the acidity of the zeolite by modification can enhance the ethene methylation reaction to form propene, making this reaction route as the dominating one for methanol conversion.

5. CONTROL OF PRODUCT SELECTIVITY AND MTO REACTION ROUTE

5.1 Reaction Network of MTO Process

While a substantial body of zeolites and SAPO molecular sieves with different chemical compositions and topological structures have been extensively investigated as catalysts for catalyzing methanol conversion during the past decades, ZSM-5 and SAPO-34 have been generally taken as the utmost effective catalysts for MTO reaction *(9,11)*. Different from these two commercial zeotype materials, ZSM-22-catalyzed MTO reaction yields significant amounts of C_{3+} olefins and less aromatics; this exceptional product spectrum makes ZSM-22 also the subject of some studies *(113,153–156)*. Recent advances on MTO reaction mechanism mainly involve these abovementioned catalysts. The product selectivity largely varies over zeolites with different topology structures. One reason for this discrimination is related to the product shape selectivity originating from the zeolite channel dimension. For ZSM-5 with 10-membered ring pore opening (around 5.6 Å), aromatics can flow out as the effluent products with great ease, and yet for SAPO-34 with 8-membered ring window (around 3.8 Å) aromatics are ever scarcely detectable in gas products. Besides, the distinctive zeolitic channel architecture can tailor methanol reaction pathway as well, further affecting product selectivity.

Polymethylbenzenes retained in the nanocage of SAPO-34 interact with acid site to form the carbenium ions, constituting the active center for methanol conversion. Ethene and propene are primarily formed via the hydrocarbon pool mechanism based on retained polymethylbenzenes *(81,82,138)*. The route for generating ethene is, however, obviously distinct from the mechanism for the formation of propene and higher olefin homologues over ZSM-5, with ethene dominatingly being produced via aromatic-based reaction route and propene and higher olefins by olefin methylation–cracking pathway *(86–88)*. Methanol conversion exhibits a

peculiar profile over ZSM-22 zeolite, comparable in size but different in topology structure compared with ZSM-5. Extremely low methanol conversion and product yields were observed under high space velocity condition *(151,152)*; however, methanol can be fully converted under the relatively low space velocity and suitable reaction temperatures conditions *(113,153,155,156,159)*. The steady-state isotope experiments definitively illustrated that olefin methylation–cracking mechanism runs as the leading methanol-converting route over ZSM-22, which accounts for the products pattern with lower ethene selectivity and higher propene and C_{3+} olefins content.

The well-established and widely accepted indirect reaction mechanism discussed in Section 4 is applicable for interpreting almost all zeotype materials catalyzed MTO reaction. It should be noted that the specific geometry and architecture for a given zeotype catalyst govern the particularity of the methanol conversion pattern. It is known that the indirect mechanism, more accurately two-cycles mechanism, consists of aromatics-based cycle and olefins-based cycle. With regard to aromatics-based mechanism, there exist considerable differences in the nature of hydrocarbon pool species on account of the space confinement conferred by a zeolite channel, and possibility for preferable inclination to the paring mechanism or side-chain alkylation mechanism. The catalysis of methanol conversion over acidic catalysts involves an extremely complicated reaction system including multiple reaction steps and diverse reaction route. Herein a simplified reaction network is proposed and illustrated in Fig. 32. The induction period with first C—C bond formation and HCP species generation from initially generated olefin products are included together with the efficient methanol conversion via the indirect reaction pathway and the deactivation.

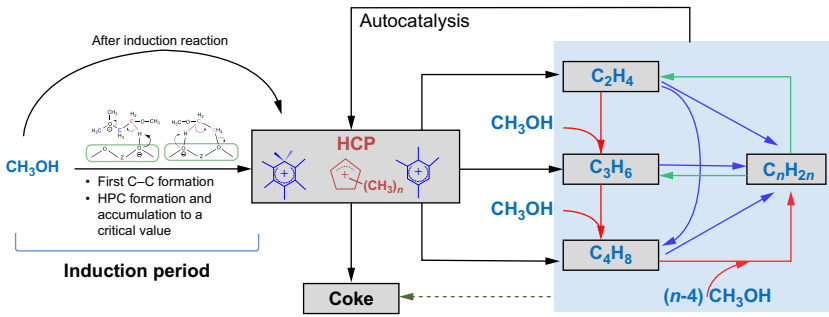

Fig. 32 Illustration of proposed reaction network of MTO process.

5.2 Methanol Conversion Route and Selectivity Control

The pore architecture and acidity of zeolites are two crucial aspects for acidic catalytic reaction. Distinguished from the common acid-catalyzed reactions, during the highly efficient MTO process proceeding via indirect reaction mechanism, BAS of zeolites provides a distinctive environment for generating and stabilizing the utterly important reaction intermediates-carbenium ions. In addition, the unique channel or the cavity structure of zeolites imposes confinement effect not only on the structure of reactive intermediates but also on the olefin formation route. Hence, both the selection of suitable topological structure and the precise variation of acidity of zeolite are of high significance for the selectivity control of olefin products.

5.2.1 Influence of Topological Structure of Zeolites on Product Selectivity

In 1982, the reactions of methanol on zeolites with different topological structures (e.g., H-T, NaH-Y, H-ZSM-5, and H-L) were thoroughly studied by Langner *(91)*. The results showed that H-ZSM-5 produces predominantly C_3–C_5 paraffins and monoaromatics and H–T generates linear C_2–C_4 olefins, whereas isobutane and isopentane are the main products for the large pore zeolites H-L and NaH-Y *(91)*. Since then, the structure–activity relationship has been perceived as one of the central concerns for methanol conversion. In recent years, with the advance of mechanistic research, substantial efforts have been devoted to interpreting reaction mechanism at the molecular level and to correlate the mechanistic insight with the discrepancy of product selectivity of actual catalytic reaction.

For a direct comparison of the product distribution with different topologies, H-SAPO-34-, H-ZSM-22-, H-ZSM-5-, and H-beta-catalyzed MTO reactions were tested by Teketal under identical conditions *(155)*. Both H-SAPO-34 and H-ZSM-22 produce the products mainly composed of olefins, but there exists a significant difference in olefins selectivity. H-SAPO-34 produces mainly light olefins, especially ethene and propene; H-ZSM-22 generates the highest amount of C_3 relative to C_2, simultaneously giving significant amounts of C_{4+} olefins. The previous experiments have evidenced that methanol conversion over H-SAPO-34 follows aromatics-based mechanism *(81,82,138)* and olefin methylation–cracking mechanism prevails over H-ZSM-22 as the space constraint of narrow one-dimensional 10-ring straight channels inhibits the effective operation of aromatics cycle *(113,153,155, 156,159)*. The dominating production of ethene and propene over

H-ZSM-5 and H-beta is ascribed to the contribution of aromatics cycle working on these two catalysts. It is noteworthy that the propene to ethene ratio would be variable with reaction proceeding or with the change of reaction conditions, albeit the olefins formation route is not varied. Song et al. *(81)* found the selectivity distinction of ethene and propene and suggested that it is relevant to the number of methyl groups on benzene rings trapped in the nanocages of H-SAPO-34. Propene is favorably generated by methylbenzenes with four to six methyl groups, while ethene is predominantly obtained from those with two or three methyl groups. The differences in the size and the consequent reactivity of polymethylbenzenes species can successfully explain the differing selectivity of ethene and propene over H-ZSM-5 and H-beta *(88)*.

Conversion of methanol to olefins carried out in pulse feeding mode was comparatively studied over three zeolites with different topologies (i.e., SAPO-34, H-ZSM-5, and H-ZSM-22) *(113)*. The total ^{13}C contents in the olefin products against the pulse numbers of ^{13}C-methanol via isotope transient $^{12}C/^{13}C$ CH_3OH switch experiment are presented in Fig. 33 *(113)*. While the olefins generated over all these three catalysts contain ^{12}C atoms from ^{12}C CH_3OH, more ^{12}C atoms were present in olefin products, especially in ethene, over SAPO-34 than ZSM-5 and ZSM-22. This signifies that the aromatics-mediated cycle is the leading reaction route over SAPO-34, allowing for the multitude of ethene formation. The relatively high ^{13}C content of the olefin products over ZSM-5 relative to SAPO-34, however, suggests the significance of olefin methylation–cracking

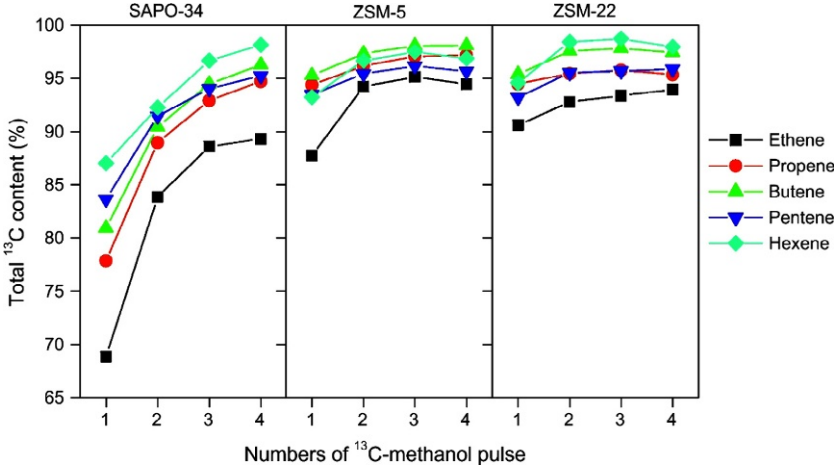

Fig. 33 Total ^{13}C content in the effluent products of successive ^{13}C-methanol pulse reaction at 450°C after the prereaction of 15 pulses of ^{12}C-methanol, CT = 0.08 s *(113)*.

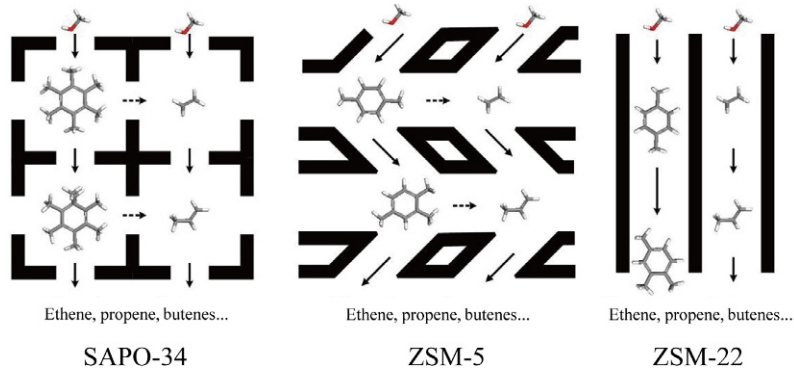

Fig. 34 Illustration of reaction routes of methanol conversion over SAPO-34, ZSM-5, and ZSM-22 *(113)*.

pathway operating over ZSM-5 zeolite, and yet the appreciable incorporation of ^{12}C atoms into ethene points to the fact that ethene is mainly resulted from the aromatics-mediated mechanism over ZSM-5. The total ^{13}C contents of C_{3+} olefins exceeding 95% indicate that olefin methylation–cracking route is operative for methanol conversion over ZSM-22. The less degree of ^{13}C atoms incorporation into aromatics associated with rather low ethene selectivity is indicative of the aromatics-mediated mechanism being strongly suppressed over ZSM-22 *(153)*. For clarity, the reaction routes of methanol conversion over the three zeolites with different pore structures are illustrated in Fig. 34 *(113)*. The further experiments performing by the co-reactions of ^{13}C-methanol and ^{12}C-*p*-xylene or ^{12}C-butene over the three zeolites imply that the aromatics and olefins, respectively, participate the catalytic process in a quite different way. Ethene, obtained from the aromatics-mediated mechanism, could be enhanced by the co-feeding of xylene; however the higher olefins derived from the olefin methylation–cracking route were more beneficial from the olefin addition. These findings demonstrate the possibility of definitive controlling of methanol-converting route and delicate tuning the weight of demanding light olefins to a certain extent, realized by selecting the zeolites with a distinct topological structure and, further for a specific zeolite, by introducing additional olefins or aromatics into the reaction system.

5.2.2 Influence of Cavity Structures on Product Selectivity

Cavity-type eight-membered ring small pore molecular sieves represented by SAPO-34 have universally been considered as one of most effective

and premium catalysts for catalyzing MTO reaction, owing to their unique topology structure, with nanocavity being spacious enough to accommodate large active aromatic intermediates and then promoting aromatic-mediated cycle, besides bearing eight-membered ring pore opening being effective for sieving the light olefins as target products and prohibiting the exiting of larger hydrocarbons *(8,11)*. Haw et al. *(81)* reported that the selectivity of light olefins over H-SAPO-34 is closely related to the number of methyl groups on the benzene ring of aromatics retained in the cage, in such a way that propene is favorably formed by methylbenzenes with four to six methyl groups but ethene predominantly derived from the lower analogues with two or three methyl groups. Hence, as cage-structured small pore molecular sieves are adopted for catalyzing methanol conversion, the spatial constraint of the well-defined cavity structure can exert a significant effect on the subtle structural variation and consequently the reactivity of active aromatic entities, allowing for the cavity-controlled catalysis *(109,111)*.

Three kinds of eight-membered ring SAPO molecular sieves (i.e., SAPO-34 (CHA), SAPO-18 (AEI), and SAPO-35 (LEV)), with comparable moderate acid strength but with different cavity structures, were tested for MTO reaction at the temperature range of 300–400°C and the outcomes are displayed in Fig. 35 *(111)*. Varied product distribution over different SAPO catalysts was observed. Ethene and propene, especially ethene, are predominantly generated over SAPO-35, while propene and butene are formed as the main products over SAPO-18 and SAPO-34 under the same conditions, associated with the relatively large cavity of CHA and AEI topology. In addition, SAPO-18 yields more butene than SAPO-34, possibly due to the slightly larger space provided by pear-like AEI cavity of SAPO-18 compared with the CHA cavity of SAPO-34 *(111)*.

The cavity structures show spatial confinements on the formation of the active intermediates confined inside the cage. Analysis of retained species in

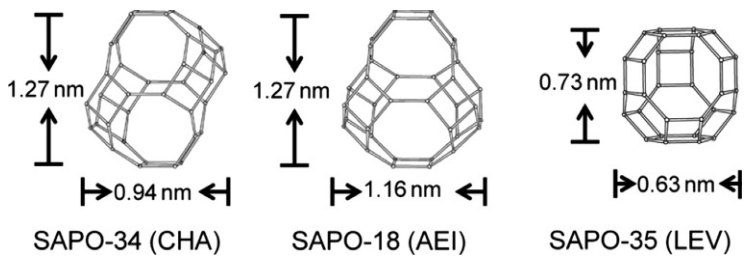

Fig. 35 Illustration of cavity structures of SAPO-34, SAPO-18, and SAPO-35 *(111)*.

cages of SAPO catalysts with TOS = 15 min at 300°C illustrates that tetra-, penta-, and hexamethylbenzenes compose of the dominating retained compounds in SAPO-34 and SAPO-18, but over SAPO-35 with small LEV cavity, tri-, tetra-, and pentamethylbenzenes appear as the main confined organics and dimethylbenzene is also detected in a certain quantity. The relative reactivity of retained organics inside different cages was successfully distinguished by $^{12}C/^{13}C$-methanol switch experiments demonstrated in Fig. 36 *(111)*. Polymethylbenzenes are unambiguously identified as the utmost active hydrocarbon species, with penta- and hexamethylbenzene being the substantially more active species over SAPO-34, hexamethylbenzene acting as the main catalytic active intermediate over SAPO-18, and tetramethylbenzene being the dominating operative organics over SAPO-35. The manifested discrimination of these active organics retained in different cavities suggests that the cavity structure acts as a key factor for determining the type of active hydrocarbon pool species and then selectively modulating the product distribution. Higher methyl-substituted polymethylbenzenes, i.e., penta- and hexamethylbenzene, are favorable for propene formation, yet lower homologues with di-, tri-, and tetramethyl-substituted counterparts lead predominantly to ethene. The distinct reactivity of polymethylbenzenes confined in SAPO-34, SAPO-18 and SAPO-35 cavities rationalizes the different yields of light olefins, lending a hint to an applicable alternative to realize the selectivity control of light olefin products by rationally designing and delicately tuning the cavity structures of the cavity-type catalysts *(109,111)*.

Pretty solid experimental evidences have been offered to interpret the confinement effect of cavity structures on the formation of reactive intermediates over SAPO molecular sieves. Based on the foundation work of direct observation of heptaMB$^+$ over DNL-6 catalyst *(108)*, methanol conversion and the role and activity of active intermediates were comparatively investigated on SAPO-35 with smaller cavity (6.3 × 7.3 Å), SAPO-34 with medium cavity of 6.7 × 10 Å, and DNL-6 with large cavity (11.4 × 11.4 Å) *(109)*. Under real working conditions of MTO reaction, two types of carbenium intermediates, polyMB$^+$ and polyMCP$^+$, were directly observed and verified by isotopic tracing technique and theoretical calculations. Different from the relatively large-sized pentaMCP$^+$ and heptaMB$^+$ cations captured over DNL-6 catalyst, tri-, and tetraMCP$^+$ and pentaMB$^+$ cations were observed over SAPO-35, but MCP$^+$ cations (i.e., tri-, tetra-, and pentaMCP$^+$) were merely obtained over SAPO-34. $^{12}C/^{13}C$-methanol switch experiments were further implemented to discriminate the active intermediates from the spectators. The ^{13}C contents of methylbenzenes, as to SAPO-34 and DNL-6,

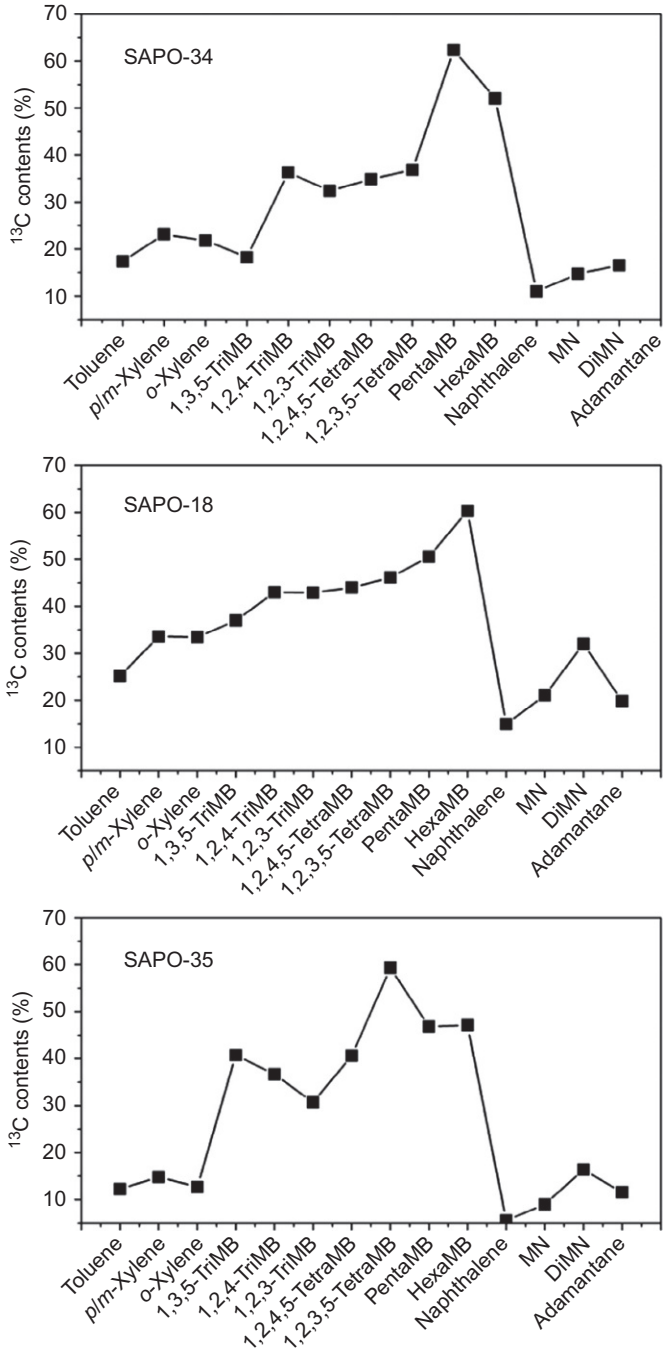

Fig. 36 Total ^{13}C contents of the retained organics after ^{12}C/^{13}C-methanol switch experiment over SAPO-34, SAPO-18, and SAPO-35 *(111)*.

scramble parallel with the number of methyl groups, with hexaMB being the most very active intermediates, especially for SAPO-34. However, over SAPO-35, pentaMB exhibits more ^{13}C content than hexaMB owing to the steric constraint of the small LEV cavity. The theoretical calculations were also conducted using DFT-D2 method in order to gain more insight into the confinement effects of cavity on the reactivity of carbenium ions. The performance of methylation of tetraMB, pentaMB, and hexaMB to form the corresponding polymethylbenzenium cations was compared with the intrinsic Gibbs free-energy barriers as an activity indicator (shown in Fig. 37) *(109)*. Over SAPO-34 and DNL-6, the estimated barriers decrease with the increase of the number of methyl groups. However, this trend does not hold for SAPO-35, where the methylation of hexaMB is subject to the highest Gibbs free-energy barriers. This suggests the transition-state selectivity effect of cage-structured molecular sieves on the generation of active carbenium ions. The steric constraints exerted by the smaller LEV cavity limit the molecular size of bulky intermediates and consequently lead to higher ethene selectivity *(109)*. Hence, cavity-controlled selectivity, that is, cavity structure determines the generation of confined reactive organics, in turn controls the MTO reaction activity, and possesses great potential to be a feasible approach to selectively regulate the olefin products pattern.

5.2.3 Influence of Zeolitic Acidity on Product Selectivity

Acidic zeolites are usually utilized as the catalysts for catalyzing methanol conversion to olefins. MTO process follows the indirect reaction route, i.e., hydrocarbon pool mechanism *(15,47,75–77)*, with multistep proceedings of

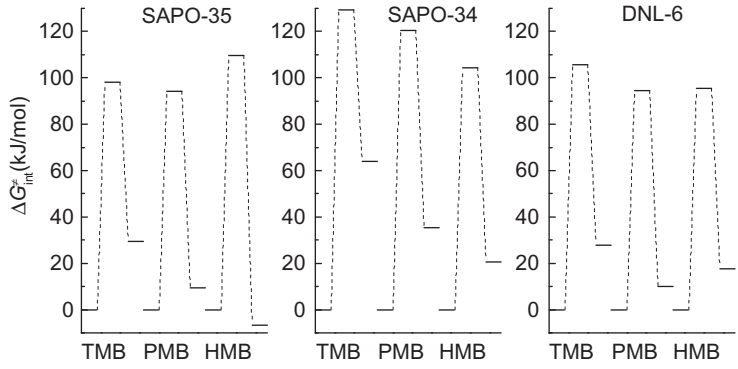

Fig. 37 Intrinsic free-energy barriers of the methylation of tetraMB (TMB), pentaMB (PMB), and hexaMB (HMB) over SAPO-35, SAPO-34, and DNL-6 at 275°C *(109)*.

reaction. The formation and stabilization of carbenium ions, alkylation reaction, rearrangement reaction, cracking for light olefins formation, etc., involve the participation of acidic sites. Parallel to the generation and desorption of olefin products, the residing olefins inside the zeolite channel can be subject to further condensation to heavier coke resulting in the deactivation of catalyst. These sequential reactions occurring on the acidic center of zeolite progressively build up the complex reaction network. The acid strength and acid density work as two critical factors that modulate the methanol conversion pathway and resultantly the olefins selectivity.

5.2.3.1 Influence of Zeolitic Acidity Strength

Yuen et al. *(160)* comparatively explored the effect of acid strength of isostructural zeotype catalysts, SAPO-34 and H-SSZ-13 with CHA topology and SAPO-5 and H-SSZ-24 with AFI topology, on the methanol conversion performances. The differing acid strength of isostructural molecular sieves considerably influences the methanol conversion route. Albeit the full conversion of methanol in the initial period on both categories of catalysts, in stark contrast to SAPO molecular sieves, the methanol reactant is liable to penetrate the aluminosilicate catalysts bed and deactivate the zeolites quickly. Similarly, Bleken et al. *(161)* also compared the methanol reaction over SAPO-34 and H-SSZ-13 and drew the conclusion that H-SSZ-13 with stronger acidity facilitates the formation of olefin products as well as the aromatics retained in the cavity, causing the quick deactivation of H-SSZ-13.

The MTH reaction performance was further studied by Erichsen et al. *(162,163)* over two 12-membered ring zeotype materials, moderately acidic molecular sieve H-SAPO-5 and stronger acidic zeolite H-beta at 350–450°C. H-SAPO-5 was found to be more selective toward the production of C_3–C_5 olefins, while H-beta-catalyzed methanol reaction produced more ethene and aromatics except for C_3–C_5 products. The isotope transient $^{12}C/^{13}C$ CH_3OH switch experiments were performed at 450°C to study the activity of reactive intermediates on H-SAPO-5. The results exhibited that more ^{13}C atoms are incorporated into the alkene products than the retained polymethylated benzene organics, suggesting governing role of olefins methylation–cracking route on H-SAPO-5 *(162,163)*. Co-reactions of CH_3OH and benzene drove the product selectivity toward ethene and propene, which means that aromatics can also serve as a cocatalyst for light olefins formation over H-SAPO-5. Dissecting the isotope labeling patterns of C_2–C_5 olefins through co-feeding reaction of ^{13}C CH_3OH and benzene

indicates that polymethylated benzenes present in excessive amounts may contribute to ethene and propene formation via paring mechanism; however, isobutene and isopentene are unquestionably derived from the olefin methylation–cracking mechanism. Taken together, a reaction scheme for methanol conversion over SAPO-5 is suggested and illustrated in Fig. 38 *(163)*, analogous to the proposed dual-cycle mechanism on H-ZSM-5. However, the proposed alkene and arene cycles over H-SAPO-5 consist of apparently larger intermediates due to the spacious channel space of H-SAPO-5 relative to H-ZSM-5. When turning to H-beta, which has pore dimensions similar to H-SAPO-5 but with stronger acidity, methanol conversion mainly follows the aromatic-mediated route, different from the dominating olefin methylation–cracking mechanism on H-SAPO-5 *(163)*. The difference in reaction direction is attributed to the distinct acid strength. The essential factor for building mature aromatics cycle highly relies on the facile generation of active five- and/or six-membered ring carbenium ions. The stronger acidic aluminosilicate zeolites are prone to produce carbenium ions as compared to moderate acidic SAPO molecular sieves. As for CHA-type catalysts, heptaMB$^+$ ions, important carbenium ions involved in the MTO reaction, can easily form and will be successfully captured under the real reaction conditions over SSZ-13 with stronger acidity, not the case for medium acidic SAPO-34 *(74)*.

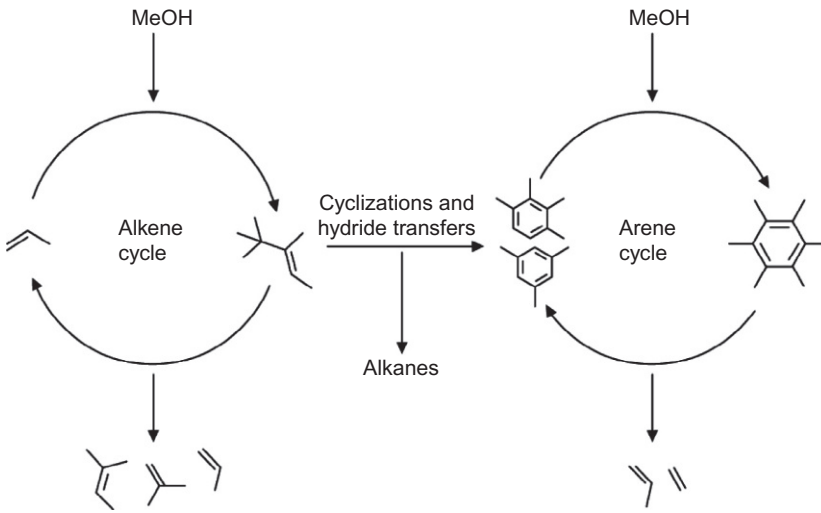

Fig. 38 Scheme of the proposed dual-cycle mechanism in operation during methanol-to-hydrocarbons reaction over H-SAPO-5 *(163)*.

5.2.3.2 Influence of Zeolitic Acidity Density

Brønsted acid center plays a vital role in MTO reaction catalyzed by the zeotype catalysts. Regarding the propagation of aromatics cycle, Brønsted acidity is closely correlated with the formation of active intermediate species (polymethylbenzenes and the corresponding carbenium ions) and consequentially the generation of light olefins *(74,108)*. Excessive Brønsted acid centers are capable of accelerating the hydrocarbon pool species to further condense to heavier aromatics, leading to final deactivation *(15)*. Dai et al. *(164–166)* found that Brønsted acid center significantly affects the catalytic activity and life span of MTO catalysts. Given the complication of reaction mechanism, acid density is taken as an important design parameter for reaction route controlling and selectivity optimization in MTO reaction.

The MTO reaction activity and mechanism over AlPO-18 (without BAS) and series of SAPO-18 (with different BAS densities) catalysts were systematically investigated *(148)*. The methanol conversion capacity was obviously improved with the concurrent increment of BAS densities. Using ^{13}C MAS NMR technique, pentaMCP$^+$ ions were directly captured over SAPO-18 with higher BAS densities under the working MTO reaction conditions. The pentaMCP$^+$ ions can be observed, with low intensity, on the catalyst with less BAS, but no carbenium ions were detected over AlPO-18 *(148)*. This indicates that BAS densities play a critical role in the formation of reactive intermediates and that higher BAS densities are advantageous for the generation and accumulation of important hydrocarbon pool species-pentaMCP$^+$ ions.

With the aid of $^{12}C/^{13}C$-methanol switch technique, the effect of BAS densities on methanol conversion mechanism was further elaborated *(148)*. Over SAPO-18 with relatively high BAS density, polymethylbenzenes were largely formed and light olefins mainly follow the aromatic-based mechanism. The slight discrepancy of ^{13}C incorporation into retained polymethylated benzene and light olefins implies that the olefin methylation–cracking route cannot be ruled out for methanol conversion over SAPO-18 with low BAS density. However, over AlPO-18 without BAS, ^{13}C atoms are much more incorporated into the olefins product than the retained pentaMB and hexaMB, suggesting the dominance of olefin methylation–cracking mechanism. Thereby, BAS significantly affects the preference of olefin-based or arene-based route for the methanol conversion to a great extent. The proposed methanol conversion pathways over AlPO-18 and SAPO-18 are illustrated in Fig. 39 *(148)*.

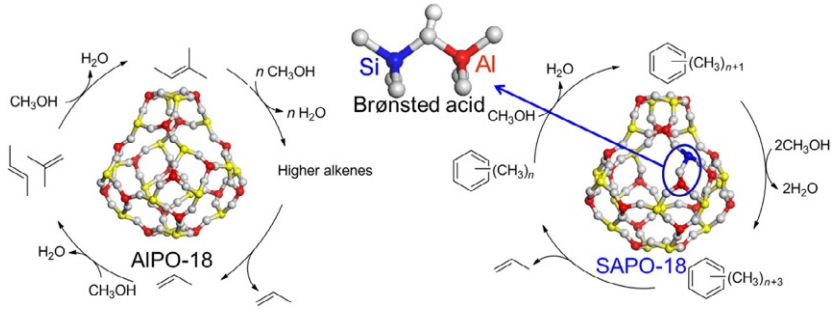

Fig. 39 Illustration of methanol conversion pathways over AlPO-18 and SAPO-18 *(148)*.

As co-feeding reactions of ethene and methanol were conducted over H-ZSM-22 and H-ZSM-5, the reaction pathway was also found to be highly related to BAS density of catalysts *(156,157)*. Lowering the BAS density of catalysts via P and La modification helps to overwhelmingly suppress the respective conversions of methanol or ethene. Meanwhile, the methylation reaction of methanol and ethene turns to be the leading reaction in the catalytic system accounting for the high propene selectivity.

6. DEACTIVATION OF MTO REACTION

6.1 Two Deactivation Modes

MTO reaction is the acid-catalyzed reaction. As other acid-catalyzed reactions of hydrocarbons conversion, the product formation in the MTO reaction is accompanied by the coke formation and catalyst deactivation. The MTO catalysts used in industrial processes, SAPO-34 and ZSM-5, present different deactivation modes in the methanol conversion. SAPO-34 is a molecular sieve with a cavity-type structure. The deactivation of SAPO-34 results from the transformation the confined intermediates, such as polymethylbenzenes, to bulky polyaromatics, which depresses the mass transfer of the reactant largely *(15)*. When most of the cavities are occupied by the polyaromatics and the reaction centers of the catalyst become inaccessible to the reactant methanol, the deactivation would occur (Fig. 40, left) *(15)*. Hereijgers and coworkers supported the view of deactivation from the mass transfer reduction in SAPO-34 *(14)*. Limited by the eight-membered ring window of SAPO-34, large coke species cannot diffuse out the channel of the catalyst; thus, the MTO reaction over SAPO-34 is characteristic of the high coke amount and quick deactivation. Different from SAPO-34 with a relatively big supercage, the intersectional 10-mermered ring channel

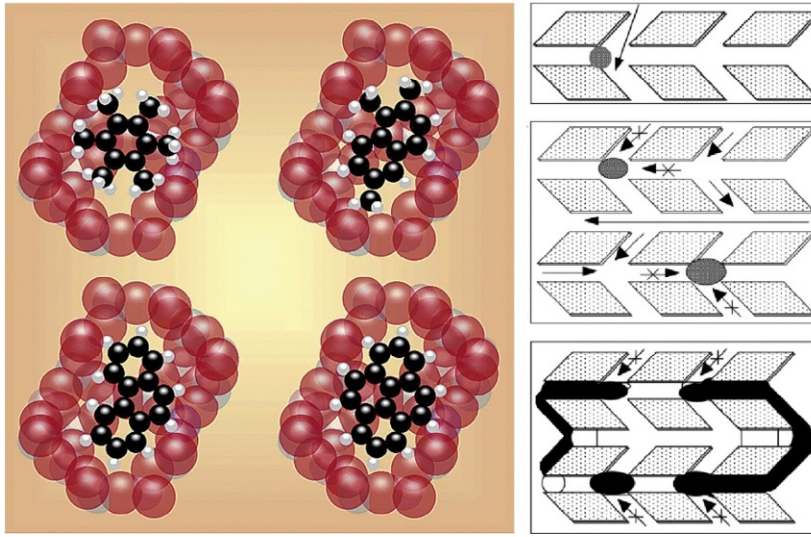

Fig. 40 Deactivation of MTO reaction over SAPO-34 (*left*) *(15)* and H-ZSM-5 (*right*) *(167)*.

cannot provide the space for the formation of bulky aromatic compounds, such as polyaromatics, phenanthrene and pyrene. The channel of ZSM-5 can only accommodate methylbenzenes with less methyl substitution groups, and most of these methylbenzenes can diffuse out to the gas phase. The structure of ZSM-5 determines that no bulky coke species deposition in the 10-membered ring channel *(86)*. The deactivation of H-ZSM-5 is not related to the coke formation on the internal surface of the zeolite, but the coke deposition on the external surface (Fig. 40, right) *(167,168)*. Mores and coworkers studied the reaction over H-ZSM-5 and SAPO-34 and found the difference in the coke formation over the two catalysts *(169,170)*. Under the identical reaction condition, methanol reaction over SAPO-34 encounters quicker deactivation than H-ZSM-5, and therefore, in the industrial application of MTO process, fluid-bed reaction-regeneration technology is designed for SAPO-34-catalyzed MTO process for solving the deactivation problem and assuring the highly efficient conversion; while for H-ZSM-5-catalyzed MTP process, fixed-bed reaction technology is utilized.

6.2 The Factors Influencing Deactivation

In the discussion of catalyst deactivation with coke deposition, the coke species causing the deactivation usually refer to the species that can block the

channel or cover the active sites of the molecular sieve catalysts. For the reaction catalyzed by the acidic molecular sieves, such as MTO reaction, some products are too large or have a strong proton affinity, cannot diffuse out of the molecular sieve pores, and accommodate in the pore or supercage. These confined species, which limit the mass transfer or occupy the acid sites, cause the deactivation. The mode of coke deposition and deactivation is closely related to the reaction temperature, the topology, and the acidity of the catalysts.

6.2.1 The Effect of Reaction Temperature

Coke deposition over molecular sieve catalysts in the MTO reaction is closely related to the reaction temperature. Schulz and coworkers *(171,172)* found that the increase of reaction temperature of methanol conversion over H-ZSM-5 would vary the catalyst life span and the deactivation mode. For the reaction performed at relatively low temperature, such as 270–300°C, bulky alkylbenzenes that generated in the catalyst and occupying the channel of H-ZSM-5 are responsible for the catalyst deactivation. When the reaction performed at relatively high temperature, such as 350°C, these bulky aromatic compounds retained in the channel of the H-ZSM-5 would transform to small-sized aromatics with the elimination of alkene products. When the reaction temperature is higher than 350°C, coke deposition on the catalyst external surface becomes the main deactivation mode. The methanol conversion at different reaction temperatures corresponds to two deactivation modes, channel blockage and external surface coverage. The coke amount and catalyst lifetime also vary with reaction temperature. The catalyst life is 0.5 h at 290°C with the coke amount of 10%, but at 380°C, the catalyst life is 400 h with the coke amount of 0.3% *(171)*.

For the study of coke formation in methanol conversion catalyzed by cavity-type molecular sieves, it is generally accepted that the generated methylbenzenes in the cavity of the catalysts will transform to methylnaphthalenes during the reaction, and further transform to phenanthrene and pyrene derivatives. When most of the cavities of the catalysts are occupied by the polyaromatics, the mass transfer of the reactants will be severely depressed, which causes the sharp decline of the methanol conversion to hydrocarbons products *(15)*. Bleken and coworkers studied the coking behavior in the methanol conversion over SAPO-34 and H-SSZ-13 with identical CHA topology *(161)*. Even the difference in the acid strength of zeolite and SAPO catalysts, the reaction shows a very similar trend in catalyst lifetime and coke formation of methanol reaction performed over the two

catalysts at varied reaction temperature. When the methanol conversion was performed over SAPO-34 at 300°C for 20 min, the coke amount attains to 16%; however, the coke amount is lowered down to 6% at 400°C. Under the same reaction condition, the coke amount of H-SSZ-13 declines from 20% at 300°C to 9% at 400°C. Both SAPO-34-and H-SSZ-13-catalyzed methanol reaction could exhibit a prolonged catalyst life span at an optimized temperature condition, but under lower or higher temperature conditions, both catalysts suffer from quick deactivation. The deactivation of the two catalysts stems from the polyaromatics formation. However, the difference also exists. The bulky aromatics, such as phenanthrene and pyrene with three or four benzene rings, and much bulkier and insoluble coke are found in the deactivated H-SSZ-13 catalyst with stronger acid strength, but for the reaction performed over SAPO-34, the coke species are mainly composed of naphthalene and its derivatives.

Liu and coworkers studied methanol reaction and coke formation over SAPO-34 catalyst and found a special evolution of methanol conversion in reaction under the temperature-programmed increase (Fig. 41) *(173)*. Methanol was fed to the reactor at 250°C and the reactor was heated with the temperature-programmed increase, while no hydrocarbon products are generated in the temperature range of 250–300°C. The methanol reaction

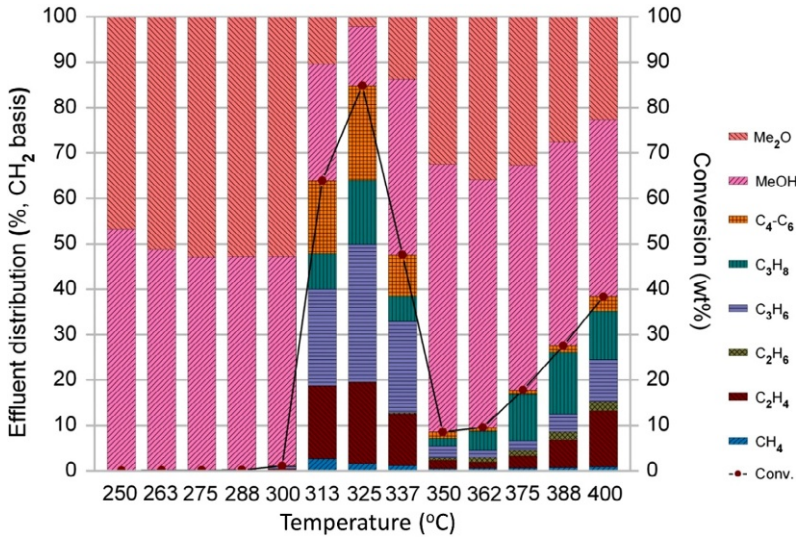

Fig. 41 The effluent product distribution of methanol conversion under the reaction condition of programmed temperature increase from 250°C to 400°C *(173)*.

starts from 300°C, attains to maximum at 325°C, then declines with the temperature from 325 to 350°C, and eventually increases again as the temperature higher than 350°C.

To explain this phenomenon, the performance of methanol conversion associated with coke formation and evolution at different reaction temperatures was studied in detail. Methanol conversion exhibits quite different characteristics over the SAPO-34 catalyst at low and high temperatures *(173–175)*. Low-temperature reaction shows an apparent induction period and the feature of fast deactivation. With the increase of temperature, the induction period is shortened gradually. It is observed from Fig. 42 *(175)* that at both rather low and high temperature, the catalyst suffers from fast deactivation with quick coke deposition. But at the temperature range of 400–450°C, the reaction presents slight coke deposition and longer catalyst life span. By analyzing the retained coke species in the deactivated catalyst, it is evidenced that the deactivation of SAPO-34 at high-temperature results from the deposition of polyaromatics. But for the fast deactivation at low temperature, no polyaromatics are detected on the spent catalyst. After the reaction at 300°C, the deactivated catalyst appears in white color, while the extracted organics by dissolving the spent catalyst in the HF solution followed by organic solvent extraction looks colorless. But it is proved that a large amount of organics retain on the deactivated catalyst after reaction at low temperature. A kind of newly found coke species, adamantane hydrocarbons, are carefully identified as the cause for the fast deactivation at low temperature (Fig. 43) *(174)*. Different from the methylbenzenes acting as the active HCP species, adamantane hydrocarbon cannot function

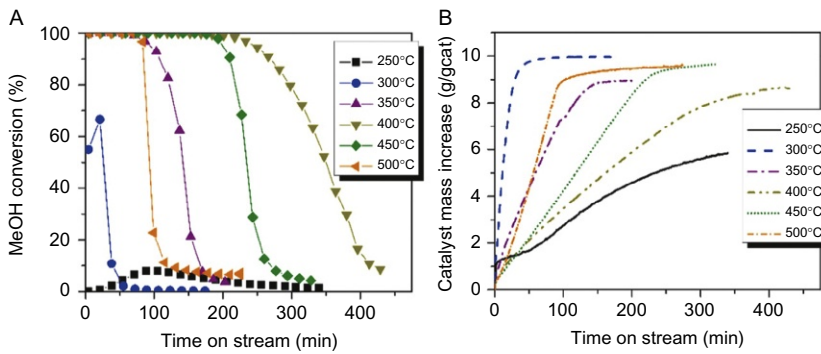

Fig. 42 The variation of methanol conversion and catalyst mass increase at different reaction temperatures with time on stream *(175)*.

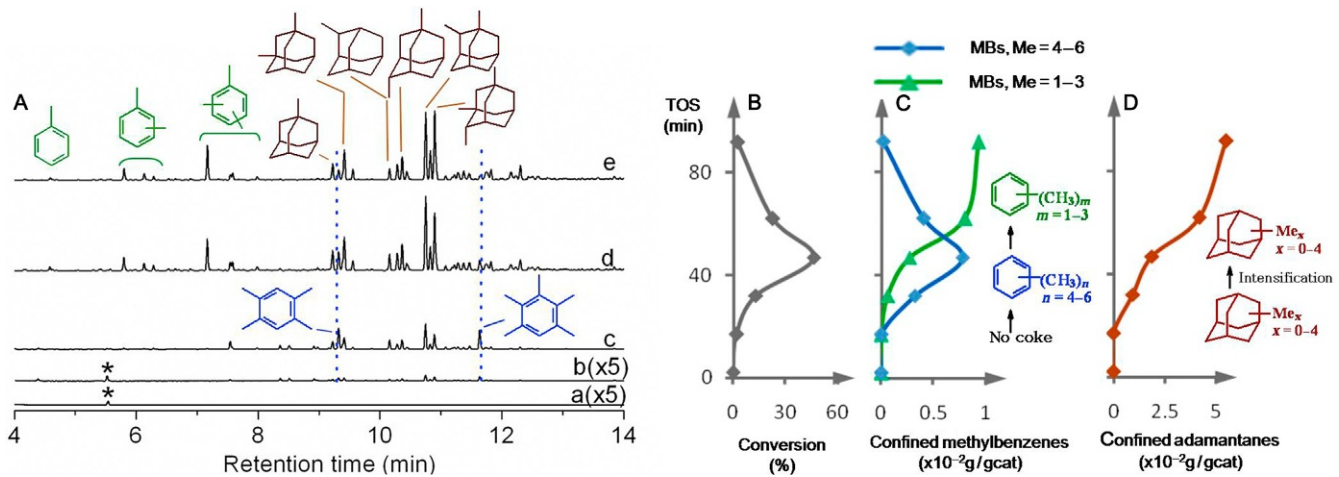

Fig. 43 GC–MS analysis of the retained organics after methanol conversion at 300°C (A), the variation of methanol conversion (B), the amount of methylbenzenes (C), and the amount of adamantane hydrocarbons (D) *(174)*. (for (A), a. 17 min; b. 32 min; c. 47 min; d. 62 min; e. 92 min; *internal standard).

as the reaction center for the assembly of C—C bond from C1 reactant. The occupation of adamantane species in the catalyst cages inhibits the effective mass transfer and thus depresses the continuous generation of the HCP species, finally causing the quick catalyst deactivation.

According to the coke species evolution with reaction temperature as presented in Scheme 2 *(172)*, the special variation trend of methanol conversion with the temperature-programmed reaction shown in Fig. 41 can be well explained. Deactivation at low-temperature results from the formation and accumulation of adamantanes in the cage-type catalyst of SAPO-34. With the increase of reaction temperature, adamantane hydrocarbons will be transformed to naphthalene derivatives and further to phenanthrene and pyrene. The evolution of the confined coke species with reaction temperature corresponds to the dynamic course that deactivation initially occurs at relatively low temperature (300–325°C), then the catalytic activity is gradually restored with temperature increase (325–350°C), and eventually the catalyst loses activity again with further increasing temperature (350–400°C).

In the case of H-ZSM-5, over which temperature-programmed methanol to hydrocarbon (TP-MTH) reactions was also performed, similar to the abovementioned methanol reaction over SAPO-34, four different reaction

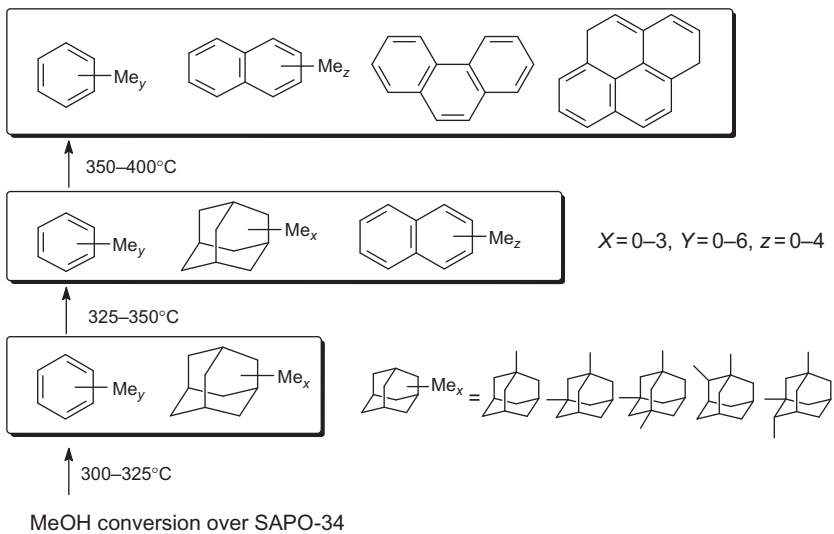

Scheme 2 Coke species evolution in methanol reaction with reaction temperature increase *(173)*.

stages could be clearly observed: the initial reaction stage, the autocatalysis reaction stage, the deactivation stage, and the activity recovery stage *(176)*. 1,2,3,5-TetraMB was found to be the main active species during the initial autocatalytic stage and its "overloading" effect resulted in the unusual deactivation phenomenon; i.e., despite its high intrinsic reactivity, too quick formation of 1,2,3,5-tetraMB and lower methylbenzenes with poor mobility will lead to the occupation of most catalyst channels and channel intersections and cause the deactivation of H-ZSM-5 at low temperature. With the temperature increase, the reactivity of these polymethylbenzenes can be recovered, which is in accordance with the "reanimation" of H-ZSM-5 at increased reaction temperature as proposed by Schluz *(171,172)*.

According to the reaction mechanism of methanol conversion catalyzed by the catalysts with a three-dimensional channel or a cavity structure, polymethylbenzenes are generally known as the most reactive intermediates serving as the accelerant for methanol autocatalytic reaction, but naphthalene and its derivatives are less reactive in methanol reaction and are often regarded as the coke species together with polyaromatics, which causes the deactivation of methanol reaction *(174)*. Bulky aromatic hydrocarbon generation requires a wide space provided by the zeolite or molecular sieve catalysts, so the component of the coke species is related closely to the topology of the catalysts. The study of the retained compounds during methanol conversion indicated that the polymethylbenzenes behave not only as the important intermediates for olefins production but also as the precursor for forming the polyaromatics as the coke species. Sassi studied the reaction of co-feeding methanol and methylbenzene on H-beta *(95,126)* and speculated that one benzene ring of naphthalene is directly derived from polymethylbenzene itself and another one is formed by the coupling of two isopropyl groups on the benzene ring. Bjørgen and coworkers *(139)* suggested one possible route for the formation of coke precursor over acidic zeolite (Fig. 44), in which heptamethylbenzenium ion, formed by methylation of hexamethylbenzene, can transform through carbenium ion rearrangement and hydrogen transfer reaction to dihydrotrimethylnaphthalene, a key precursor for naphthalene derivatives. This work offers the possibility of the evolution route of polymethylbenzenes to coke precursor, accompanying by the hydrogen transfer reaction converting the olefins to the corresponding alkanes; however, the definite experimental evidence for building up such an evolution route remains lacking *(139)*.

Different from zeolite or molecular sieve catalysts with a spacious channel or a large cage structure, coke deposition of methanol conversion

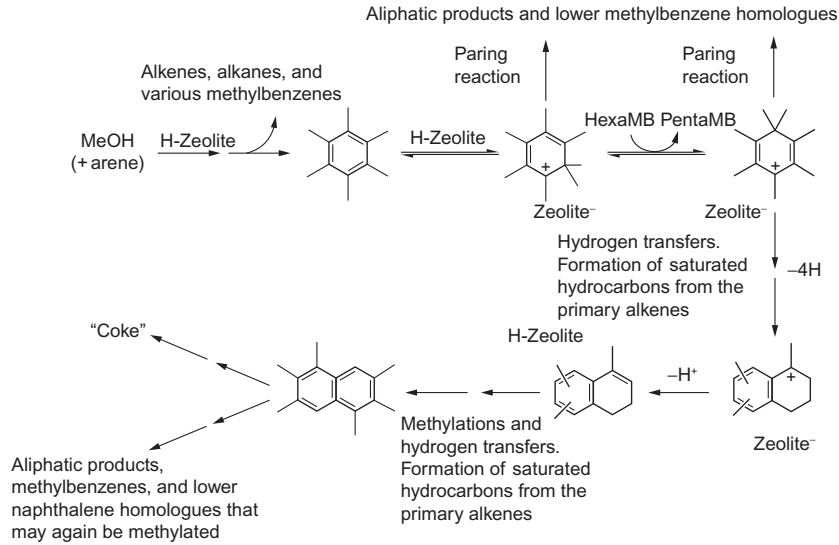

Fig. 44 The possible route for the hexamethylbenzene to dihydrotrimethylnaphthalene *(139)*.

over H-ZSM-5 mainly results from insoluble coke deposited on the external surface *(167)*. Due to the 10-membered ring intersectional channel structure, only lower methylbenzenes can be formed inside the channel, while the formation of heptamethylbenzenium ion and heavier polyaromatics is more difficult due to the steric hindrance effect exerted by the relatively narrow channel of H-ZSM-5 *(133,167)*. Bleken and coauthors *(133)* comparatively studied the methanol conversion over four kinds of three-dimensional and 10-membered-ring channel structure zeolites (IMF, TUN, MEL, and MFI) and found that the subtle variation in the 10-membered ring channel structure can cause a remarkable difference in the deactivation mode. Although the four zeolites give very close effluent product distribution, the lifetime duration differs significantly with the specific topology of the zeolite and decreases in the order: ZSM-11 > ZSM-5 > TNU-9 > IM-5. Polyaromatics can be fast formed in the much larger cavities of TNU-9 and IM-5, which cause a more rapid deactivation compared to ZSM-5 and ZSM-11. ZSM-11 and ZSM-5 with MEL and MFI structures illustrate relatively a long life span since no bulky coke species are formed in these two catalysts with smaller channel intersections. Moreover, the reduced deactivation results from the coke formation at the external surface *(133)*.

6.2.2 The Effect of Catalyst Acidity

The catalyst deactivation of MTO reaction over zeolite and SAPO catalysts is closely related to the catalyst acidity. The catalysts with stronger acid strength and higher acid site density are generally subject to quick deactivation *(160,177,178)*. Guisnet and coworkers *(167)* summarized the role played by the acidity and pointed out that (i) the catalyst with stronger acid strength would cause the faster chemical elemental reactions and more pronounced formation rate of coke precursors, consequently leading to the faster coking rate; (ii) the higher acid site density reducing the distance of two adjacent acid sites would enhance the probability of reactants and/or intermediates reacting with each other in more successive chemical steps (e.g., condensation reactions) along the diffusion path within the zeolite channel, which favorably accelerates the coke formation (Fig. 45) *(167)*.

Yuen and coworkers *(160)* evaluated the effect of acid strength on MTO reaction over SAPO-34 and H-SSZ-13 with the identical chabazite structure. The total methanol conversion can be achieved at the initial stage for both catalysts, but stronger acidic H-SSZ-13 exhibited more rapid deactivation than SAPO-34. The careful analysis of the coke composition after catalyst deactivation indicated that the C/H ratio of coke species over SAPO-34 is lower than that over H-SSZ-13 (Table 3) *(160)*, indicating that more H-unsaturated coke species, such as polyaromatics, are formed over H-SSZ-13 with stronger acid strength. Bleken and coworkers *(161)* also investigated the influence of acid strength on the MTO reaction performance

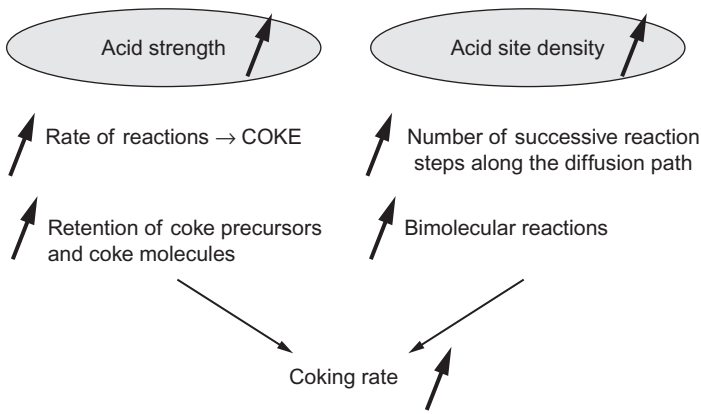

Fig. 45 The influences of acid properties on the coking rate of the catalysts *(167)*.

Table 3 Coke Composition of the Catalysts After Reaction Over SAPO-34 and H-SSZ-13 *(160)* (400°C, LHSV = 0.27, 22% Methanol Solution)

Material	SiO_2/Al_2O_3	Carbon Percent (%)	Hydrogen Percent (%)	Time on Stream (h)
SAPO-34	—	19.06	1.70	54
SSZ-13	9	16.60	1.46	18
SSZ-13	18	19.25	1.47	18
SSZ-13	58	15.00	1.35	18

and deactivation behavior over H-SAPO-34 and H-SSZ-13 with the same topology, close density of acid sites (approximately one acid site per cage), and comparable crystal size. The results showed that the more acidic H-SSZ-13 presents higher methanol conversion activity than SAPO-34, but suffers from quicker deactivation at high reaction temperature. The coke species over H-SAPO-34 are mainly composed of methylbenzene and methylnaphthalenes, while over H-SSZ-13, besides the formation of 1-ring and 2-ring compounds, 3-ring compounds, such as phenanthrene and its derivatives, are also formed, indicating that the polyaromatics are readily formed over H-SSZ-13 than H-SAPO-34 *(161)*.

Hydrogen transfer reaction is the major route of coke species formation in the reaction network of methanol conversion over zeolite catalysts. Hydrogen transfer over acidic zeolite catalysts gives rise to the nonolefinic by-products, including alkanes, aromatics, and coke. Muller and coworkers studied the role of BAS and LAS on hydrogen transfer reaction in the reaction network of methanol conversion *(179)*. Two hydrogen transfer routes were identified for the conversion of methanol to hydrocarbons. One hydrogen transfer way occurs between methanol and alkenes, involving the formation of HCHO by transferring the hydrogen from methanol to alkenes with the aid of BAS and LAS. The other hydrogen transfer reaction operates in the absence of methanol, transferring hydrogen between alkenes catalyzed by BAS only *(179)*. In the comparative study of methanol reaction over H-SAPO-5 and H-SSZ-24 catalysts with the same AFI topology, but different acid strengths for the MTH reaction, it was also found that the more acidic H-SSZ-24 yields much higher selectivities to arenes than the less acidic H-SAPO-5, thus suggesting that a higher acid strength favors intermolecular hydrogen transfer reactions *(162)*.

7. CONCLUSION AND OUTLOOK

Research and development of methanol-to-olefins process over the past three decades have made very fruitful achievements, including not only the successful process commercialization but also the fundamental understanding of reaction mechanism. Researchers proposed the direct reaction mechanism of C—C bond formation in the early studies, then the subsequent energetically favorable indirect pathway, and varied reaction routes for olefin generation according to different catalyst structures. Indirect reaction mechanisms for methanol-to-hydrocarbon conversion have been widely accepted. The studies of the direct mechanism for the initial C—C bond generation during the early reaction stage of methanol reaction over zeotype catalysts have attracted great interests again in the very recent years, and some very important progresses have been made. From the initial C—C bond generation to the efficient methanol-to-olefins reactions, further to the deactivation of the zeotype catalysts, the studies discussed in this chapter explain the special catalysis of methanol conversion—an organic species-induced reaction and deactivation over zeolite and SAPO catalysts. All these contributions help to understand the structure–function relationship of methanol reaction over molecular sieve catalysts, which lay the foundation for the development of catalysts and the optimization of the catalytic properties.

In the field of MTO reaction over solid acidic catalysts, the combined action from the acidity and structure of the catalysts has been revealed continuously based on the fundamental studies, while still many puzzles have not yet been solved completely due to the complexity of MTO conversion with a complicated reaction network. More research should be conducted in the future to clarify the issues of common concerns, including the reaction path for the initial C—C bond formation, the origin of the hydrocarbon pool species, the occurrence of the autocatalysis of methanol reaction, the specific reaction routes and the modulation of the reaction routes, the catalyst development for the improved selectivity of specifically desired olefin products and the reduced coke generation. The further progress in fundamental MTO research also relies on in situ techniques for the observation and characterization of the reaction, theoretical calculation on the catalytic reaction pathways and key intermediates, and advanced catalytic material synthesis to promote the development of new-generation of industrial catalyst and process.

ACKNOWLEDGMENTS

The authors acknowledge the financial support from the National Natural Science Foundation of China (Nos. 91545104, 21473182, and 21603223), the Frontier Science Key Program of the Chinese Academy of Sciences, and the Youth Innovation Promotion Association of the Chinese Academy of Sciences (2014165).

REFERENCES

1. Chang, C. D.; Silvestri, A. J. *J. Catal.* **1977**, *47*(2), 249–259.
2. Chang, C. D.; Silvestri, A. J.; Smith, R. L. Production of Gasoline Hydrocarbons. US Patent, 3 928 483, 1975.
3. Chang, C. D.; Silvestri, A. J.; Smith, R. L. Aromatization Reactions. US Patent, 3 894 103, 1975.
4. Chang, C. D. *Catal. Rev.* **1984**, *26*(3–4), 323–345.
5. Stocker, M. *Microporous Mesoporous Mater.* **1999**, *29*(1–2), 3–48.
6. Tian, P.; Wei, Y. X.; Ye, M.; Liu, Z. M. *ACS Catal.* **2015**, *5*(3), 1922–1938.
7. Liang, J.; Li, H. Y.; Zhao, S.; Guo, W. G.; Wang, R. H.; Ying, M. L. *Appl. Catal.* **1990**, *64*(1–2), 31–40.
8. Liu, Z. M.; Liang, J. *Curr. Opin. Solid State Mater. Sci.* **1999**, *4*(1), 80–84.
9. Koempel, H.; Liebner, W. *Stud. Surf. Sci. Catal.* **2007**, *167*, 261–267.
10. Brent, M. T. L.; Celeste, A. M.; Patton, R. L.; Gajek, R. T.; Cannan, T. R.; Lanigen, E. M.; Lok, B. M.; Messina, C. A.; Flanigen, E. M. New Family of Silico-Alumino-Phosphate Molecular Sieves—Prepared by Hydrothermal Crystallisation Are Useful for Sepn. and as Catalysts. EP103117-A1; EP103117-A; JP59035018-A; NO8302712-A; US4440871-A; DK8303398-A; ES8504077-A; CA1202016-A; ES8602094-A; EP103117-B; ES8604783-A; DE3366290-G; US5114563-A, EP103117-A1 EP103117-A, Mar 21, 1984 198413.
11. Liu, Z. M.; Qi, Y. *Bull. Chin. Acad. Sci.* **2006**, *21*(5), 406–408.
12. Argauer, R. J.; Landolt, G. R.; Audubon, N. J. Crystalline Zeolite ZSM-5 and Method of Preparing the Same. US Patent, 3702886, 1972.
13. Chang, C. D.; Lang, W. H.; Silvestri, A. J. Aromatization of Hetero-Atom Substituted Hydrocarbons. US Patent 3894104, 1975.
14. Hereijgers, B. P. C.; Bleken, F.; Nilsen, M. H.; Svelle, S.; Lillerud, K. P.; Bjorgen, M.; Weckhuysen, B. M.; Olsbye, U. *J. Catal.* **2009**, *264*(1), 77–87.
15. Haw, J. F.; Song, W.; Marcus, D. M.; Nicholas, J. B. *Acc. Chem. Res.* **2003**, *36*(5), 317–326.
16. Zhang, S.; Zhang, L.; Li, W. *Acta Phys. Chim. Sin.* **2014**, *30*(3), 535–543.
17. Gu, D. B. *Petrochem. Indus. Tech.* **2012**, *19*(4), 39.
18. Cormerais, F. X.; Chen, Y. S.; Kern, M.; Gnep, N. S.; Guisnet, M. *J. Chem. Res. S* **1981**, *9*, 290–291.
19. Marchi, A. J.; Froment, G. F. *Appl. Catal. A Gen.* **1993**, *94*(1), 91–106.
20. Santiesteban, J. G.; Chang, C. D.; Vartuli, J. C. *Zeolites* **1997**, *18*(2), 234.
21. Inui, T.; Morinaga, N.; Takegami, Y. *Appl. Catal.* **1983**, *8*(2), 187–197.
22. Zhou, F.; Tian, P.; Liu, Z. M.; Liu, G. Y.; Chang, F. X.; Li, J. Z. *Chin. J. Catal.* **2007**, *28*(9), 817–822.
23. Lok, B. M.; Messina, C. A.; Patton, R. L.; Gajek, R. T.; Cannan, T. R.; Flanigen, E. M. *J. Am. Chem. Soc.* **1984**, *106*(20), 6092–6093.
24. Wilson, S.; Barger, P. *Microporous Mesoporous Mater.* **1999**, *29*(1–2), 117–126.
25. Chen, D.; Moljord, K.; Fuglerud, T.; Holmen, A. *Microporous Mesoporous Mater.* **1999**, *29*(1–2), 191–203.

26. Liu, G. Y.; Tian, P.; Zhang, Y.; Li, J. Z.; Xu, L.; Meng, S. H.; Liu, Z. M. *Microporous Mesoporous Mater.* **2008**, *114*(1–3), 416–423.
27. Tan, J.; Liu, Z.; Bao, X.; Liu, X.; Han, X.; He, C.; Zhai, R. *Microporous Mesoporous Mater.* **2002**, *53*(1–3), 97–108.
28. Liu, G.; Tian, P.; Li, J.; Zhang, D.; Zhou, F.; Liu, Z. *Microporous Mesoporous Mater.* **2008**, *111*(1–3), 143–149.
29. Inui, T.; Kang, M. *Appl. Catal. A Gen.* **1997**, *164*(1–2), 211–223.
30. Van Niekerk, M. J.; Fletcher, J. C. Q.; OConnor, C. T. *Appl. Catal. A Gen.* **1996**, *138*(1), 135–145.
31. Xu, L.; Liu, Z. M.; Du, A. P.; Wei, Y. X.; Sun, Z. G. *Stud. Surf. Sci. Catal.* **2004**, *147*, 445–450.
32. Song, W. G.; Haw, J. F. *Angew. Chem. Int. Ed.* **2003**, *42*(8), 892–894.
33. Mees, F. D. P.; Voort, P. V. D.; Cool, P.; Martens, L. R. M.; Janssen, M. J. G.; Verberckmoes, A. A.; Kennedy, G. J.; Hall, R. B.; Wang, K.; Vansant, E. F. *J. Phys. Chem. B* **2003**, *107*, 3161–3167.
34. Chang, C. D. *J. Catal.* **1981**, *69*(1), 244–245.
35. Chang, C. D. *Catal. Rev.* **1983**, *25*(1), 1–118.
36. Keil, F. J. *Microporous Mesoporous Mater.* **1999**, *29*(1–2), 49–66.
37. Mokrani, T.; Scurrell, M. *Catal. Rev.* **2009**, *51*(1), 1–145.
38. Maiden, C. J. *Stud. Surf. Sci. Catal.* **1988**, *36*, 1–16.
39. Tabak, S. A.; Krambeck, F. J.; Garwood, W. E. *AIChE J.* **1986**, *32*(9), 1526–1531.
40. Vora, B. V.; Lentz, R. A.; Marker, T. L.; Nilsen, H.; Kvisle, S.; Fuglerud, T., 5th World Congress of Chemical Engineering 1996, San Diego.
41. Bertau, M.; Wernicke, H. J.; Schmidt, F. In: *Chapter 6: Methanol Utilisation Technologies*; Bertau, M., Offermanns, H., Plass, L., Schmidt, F., Wernicke, H. J., Eds.; Springer: Berlin, Heidelberg, 2014; pp 327–601.
42. Trabold, P. In: *Sustainable Routes to Petrochemical Products*; *The 7th International Petrochemical Conference, Athene*; 2007.
43. Vora, B. V.; Marker, T. L.; Barger, P. T.; Nilsen, H. R.; Kvisle, S.; Fuglerud, T. *Stud. Surf. Sci. Catal.* **1997**, *107*, 87–98.
44. Chen, J. Q.; Bozzano, A.; Glover, B.; Fuglerud, T.; Kvisle, S. *Catal. Today* **2005**, *106*(1–4), 103–107.
45. Liu, Z. M.; Sun, C. L.; Wang, G. W.; Wang, Q. X.; Cai, G. Y. *Fuel Process. Technol.* **2000**, *62*, 161–172.
46. Liu, Z. M. *Methanol to Olefins*. SciencePress: Beijing, 2015; pp 40–83.
47. Olsbye, U.; Svelle, S.; Bjorgen, M.; Beato, P.; Janssens, T. V. W.; Joensen, F.; Bordiga, S.; Lillerud, K. P. *Angew. Chem. Int. Ed.* **2012**, *51*(24), 5810–5831.
48. Berg, J. P.; Wolthuizen, J. P.; Hooff, J. H. In: *The Conversion of Dimethyl Ether to Hydrocarbons on Zeolite H-ZSM-5: The Reaction Mechanism for Formation of Primary Olefins*; *Proceedings of the Fifth International Conference on Zeolites*; 1980; pp 649–660.
49. Hutchings, G. J.; Gottschalk, F.; Hall, M. V. M.; Hunter, R. *J. Chem. Soc. Farad. T 1* **1987**, *83*, 571–583.
50. Olah, G. A. *Pure Appl. Chem.* **1981**, *53*(1), 201–207.
51. Kagi, D. *J. Catal.* **1981**, *69*(1), 242–243.
52. Ono, Y.; Mori, T. *J. Chem. Soc. Farad. T 1* **1981**, *77*, 2209–2221.
53. Swabb, E. A.; Gates, B. C. *Ind. Eng. Chem. Fund.* **1972**, *11*(4), 540–545.
54. Clarke, J. K. A.; Darcy, R.; Hegarty, B. F.; Odonoghue, E.; Amirebrahimi, V.; Rooney, J. J. *J. Chem. Soc. Chem. Commun.* **1986**, *5*, 425–426.
55. Zatorski, W.; Kryzanowski, S. *Acta Phys. Chem.* **1978**, *29*, 347.
56. Hemelsoet, K.; Mynsbrugge, J. V. d.; Wispelaere, K. D.; Waroquier, M.; Speybroeck, V. V. *ChemPhysChem* **2013**, *14*(8), 1526–1545.

57. Li, J. F.; Wei, Z. H.; Chen, Y. Y.; Jing, B. Q.; He, Y.; Dong, M.; Jiao, H. J.; Li, X. K.; Qin, Z. F.; Wang, J. G.; Fan, W. B. *J. Catal.* **2014**, *317*, 277–283.
58. Peng, C.; Wang, H. F.; Hu, P. *Phys. Chem. Chem. Phys.* **2016**, *18*(21), 14495–14502.
59. Tajima, N.; Tsuneda, T.; Toyama, F.; Hirao, K. *J. Am. Chem. Soc.* **1998**, *120*(32), 8222–8229.
60. Lesthaeghe, D.; Van Speybroeck, V.; Marin, G. B.; Waroquier, M. *Angew. Chem. Int. Ed.* **2006**, *45*(11), 1714–1719.
61. Lesthaeghe, D.; Van Speybroeck, V.; Marin, G. B.; Waroquier, M. *Ind. Eng. Chem. Res.* **2007**, *46*(26), 8832–8838.
62. Comas-Vives, A.; Valla, M.; Coperet, C.; Sautet, P. *ACS Cent. Sci.* **2015**, *1*(6), 313–319.
63. Liu, Y.; Muller, S.; Berger, D.; Jelic, J.; Reuter, K.; Tonigold, M.; Sanchez-Sanchez, M.; Lercher, J. A. *Angew. Chem. Int. Ed.* **2016**, *55*(19), 5723–5726.
64. Olah, G. A.; Doggweiler, H.; Felberg, J. D.; Frohlich, S.; Grdina, M. J.; Karpeles, R.; Keumi, T.; Inaba, S.; Ip, W. M.; Lammertsma, K.; Salem, G.; Tabor, D. C. *J. Am. Chem. Soc.* **1984**, *106*(7), 2143–2149.
65. Munson, E. J.; Kheir, A. A.; Haw, J. F. *J. Phys. Chem.* **1993**, *97*(28), 7321–7327.
66. Howe, R. F.; Taylor, M. J. *Spectrochim. Acta A* **1987**, *43*(1), 73–78.
67. Chowdhury, A. D.; Houben, K.; Whiting, G. T.; Mokhtar, M.; Asiri, A. M.; Al-Thabaiti, S. A.; Basahel, S. N.; Baldus, M.; Weckhuysen, B. M. *Angew. Chem. Int. Ed.* **2016**, *55*(51), 15840–15845.
68. Blaszkowski, S. R.; vanSanten, R. A. *J. Am. Chem. Soc.* **1997**, *119*(21), 5020–5027.
69. Wu, X. Q.; Xu, S. T.; Zhang, W. N.; Huang, J. D.; Li, J. Z.; Yu, B. W.; Wei, Y. X.; Liu, Z. M. *Angew. Chem. Int. Ed.* **2017**, *56*(31), 9039–9043.
70. Kolboe, S. *Acta Chem. Scand. Ser.* **1986**, *40*(10), 711–713.
71. Kolboe, S. *Stud. Surf. Sci. Catal.* **1988**, *36*, 189–193.
72. Wang, W.; Buchholz, A.; Seiler, M.; Hunger, M. *J. Am. Chem. Soc.* **2003**, *125*(49), 15260–15267.
73. Haw, J. F.; Marcus, D. M. *Top. Catal.* **2005**, *34*(1–4), 41–48.
74. Xu, S. T.; Zheng, A. M.; Wei, Y. X.; Chen, J. R.; Li, J. Z.; Chu, Y. Y.; Zhang, M. Z.; Wang, Q. Y.; Zhou, Y.; Wang, J. B.; Deng, F.; Liu, Z. M. *Angew. Chem. Int. Ed.* **2013**, *52*(44), 11564–11568.
75. Dahl, I. M.; Kolboe, S. *Catal. Lett.* **1993**, *20*(3–4), 329–336.
76. Dahl, I. M.; Kolboe, S. *J. Catal.* **1994**, *149*(2), 458–464.
77. Dahl, I. M.; Kolboe, S. *J. Catal.* **1996**, *161*(1), 304–309.
78. Arstad, B.; Kolboe, S. *J. Am. Chem. Soc.* **2001**, *123*(33), 8137–8138.
79. Arstad, B.; Kolboe, S. *Catal. Lett.* **2001**, *71*(3–4), 209–212.
80. Mikkelsen, O.; Ronning, P. O.; Kolboe, S. *Microporous Mesoporous Mater.* **2000**, *40*(1–3), 95–113.
81. Song, W. G.; Fu, H.; Haw, J. F. *J. Am. Chem. Soc.* **2001**, *123*(20), 4749–4754.
82. Song, W. G.; Haw, J. F.; Nicholas, J. B.; Heneghan, C. S. *J. Am. Chem. Soc.* **2000**, *122*(43), 10726–10727.
83. Song, W. G.; Nicholas, J. B.; Sassi, A.; Haw, J. F. *Catal. Lett.* **2002**, *81*(1–2), 49–53.
84. Dessau, R. M. *J. Catal.* **1986**, *99*(1), 111–116.
85. Dessau, R. M.; Lapierre, R. B. *J. Catal.* **1982**, *78*(1), 136–141.
86. Bjorgen, M.; Svelle, S.; Joensen, F.; Nerlov, J.; Kolboe, S.; Bonino, F.; Palumbo, L.; Bordiga, S.; Olsbye, U. *J. Catal.* **2007**, *249*(2), 195–207.
87. Svelle, S.; Joensen, F.; Nerlov, J.; Olsbye, U.; Lillerud, K. P.; Kolboe, S.; Bjorgen, M. *J. Am. Chem. Soc.* **2006**, *128*(46), 14770–14771.
88. Svelle, S.; Olsbye, U.; Joensen, F.; Bjorgen, M. *J. Phys. Chem. C* **2007**, *111*(49), 17981–17984.

89. Chen, N. Y.; Reagan, W. J. *J. Catal.* **1979**, *59*(1), 123–129.
90. Qi, L.; Wei, Y. X.; Xu, L.; Liu, Z. M. *ACS Catal.* **2015**, *5*(7), 3973–3982.
91. Langner, B. E. *Appl. Catal.* **1982**, *2*(4–5), 289–302.
92. Sullivan, R. F.; Sieg, R. P.; Langlois, G. E.; Egan, C. J. *J. Am. Chem. Soc.* **1961**, *83*(5), 1156–1160.
93. Mole, T.; Bett, G.; Seddon, D. *J. Catal.* **1983**, *84*(2), 435–445.
94. Mole, T.; Whiteside, J. A.; Seddon, D. *J. Catal.* **1983**, *82*(2), 261–266.
95. Sassi, A.; Wildman, M. A.; Ahn, H. J.; Prasad, P.; Nicholas, J. B.; Haw, J. F. *J. Phys. Chem. B* **2002**, *106*(9), 2294–2303.
96. Haw, J. F. *Top. Catal.* **1999**, *8*(1–2), 81–86.
97. Haw, J. F.; Nicholas, J. B.; Song, W. G.; Deng, F.; Wang, Z. K.; Xu, T.; Heneghan, C. S. *J. Am. Chem. Soc.* **2000**, *122*(19), 4763–4775.
98. Song, W. G.; Nicholas, J. B.; Haw, J. F. *J. Phys. Chem. B* **2001**, *105*(19), 4317–4323.
99. Xu, T.; Barich, D. H.; Goguen, P. W.; Song, W. G.; Wang, Z. K.; Nicholas, J. B.; Haw, J. F. *J. Am. Chem. Soc.* **1998**, *120*(16), 4025–4026.
100. Bjorgen, M.; Olsbye, U.; Svelle, S.; Kolboe, S. *Catal. Lett.* **2004**, *93*(1–2), 37–40.
101. Song, W. G.; Fu, H.; Haw, J. F. *J. Phys. Chem. B* **2001**, *105*(51), 12839–12843.
102. Bjorgen, M.; Bonino, F.; Kolboe, S.; Lillerud, K. P.; Zecchina, A.; Bordiga, S. *J. Am. Chem. Soc.* **2003**, *125*(51), 15863–15868.
103. Xu, T.; Haw, J. F. *J. Am. Chem. Soc.* **1994**, *116*(22), 10188–10195.
104. Wang, C.; Chu, Y. Y.; Zheng, A. M.; Xu, J.; Wang, Q.; Gao, P.; Qi, G. D.; Gong, Y. J.; Deng, F. *Chemistry* **2014**, *20*(39), 12432–12443.
105. Wang, C.; Yi, X.; Xu, J.; Qi, G.; Gao, P.; Wang, W.; Chu, Y.; Wang, Q.; Feng, N.; Liu, X.; Zheng, A.; Deng, F. *Chemistry* **2015**, *21*(34), 12061–12068.
106. Wang, C.; Xu, J.; Qi, G. D.; Gong, Y. J.; Wang, W. Y.; Gao, P.; Wang, Q.; Feng, N. D.; Liu, X. L.; Deng, F. *J. Catal.* **2015**, *332*, 127–137.
107. Wang, C.; Wang, Q.; Xu, J.; Qi, G.; Gao, P.; Wang, W.; Zou, Y.; Feng, N.; Liu, X.; Deng, F. *Angew. Chem. Int. Ed.* **2016**, *55*(7), 2507–2511.
108. Li, J. Z.; Wei, Y. X.; Chen, J. R.; Tian, P.; Su, X.; Xu, S. T.; Qi, Y.; Wang, Q. Y.; Zhou, Y.; He, Y. L.; Liu, Z. M. *J. Am. Chem. Soc.* **2012**, *134*(2), 836–839.
109. Li, J. Z.; Wei, Y. X.; Chen, J. R.; Xu, S. T.; Tian, P.; Yang, X. F.; Li, B.; Wang, J. B.; Liu, Z. M. *ACS Catal.* **2015**, *5*(2), 661–665.
110. Teketel, S.; Erichsen, M. W.; Bleken, F. L.; Svelle, S.; Petter, K. *Catalysis* **2014**, *26*, 179–217.
111. Chen, J. R.; Li, J. Z.; Wei, Y. X.; Yuan, C. Y.; Li, B.; Xu, S. T.; Zhou, Y.; Wang, J. B.; Zhang, M. Z.; Liu, Z. M. *Catal. Commun.* **2014**, *46*, 36–40.
112. Teketel, S.; Skistad, W.; Benard, S.; Olsbye, U.; Lillerud, K. P.; Beato, P.; Svelle, S. *ACS Catal.* **2012**, *2*(1), 26–37.
113. Li, J. Z.; Wei, Y. X.; Liu, G. Y.; Qi, Y.; Tian, P.; Li, B.; He, Y. L.; Liu, Z. M. *Catal. Today* **2011**, *171*(1), 221–228.
114. Dai, W. L.; Wang, X.; Wu, G. J.; Guan, N. J.; Hunger, M.; Li, L. D. *ACS Catal.* **2011**, *1*(4), 292–299.
115. Zhang, M. Z.; Xu, S. T.; Wei, Y. X.; Li, J. Z.; Chen, J. R.; Wang, J. B.; Zhang, W. N.; Gao, S. S.; Li, X. J.; Wang, C. X.; Liu, Z. M. *RSC Adv.* **2016**, *6*(98), 95855–95864.
116. Wang, C. M.; Wang, Y. D.; Xie, Z. K.; Liu, Z. P. *J. Phys. Chem. C* **2009**, *113*(11), 4584–4591.
117. Bjorgen, M.; Akyalcin, S.; Olsbye, U.; Benard, S.; Kolboe, S.; Svelle, S. *J. Catal.* **2010**, *275*(1), 170–180.
118. Bjørgen, M.; Olsbye, U.; Petersen, D.; Kolboe, S. *J. Catal.* **2004**, *221*(1), 1–10.
119. Tian, P.; Su, X.; Wang, Y. X.; Xia, Q. H.; Zhang, Y.; Fan, D.; Meng, S. H.; Liu, Z. M. *Chem. Mater.* **2011**, *23*(6), 1406–1413.
120. Li, J. Z.; Wei, Y. X.; Xu, S. T.; Tian, P.; Chen, J. R.; Liu, Z. M. *Catal. Today* **2014**, *226*, 47–51.

121. Zhang, M. Z.; Xu, S. T.; Li, J. Z.; Wei, Y. X.; Gong, Y. J.; Chu, Y. Y.; Zheng, A. M.; Wang, J. B.; Zhang, W. N.; Wu, X. Q.; Deng, F.; Liu, Z. M. *J. Catal.* **2016**, *335*, 47–57.
122. Song, W. G.; Marcus, D. M.; Fu, H.; Ehresmann, J. O.; Haw, J. F. *J. Am. Chem. Soc.* **2002**, *124*(15), 3844–3845.
123. Jiang, Y. J.; Wang, W.; Marthala, V. R. R.; Huang, J.; Sulikowski, B.; Hunger, M. *J. Catal.* **2006**, *238*(1), 21–27.
124. Vandichel, M.; Lesthaeghe, D.; Van der Mynsbrugge, J.; Waroquier, M.; Van Speybroeck, V. *J. Catal.* **2010**, *271*(1), 67–78.
125. Lesthaeghe, D.; Horre, A.; Waroquier, M.; Marin, G. B.; Van Speybroeck, V. *Chemistry* **2009**, *15*(41), 10803–10808.
126. Sassi, A.; Wildman, M. A.; Haw, J. F. *J. Phys. Chem. B* **2002**, *106*(34), 8768–8773.
127. Arstad, B.; Kolboe, S.; Swang, O. *J. Phys. Chem. A* **2005**, *109*(39), 8914–8922.
128. McCann, D. M.; Lesthaeghe, D.; Kletnieks, P. W.; Guenther, D. R.; Hayman, M. J.; Van Speybroeck, V.; Waroquier, M.; Haw, J. F. *Angew. Chem. Int. Ed.* **2008**, *47*(28), 5179–5182.
129. Kolboe, S.; Svelle, S.; Arstad, B. *J. Phys. Chem. A* **2009**, *113*(5), 917–923.
130. Kolboe, S. *J. Phys. Chem. A* **2011**, *115*(14), 3106–3115.
131. Kolboe, S. *J. Phys. Chem. A* **2012**, *116*(14), 3710–3716.
132. De Wispelaere, K.; Hemelsoet, K.; Waroquier, M.; Van Speybroeck, V. *J. Catal.* **2013**, *305*, 76–80.
133. Bleken, F.; Skistad, W.; Barbera, K.; Kustova, M.; Bordiga, S.; Beato, P.; Lillerud, K. P.; Svelle, S.; Olsbye, U. *Phys. Chem. Chem. Phys.* **2011**, *13*(7), 2539–2549.
134. Haw, J. F. *Phys. Chem. Chem. Phys.* **2002**, *4*(22), 5431–5441.
135. Bjorgen, M.; Joensen, F.; Lillerud, K. P.; Olsbye, U.; Svelle, S. *Catal. Today* **2009**, *142*(1–2), 90–97.
136. Lesthaeghe, D.; De Sterck, B.; Van Speybroeck, V.; Marin, G. B.; Waroquier, M. *Angew. Chem. Int. Ed.* **2007**, *46*(8), 1311–1314.
137. Wang, C. M.; Wang, Y. D.; Liu, H. X.; Xie, Z. K.; Liu, Z. P. *Microporous Mesoporous Mater.* **2012**, *158*, 264–271.
138. Fu, H.; Song, W. G.; Haw, J. F. *Catal. Lett.* **2001**, *76*(1–2), 89–94.
139. Bjørgen, M.; Olsbye, U.; Kolboe, S. *J. Catal.* **2003**, *215*(1), 30–44.
140. Zaidi, H. A.; Pant, K. K. *Catal. Today* **2004**, *96*(3), 155–160.
141. Kissin, Y. V. *Catal. Rev.* **2001**, *43*(1–2), 85–146.
142. Wang, X.; Dai, W. L.; Wu, G. J.; Li, L. D.; Guan, N. J.; Hunger, M. *Catal. Sci. Technol.* **2014**, *4*(3), 688–696.
143. Dai, W. L.; Dyballa, M.; Wu, G.; Li, L. D.; Guan, N. J.; Hunger, M. *J. Phys. Chem. C* **2015**, *119*, 2637–2645.
144. Dai, W. L.; Wang, C. M.; Dyballa, M.; Wu, G. J.; Guan, N. J.; Li, L. D.; Xie, Z. K.; Hunger, M. *ACS Catal.* **2015**, *5*(1), 317–326.
145. Wang, C. M.; Wang, Y. D.; Xie, Z. K. *Catal. Sci. Technol.* **2014**, *4*(8), 2631–2638.
146. Hwang, A.; Prieto-Centurion, D.; Bhan, A. *J. Catal.* **2016**, *337*, 52–56.
147. Wang, C. M.; Wang, Y. D.; Xie, Z. K. *J. Catal.* **2013**, *301*, 8–19.
148. Chen, J. R.; Li, J. Z.; Yuan, C. Y.; Xu, S. T.; Wei, Y. X.; Wang, Q. Y.; Zhou, Y.; Wang, J. B.; Zhang, M. Z.; He, Y. L.; Xu, S. L.; Liu, Z. M. *Catal. Sci. Technol.* **2014**, *4*(9), 3268–3277.
149. Wang, S.; Wei, Z. H.; Chen, Y. Y.; Qin, Z. F.; Ma, H.; Dong, M.; Fan, W. B.; Wang, J. G. *ACS Catal.* **2015**, *5*(2), 1131–1144.
150. Wang, S.; Chen, Y. Y.; Wei, Z. H.; Qin, Z. F.; Ma, H.; Dong, M.; Li, J. F.; Fan, W. B.; Wang, J. G. *J. Phys. Chem. C* **2015**, *119*(51), 28482–28498.
151. Cui, Z. M.; Liu, Q.; Ma, Z.; Bian, S. W.; Song, W. G. *J. Catal.* **2008**, *258*(1), 83–86.

152. Cui, Z. M.; Liu, Q.; Baint, S. W.; Ma, Z.; Song, W. G. *J. Phys. Chem. C* **2008**, *112*(7), 2685–2688.
153. Li, J. Z.; Wei, Y. X.; Qi, Y.; Tian, P.; Li, B.; He, Y. L.; Chang, F. X.; Sun, X. D.; Liu, Z. M. *Catal. Today* **2011**, *164*(1), 288–292.
154. Teketel, S.; Svelle, S.; Lillerud, K. P.; Olsbye, U. *ChemCatChem* **2009**, *1*(1), 78–81.
155. Teketel, S.; Olsbye, U.; Lillerud, K. P.; Beato, P.; Svelle, S. *Microporous Mesoporous Mater.* **2010**, *136*(1–3), 33–41.
156. Li, J. Z.; Qi, Y.; Liu, Z. M.; Liu, G. Y.; Zhang, D. Z. *Catal. Lett.* **2008**, *121*(3–4), 303–310.
157. Li, J. Z.; Qi, Y.; Xu, L.; Liu, G. Y.; Meng, S. H.; Li, B.; Li, M. Z.; Liu, Z. M. *Catal. Commun.* **2008**, *9*(15), 2515–2519.
158. Li, J. Z.; Qi, Y.; Liu, Z. M.; Liu, G. Y.; Chang, F. X. *Chin. J. Catal.* **2008**, *29*(7), 660–664.
159. Hemelsoet, K.; Nollet, A.; Vandichel, M.; Lesthaeghe, D.; Van Speybroeck, V.; Waroquier, M. *ChemCatChem* **2009**, *1*(3), 373–378.
160. Yuen, L. T.; Zones, S. I.; Harris, T. V.; Gallegos, E. J.; Auroux, A. *Microporous Mesoporous Mater.* **1994**, *2*(2), 105–117.
161. Bleken, F.; Bjorgen, M.; Palumbo, L.; Bordiga, S.; Svelle, S.; Lillerud, K. P.; Olsbye, U. *Top. Catal.* **2009**, *52*(3), 218–228.
162. Erichsen, M. W.; Svelle, S.; Olsbye, U. *Catal. Today* **2013**, *215*, 216–223.
163. Erichsen, M. W.; Svelle, S.; Olsbye, U. *J. Catal.* **2013**, *298*, 94–101.
164. Dai, W. L.; Li, N.; Li, L. D.; Guan, N. J.; Hunger, M. *Catal. Commun.* **2011**, *16*(1), 124–127.
165. Dai, W. L.; Wang, X.; Wu, G. J.; Li, L. D.; Guan, N. J.; Hunger, M. *ChemCatChem* **2012**, *4*(9), 1428–1435.
166. Dai, W. L.; Wu, G. J.; Li, L. D.; Guan, N. J.; Hunger, M. *ACS Catal.* **2013**, *3*(4), 588–596.
167. Guisnet, M.; Costa, L.; Ribeiro, F. R. *J. Mol. Catal. A* **2009**, *305*(1–2), 69–83.
168. Müller, S.; Liu, Y.; Vishnuvarthan, M.; Sun, X.; van Veen, A. C.; Haller, G. L.; Sanchez-Sanchez, M.; Lercher, J. A. *J. Catal.* **2015**, *325*, 48–59.
169. Mores, D.; Kornatowski, J.; Olsbye, U.; Weckhuysen, B. M. *Chemistry* **2011**, *17*(10), 2874–2884.
170. Mores, D.; Stavitski, E.; Kox, M. H. F.; Kornatowski, J.; Olsbye, U.; Weckhuysen, B. M. *Chemistry* **2008**, *14*(36), 11320–11327.
171. Schulz, H. *Catal. Today* **2010**, *154*(3–4), 183–194.
172. Schulz, H.; Wei, M. *Top. Catal.* **2014**, *57*(6–9), 683–692.
173. Yuan, C. Y.; Wei, Y. X.; Li, J. Z.; Xu, S. T.; Chen, J. R.; Zhou, Y.; Wang, Q. Y.; Xu, L.; Liu, Z. M. *Chin. J. Catal.* **2012**, *33*(2), 367–374.
174. Wei, Y. X.; Li, J. Z.; Yuan, C. Y.; Xu, S. T.; Zhou, Y.; Chen, J. R.; Wang, Q. Y.; Zhang, Q.; Liu, Z. M. *Chem. Commun.* **2012**, *48*(25), 3082–3084.
175. Wei, Y. X.; Yuan, C. Y.; Li, J. Z.; Xu, S. T.; Zhou, Y.; Chen, J. R.; Wang, Q. Y.; Xu, L.; Qi, Y.; Zhang, Q.; Liu, Z. M. *ChemSusChem* **2012**, *5*(5), 906–912.
176. Qi, L.; Li, J. Z.; Wang, L. Y.; Xu, L.; Liu, Z. M. *Catal. Sci. Technol.* **2017**, *7*(4), 894–901.
177. Dahl, I. M.; Mostad, H.; Akporiaye, D.; Wendelbo, R. *Microporous Mesoporous Mater.* **1999**, *29*(1–2), 185–190.
178. Zhu, Q. J.; Kondo, J. N.; Ohnuma, R.; Kubota, Y.; Yamaguchi, M.; Tatsumi, T. *Microporous Mesoporous Mater.* **2008**, *112*(1–3), 153–161.
179. Muller, S.; Liu, Y.; Kirchberger, F. M.; Tonigold, M.; Sanchez-Sanchez, M.; Lercher, J. A. *J. Am. Chem. Soc.* **2016**, *138*(49), 15994–16003.

ABOUT THE AUTHORS

Shutao Xu received his PhD in Physical Chemistry from Dalian Institute of Chemical Physics, Chinese Academy of Sciences, in 2011. Then he joined Prof. Zhongmin Liu's team at National Engineering Laboratory for Methanol to Olefins, Dalian Institute of Chemical Physics as a research assistant. He became an associate professor in 2013 and professor in 2017. His research interests are the development of in situ NMR techniques and their applications in material science and catalysis, especially the molecular sieve synthesis and heterogeneous catalytic reaction mechanisms as revealed by in situ 1D and 2D NMR spectroscopy.

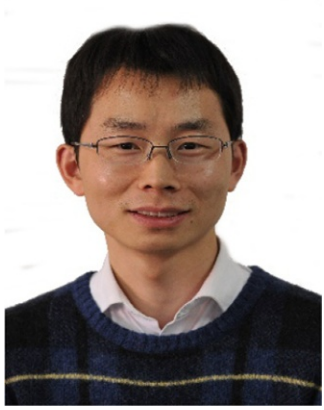

Yuchun Zhi is an associate professor in Dalian Institute of Chemical Physics, Chinese Academy of Sciences. He received his PhD degree in Industrial Catalysis from Technical University of Munich, Germany, in 2015 under the direction of Prof. Johannes A. Lercher. His doctoral work used kinetic approach associated with theoretical calculation to unravel the effect of water from molecular level on alcohol dehydration reaction. His current research field is focused on the mechanistic understanding of industry-relevant solid acid-catalyzed reactions, and more concerns are devoted to the mechanism exploration of methanol to olefins process.

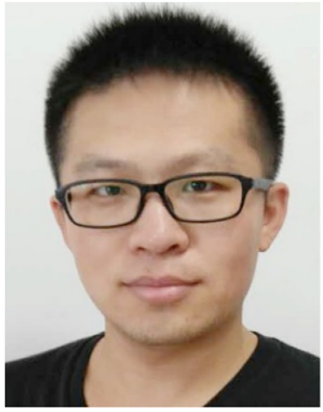

Jingfeng Han received his PhD in Physical Chemistry from Dalian Institute of Chemical Physics (DICP), Chinese Academy of Sciences, in 2015. He then spent 2 years as a postdoctoral research associate at the Methanol to Olefins, National Engineering Laboratory in DICP. His research interests are focused on the mechanism of methanol conversion reaction by operando spectroscopy and the diffusivity evolution on working catalyst for methanol to olefins reaction.

Wenna Zhang was born in 1989 in Shandong, China. She received her BS in chemistry from Inner Mongolia University, China in 2012. Currently she is a PhD candidate at National Engineering Laboratory for Methanol to Olefins, Dalian Institute of Chemical Physics, Chinese Academy of Sciences under the direction of Prof. Yingxu Wei and Prof. Zhongmin Liu. Her research interest is focused on the reaction mechanism of methanol to olefins catalyzed over zeolite via theoretical calculation.

Xinqiang Wu was born in 1988 in Shandong, China. He obtained his BS in chemical engineering and technology from Shandong Normal University in 2011. He is a PhD candidate under the direction of Prof. Yingxu Wei and Prof. Zhongmin Liu at Dalian Institute of Chemical Physics, Chinese Academy of Sciences. His research interest is focused on the mechanism of methanol conversion over zeolites during the initial stage of methanol-to-hydrocarbons process.

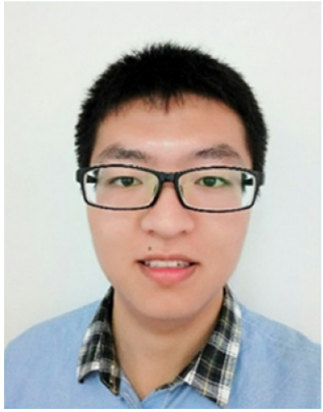

Tantan Sun was born in 1992 in Jiangsu, China. He obtained his BS in chemical engineering and technology from China University of Petroleum (East China) in 2015. He is a PhD candidate under the direction of Prof. Yingxu Wei and Prof. Zhongmin Liu at Dalian Institute of Chemical Physics, Chinese Academy of Sciences. His research is focused on host–guest interaction in zeolite-catalyzed reaction and solid-state NMR spectroscopy.

Yingxu Wei received her PhD in Dalian Institute of Chemical Physics (DICP), Chinese Academy of Sciences (CAS) in 2001. During her service at the Applied Catalysis Laboratory of DICP since graduation, she conducted the postdoctoral study at University of Namur (Belgium) from 2003 to 2004. She has been the group leader of Catalysis and New Catalytic Reactions in National Engineering Laboratory of Methanol to Olefins since 2009 and was promoted to professor in 2011. Over the years, Prof. Wei has undertaken a number of key academic research projects commissioned by NSFC, CAS, PetroChina, and other organizations. She has been involved in the researches on heterogeneous catalysis, methanol to olefins, catalysts and processes of hydrocarbon conversion, and catalytic conversion of methanol and methane derivatives. Over 70 academic papers authored by her have been published in scientific journals and more than 30 patents have been applied and granted.